ERDC/CHL TR-14-8

US Army Corps
of Engineers®
Engineer Research and
Development Center

ERDC
INNOVATIVE SOLUTIONS
for a safer, better world

Coastal Inlets Research Program

Modeling Study for Tangier Island Jetties, Tangier Island, Virginia

Zeki Demirbilek, Lihwa Lin, Donald L. Ward, and David B. King

March 2015

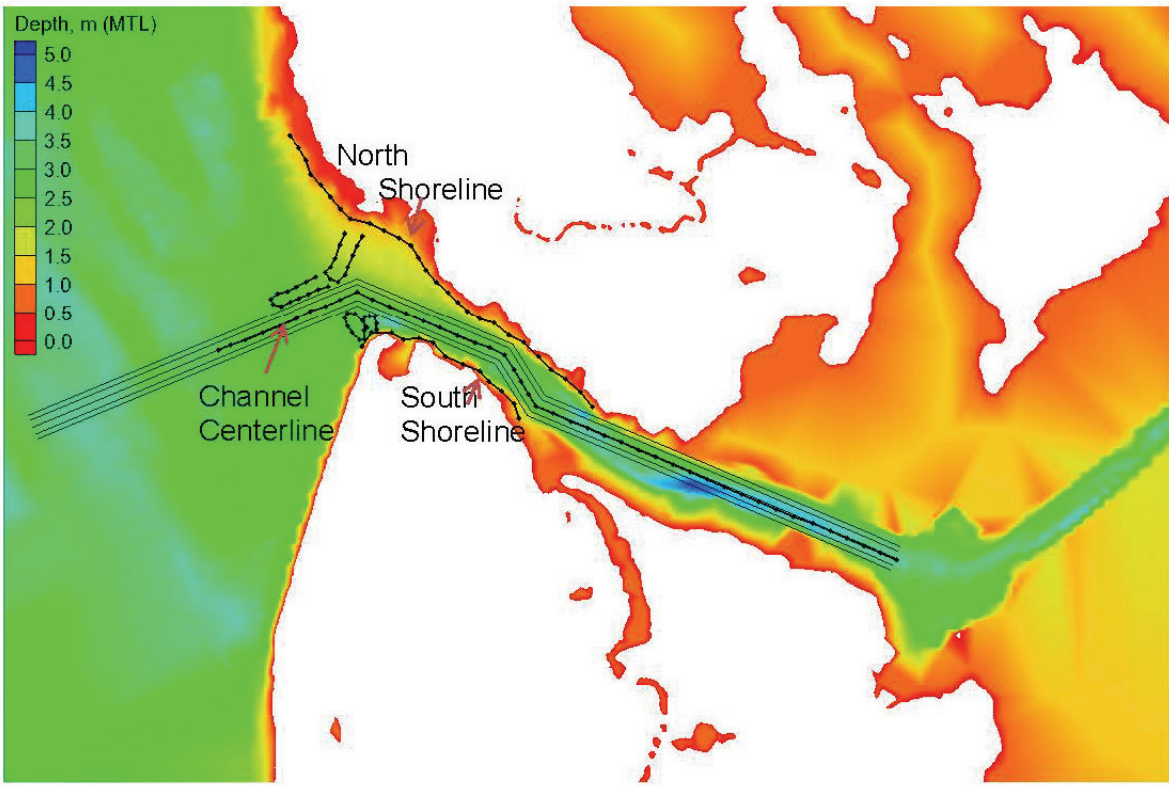

Coastal and Hydraulics Laboratory

The U.S. Army Engineer Research and Development Center (ERDC) solves the nation's toughest engineering and environmental challenges. ERDC develops innovative solutions in civil and military engineering, geospatial sciences, water resources, and environmental sciences for the Army, the Department of Defense, civilian agencies, and our nation's public good. Find out more at www.erdc.usace.army.mil.

To search for other technical reports published by ERDC, visit the ERDC online library at http://acwc.sdp.sirsi.net/client/default.

ERDC/CHL TR-14-8
March 2015

Modeling Study for Tangier Island Jetties, Tangier Island, Virginia

Zeki Demirbilek, Lihwa Lin, Donald Ward, David B. King

Coastal and Hydraulics Laboratory
U.S. Army Engineer Research and Development Center
3909 Halls Ferry Road
Vicksburg, MS 39180-6199

Final report

Prepared for U.S. Army Engineer District, Norfolk
803 Front Street, VA 23510

Under Coastal Inlets Research Program

Abstract

This report documents numerical wave and flow modeling for evaluation of the jetties on a shallow draft navigation channel on Tangier Island, VA, located in Chesapeake Bay. Because it is heavily used by the local fishing fleet, the U.S. Army Engineer District, Norfolk (CENAO) maintains the Tangier Island boat canal. CENAO is considering the construction of structures to protect the western entrance of the channel and reduce the wave energy in the lee of the structures, and asked the U.S. Army Engineer Research and Development Center (ERDC), Coastal and Hydraulics Laboratory (CHL) to perform a numerical modeling study to investigate how waves and hydrodynamics would be affected by structures, to identify the optimal location for the structures, and to develop a preliminary structure design. The primary goal of the study was to develop a quantitative estimate of waves and wave reduction in the canal for a relative comparison of alternatives investigated and for the preliminary structural design calculations.

CMS-Wave, a spectral wave model, was used to estimate waves in Chesapeake Bay and propagate waves into the entrance channel and boat canal. The numerical modeling results indicated that maximum wave energy reduction inside the canal was obtained using a dogleg jetty connecting to the north shoreline and a spur on the south shoreline.

Contents

Figures and Tables

Figures

Tables

Preface

This study was conducted for the U.S. Army Corps of Engineers (USACE), Norfolk District. This study was partially supported by the Coastal Inlets Research Program (CIRP), a research and development program in the Navigation Business Line administered by the USACE-Headquarters under the direction of W. Jeff Lillycrop, Technical Director, and Charles E. Wiggins, Associate Technical Director. Dr. Julie Rosati was Program Manager of CIRP during the period of study. Alicia Farrow and Lawrence Ives of the USACE District, Norfolk, provided input and oversight for the study.

Dr. Zeki Demirbilek of the Harbors, Entrances, and Structures Branch (HNH) of the Coastal Hydraulics Laboratory (CHL), Navigation Division and Dr. Lihwa Lin of the Coastal Engineering Branch (HNC) of the CHL Navigation Division conducted the study and wrote this report, with contributions by Dr. Donald Ward, HNH, and Dr. David King of the Coastal Processes Branch (HFC) in the Flood and Storm Protection Division.

At the time of this study, Dr. Donald Ward, was Acting Chief, HNH; Tanya Beck, was Acting Chief, HNC, and Mark Gravens was Chief, HFC. Dr. Jackie Pettway was Acting Chief, Navigation Division; Dr. Ty Wamsley was Chief, Flood and Storm Protection Division; Dr. Richard Styles was Acting Deputy Director, and Jose Sanchez was Acting Director of CHL.

COL Jeffrey R. Eckstein was the Commander of ERDC, and Dr. Jeffery P. Holland was the Director.

Unit Conversion Factors

Multiply	By	To Obtain
degrees (angle)	0.01745329	radians
feet	0.3048	meters
inches	0.0254	meters
feet^2	0.0929	meters^2
gallons (U.S. liquid)	0.003785412	cubic meters
gallons (U.S. liquid) per minute per foot	0.00020699	cubic meters per second per meter
pounds (mass)	453.59237	grams
pounds (force)	4.448222	Newtons

1 Study Needs and Plan

1.1 Background

This report describes details of a numerical modeling study conducted for Tangier Island navigation channel, which is located in Chesapeake Bay. The numerical modeling study developed wave estimates inside and outside of the shallow draft and narrow boat canal. The focus of numerical modeling was the assessment of the efficacy of proposed alternatives. Impacts of waves on navigation were examined using the CMS-Wave model. Details of numerical modeling study, tasks, results, and major findings are provided in this report.

Tangier Island (75.99° W, 37.83° N) is the southernmost of a string of islands that separate the deep portions of Chesapeake Bay to the west from shallower Tangier Sound to the east (Figure 1). The island, approximately 5 miles long by 2 miles wide, is located in the Virginia portion of Chesapeake Bay 20 miles southwest of Crisfield, MD and 70 miles north of Norfolk, VA. Tangier Island is comprised of a few low, fine-grained sand ridges with intervening marshlands having numerous islets and tidal creeks. The island's highest elevations are only a few meters above mean tide level (MTL). The populated areas are primarily three interconnected ridges on the southern portion of the island. Abundant seafood and tourism are two sources of livelihood for the island residents.

A shallow-V-shaped narrow channel, known as the Tangier Island boat canal, runs east-west across the island's mid section (Figure 2). This channel varies somewhat in width and depth, but averages approximately 265 ft (80 m) wide and 13 ft (4 m) deep. Technically termed a navigation channel, this waterway is a canal engineered and maintained by the U.S. Army Corps of Engineers for small-boat traffic. Numerous mooring docks and seafood-processing sheds line both north and south shorelines and are key infrastructure for the bay's fishing fleet. Maintenance and improvement of this canal are critical to the economy of the island.

The east side of the island is well-sheltered from the effects of storms, northeasters, and hurricanes because the short fetch distances from the Delmarva Peninsula do not provide sufficient space for large wind waves to generate and grow. The western side of Tangier Island is more exposed to large wind waves approaching the island from the northwest through

southwest quadrants. Consequently, the western shoreline has long experienced progressive flooding and erosion. Due to prevailing wind patterns, the longshore transport along the island's west shoreline is southerly.

Figure 1. Location of Tangier Island, VA, in Chesapeake Bay.

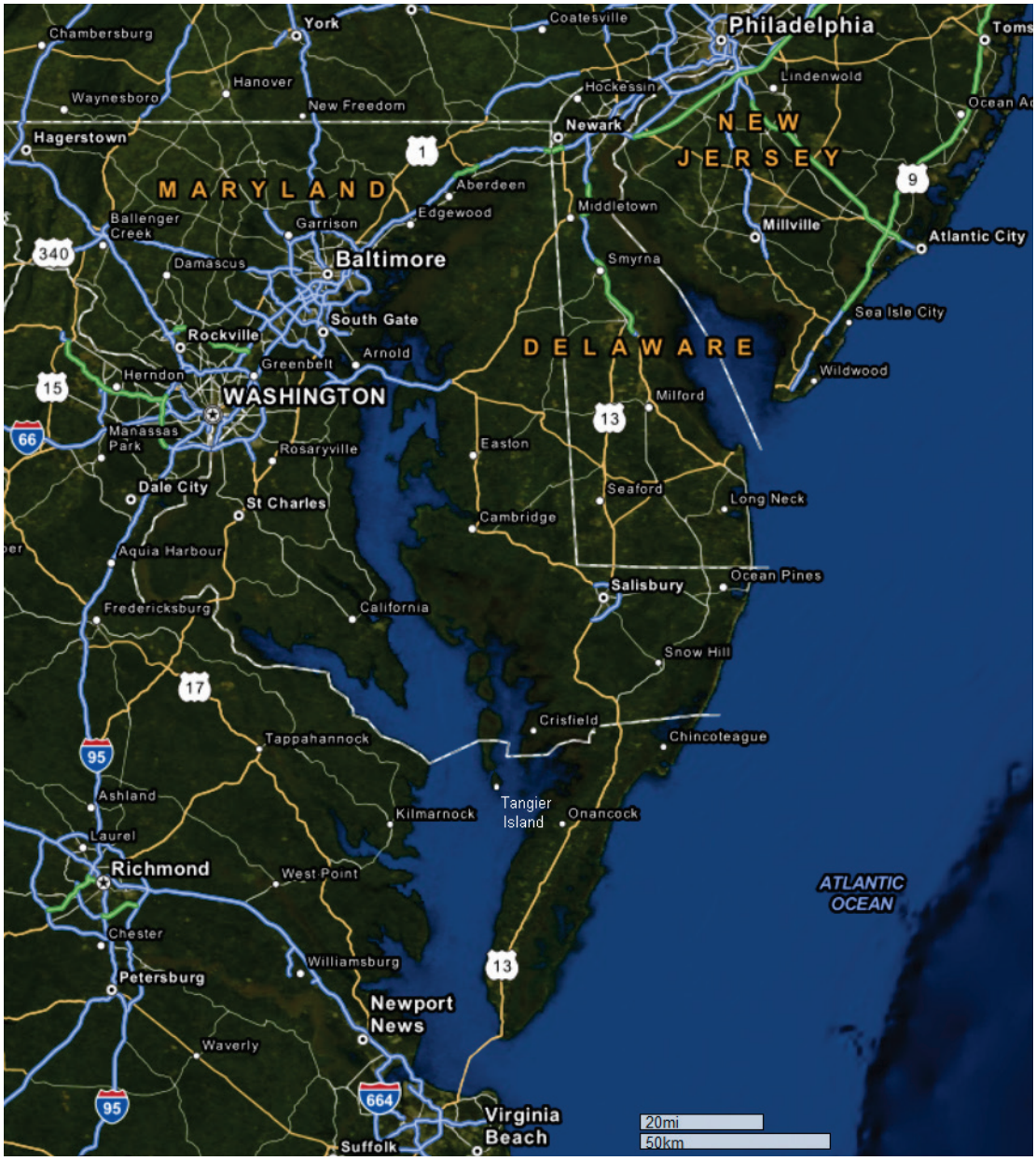

Figure 2. Tangier Island, VA.

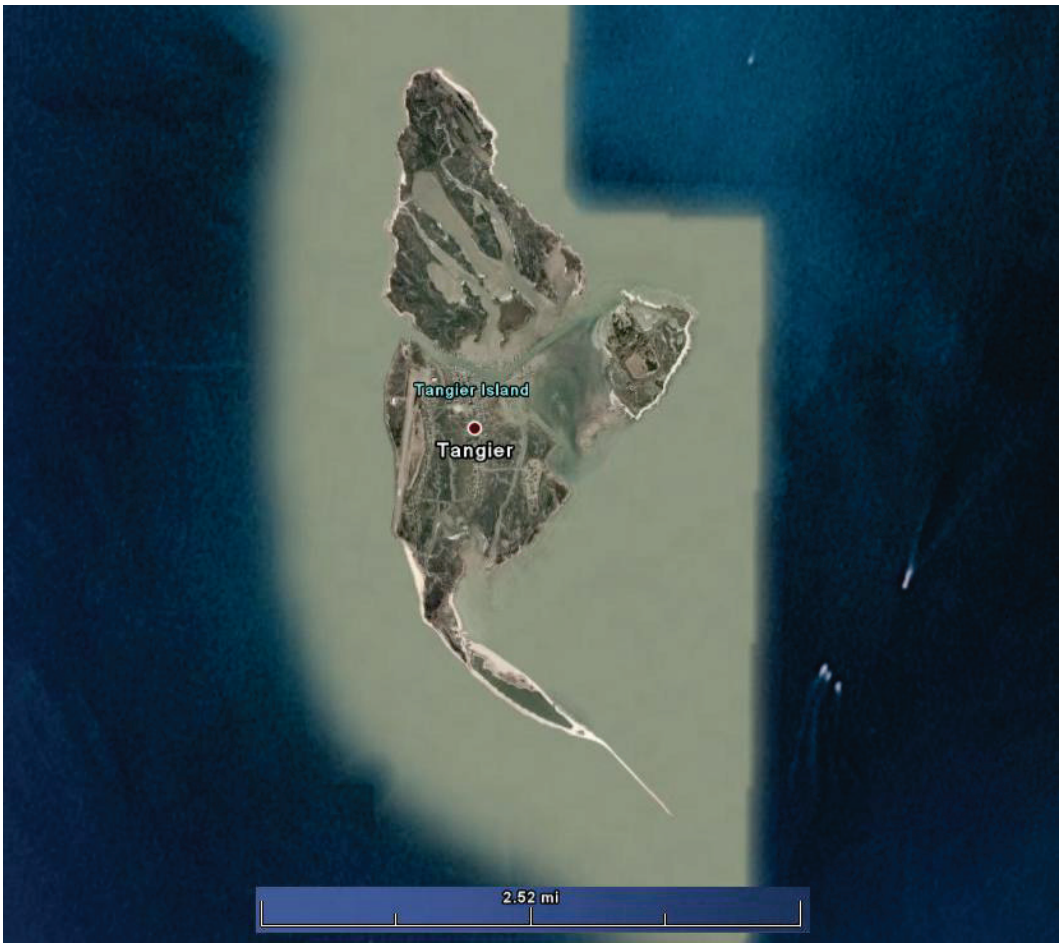

1.2 Objectives

In the past, storm waves have frequently entered the western end of the Tangier Island boat canal and caused damage to shoreline structures. The objectives of this project are to perform a numerical modeling study for engineering design of a structure intended to reduce wave energy in the western portion of the canal and to provide preliminary structural design guidance. Figure 3 shows an example of a hypothetical structure location attached to the northern shoreline.

1.3 Approach

Idealized wind and wave simulations were performed for nine wind directions (see Chapter 2 for details) and two water levels, 0 and 5 ft (0 and 1.5 m). The idealized wind conditions, representing the 50 yr return period, were used in the numerical simulations for the existing west channel without a structure (without project) and for five alternatives with structures

(with project). The 50 yr wind condition was based on a previous study. The calibration and validation of CMS has been described in detail in a series of four reports (see Demirbilek and Rosati 2011 for a summary), which included approximately 30 test cases. For field testing at bays and estuaries, Grays Harbor, WA, and Matagorda Bay, TX, were amongst the calibration and validation cases. The primary goal of the study was to develop a quantitative estimate of waves and wave reduction in the canal for a relative comparison of alternatives investigated and preliminary structural design calculations. Because there was no field data at Tangier Island, the qualitative estimates of flow and sediment transport developed were not used in the selection of recommended solutions. This report presents details of modeling tasks and findings of the study and results of structure design.

Figure 3. An example breakwater location (in red) at the western entrance of the Tangier Island boat canal.

Structural designs were estimated based on numerical wave and hydrodynamic modeling conducted for 50 yr design wind speeds, waves, and water level conditions. The 50 yr wind speed was considered as idealized condition and was based on a previous study by Basco and Shin (1993). Differ-

ent structure alternatives were evaluated to determine an optimal design based on the level of wave-energy reduction in the navigation channel. The wave and hydrodynamic modeling study results (e.g., wave height, period, direction, and water level) along the western side of the proposed structure footprint were used in the preliminary wave-control structural design calculations. These calculations included structural stability, run-up/overtopping, and transmission through and over the structure.

1.4 Data

A variety of field data were required to generate model grids and other inputs for numerical models used in this study. These data can be grouped into two general categories: (1) bathymetric, shoreline and land-elevation data, and (2) meteorological and oceanographic (metocean) inputs used as forcing conditions. CENAO provided survey data available for Tangier Island from a recent lidar (Light Detection and Ranging) survey, past study reports, and other pertinent GIS (Geographic Information System) images and data files.

The CHL identified metocean data (winds, waves, and water levels) available from various data sources and previous studies by Corps, other government agencies, and academic institutes. Land-based wind data have been modified to "over water" conditions as needed. Storm-wind fields for hurricanes Sandy and Isabel were assembled. Hurricane Isabel was selected as the 50 yr representative design hurricane event. Numerical models were set up with these data and conditions. Simulations were performed for "as is" and "with project" alternatives described in Chapter 2.

1.5 Tasks

The scope of work for this study was initially formulated between the CENAO and CHL engineers in 2009, and refined in 2012. The main elements of the study plan were to: a) collect, generate, and format input data for numerical models; b) set up and run models for "with project" and "as is" conditions; c) analyze model results to develop a structure design; and d) discuss issues, progress, findings with the District on a regular basis; and e) make appropriate adjustments to study plan as executed. The following tasks were performed in the implementation of study plan.

1.5.1 Task 1. Metocean forcing (winds, waves, tides, currents, water levels)

Because Tangier Island is not exposed to open ocean waves, locally generated wave climates for the west side of the island were derived by using local winds as input to the Coastal Modeling System (CMS) described in Appendix A.

1.5.2 Task 2. Investigation of jetty location and geometry.

A spectral (phase-averaged) wave model, CMS-Wave (Lin et al. 2008; Demirbilek et al. 2007; Lin and Demirbilek 2005), was used to provide locally generated wind-wave estimates at the project site. This model can run on a grid with variable rectangular cells. It is suited to large area applications in which wider spacing cells can be specified in the far site, where wave property variation is small and away from the area of interest, to save computational time. Wave diffraction, reflection, and transmission caused by structures are approximated in this class of wave models.

1.5.3 Task 3. Modeling channel hydrodynamics

The Tangier Island boat canal (Figures 2 and 3) is a federally maintained waterway which is regularly dredged by CENAO. One of the project design parameters was that the proposed structure should not exacerbate shoaling problems in the channel. Channel sediments are a mixture of sands and fine-grained material at Tangier Island, which were modeled with the CMS (Demirbilek and Rosati, 2011). Model simulations with and without structures were conducted to calculate water levels, currents, and sediment transport in the channel. Model results were used to identify potential depositional and erosional areas in the west channel and possible impacts of proposed structures.

1.5.4 Task 4. Structure design

Once the optimal structure location was determined, CMS-Wave was used to generate storm wave conditions at the seaward face of the structure. A joint-probability wave-distribution curve was calculated to compute stable stone sizes, damage progression, run-up, and overtopping transmission for different structure designs. The result of these analyses formed the basis of an optimal structural cross-section design that included the specification of the crest elevation, crest width, side slopes, and armor stone

sizes. The structure design incorporated the latest Corps guidance on sea-level rise. Local soil subsidence due to weight of the structure was not considered in structure design calculations because geotechnical data of the soil at the footprint of the breakwater were not available. For the present level of design, zero local structural settlement was assumed. However, regional settlement of the Chesapeake Bay is considered.

1.5.5 Task 5. Technical report

CHL and CENAO personnel conducted two site visits at the beginning and during the study. The two groups conducted regular monthly telephone meetings to discuss issues and progress. There were frequent additional communications via telephone and e-mail. The findings of the modeling study are documented in this Technical Report.

1.6 Report layout

Chapter 2 describes details of the numerical modeling study tasks, including model domain, bathymetry, grids, forcing types, structural alternatives, save stations, conditions simulated, comparison of alternatives, and study findings and recommendations. Chapter 3 describes the structural design calculations that examine three different crest elevations and include determination of structure stone size on both the seaside and leeside of the structures and transmitted wave heights for each of the crest elevations. The effects of sea-level rise and the general subsidence of the Chesapeake Bay are also considered. The study's conclusions are presented in Chapter 4.

2 Numerical Modeling for Wave-Energy Reduction in the Tangier Island Boat Canal

2.1 Purpose

A numerical modeling study investigated waves and hydrodynamics in and adjacent to the western portion of the Tangier Island boat canal. The study developed wave- and water-level estimates for design of a structure to reduce wave energy entering the western end of the navigation channel. The modeling study's results included the selection of the appropriate location, size, and geometry of a wave-control structure that reduced wave energy entering the channel, did not exacerbate the channel dredging requirements, and ensured continued boat traffic use of the channel.

2.2 Numerical models

The CMS was used to simulate waves, currents, sediment transport, and morphology change in this study. The CMS includes wave, flow, and sediment transport modeling tools for coastal inlets and navigation projects. Development and enhancement of CMS capabilities continues to evolve as a research and engineering tool for desk-top computers. The CMS uses the Surface-water Modeling System (SMS) (Zundel 2006) interface for grid generation and model setup, as well as plotting and post-processing. See Appendix A for additional information about the CMS and its capabilities.

The development of a number of advances to CMS-Wave to address the project's specific needs was funded by the CIRP. These included testing of the full-plane and parent-child capabilities of model for hurricanes and northeasters in an estuary, and development of pre- and post-processing analysis codes for model setup and structural design calculations. The calibration and validation of CMS has been described in detail in a series of four reports. See Demirbilek and Rosati (2011) for a summary, which included approximately 30 test cases. For field testing at bays and estuaries, the Grays Harbor, WA, and Matagorda Bay, TX, were amongst the calibration and validation cases. The primary goal of the study was to develop a quantitative estimate of waves and wave reduction in the canal for a relative comparison of alternatives investigated and preliminary structural de-

sign calculations. Due to absence of field data at Tangier Island, the qualitative estimates of flow and sediment transport developed were not used in the selection of recommended solutions. Details of modeling tasks and findings of the study and results of structure design follow.

2.3 Model domain, bathymetry, and forcing

The primary area of interest in this modeling study is the west channel section of the Tangier Island boat canal (Figure 4). This shallow and narrow canal is the only navigation route that cuts through the middle of Tangier Island and connects the east and west sides of island. The average west-channel base width is 60 ft (18.3 m), top width is 100 ft (30.5 m), and channel depth varies from 7.5 to 13 ft (2.3 to 4 m). The narrowest cross section (bank-to-bank) of the west channel is 230 ft (70 m).

Figure 4. Footprint of the western portion of the Tangier Island boat canal.

CENAO provided available survey data to the CHL modeling team for the east channel, west channel, and adjacent areas. To properly resolve the details of channel geometry and bathymetry, irregularly shaped shorelines, and elevations of the joining land areas for numerical modeling purposes,

these survey data were augmented with data from other sources including USGS coastal shoreline data, USACE LIDAR data, and NOAA digital elevation model (DEM) data. The extent of all available bathymetry data and surveys is shown in Figures 5 through 9, where survey points are sparse in some areas and denser in others.

Figure 5 shows the NOAA DEM data available in the Chesapeake Bay. Figure 6 shows the lidar data available for the post-Hurricane Sandy elevations in Tangier Island and vicinity area. Figure 7 shows the coverage area of the west channel entrance and vicinity depth contours. Figure 8 shows the west channel and north shoreline survey depth contours. Figure 9 shows the east channel survey-depth contours.

Figure 5. DEM bathymetry data covering Chesapeake Bay and vicinity.

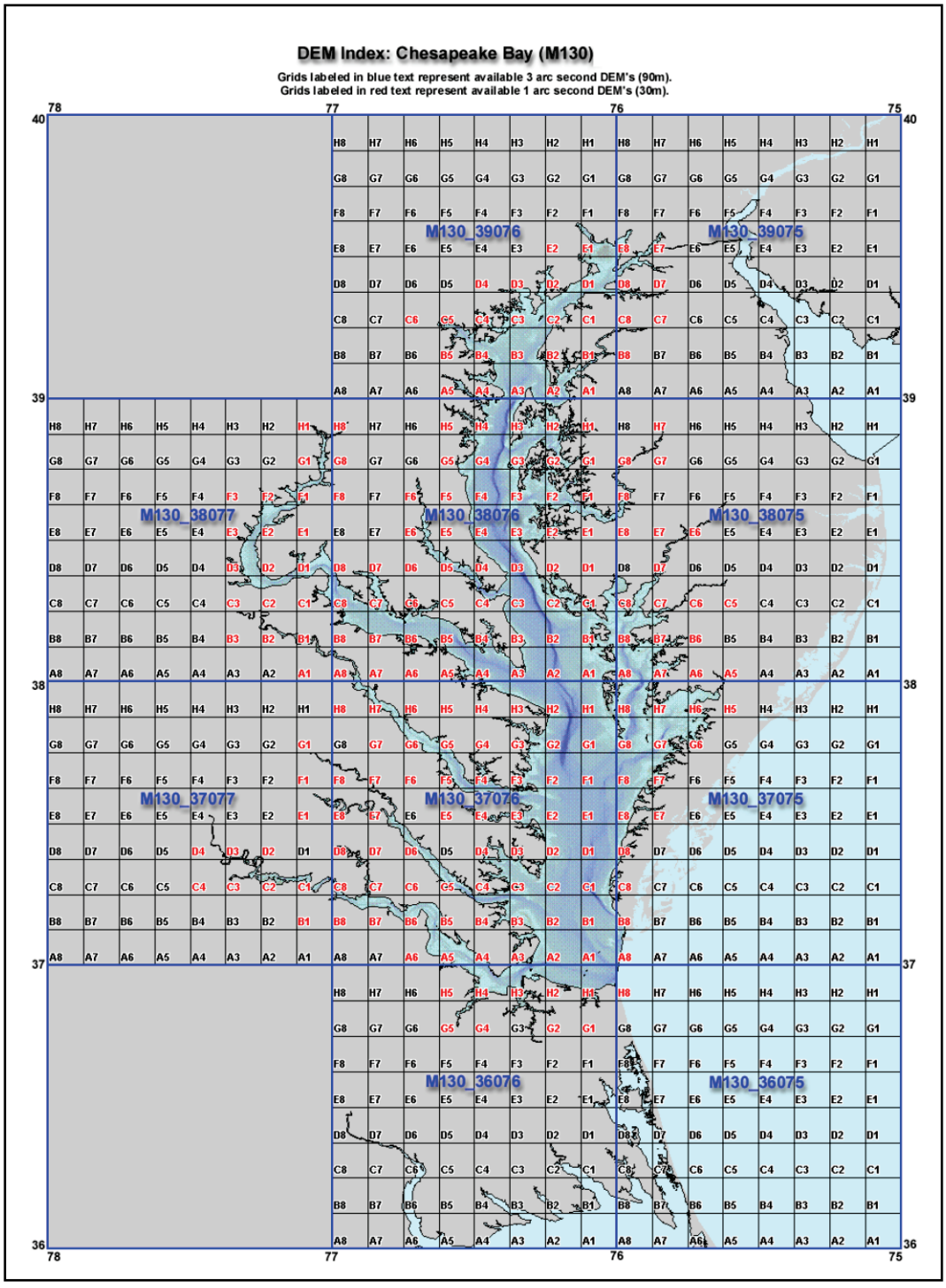

Figure 6. Post-Hurricane Sandy (2012) elevation contours (m, MTL) for Tangier Island and vicinity.

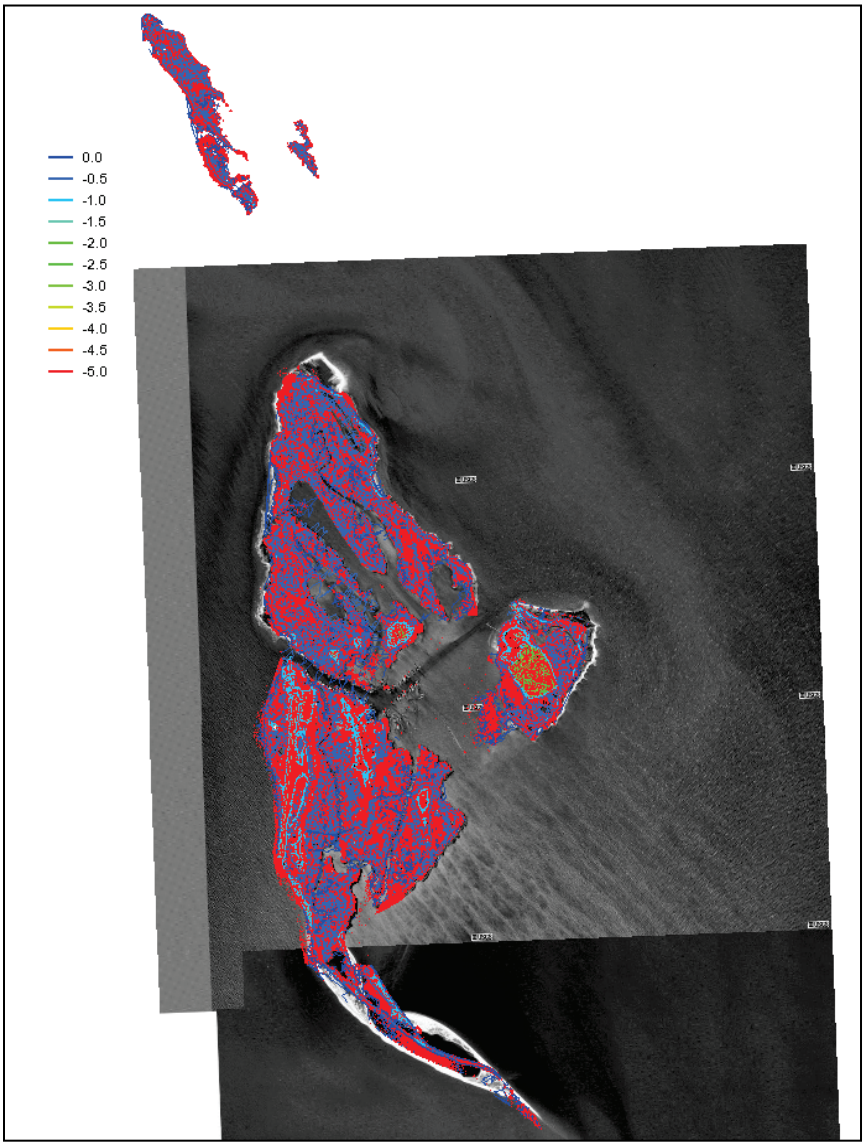

Figure 7. West channel entrance and vicinity depth contour lines (m, MTL); data locations shown as red points.

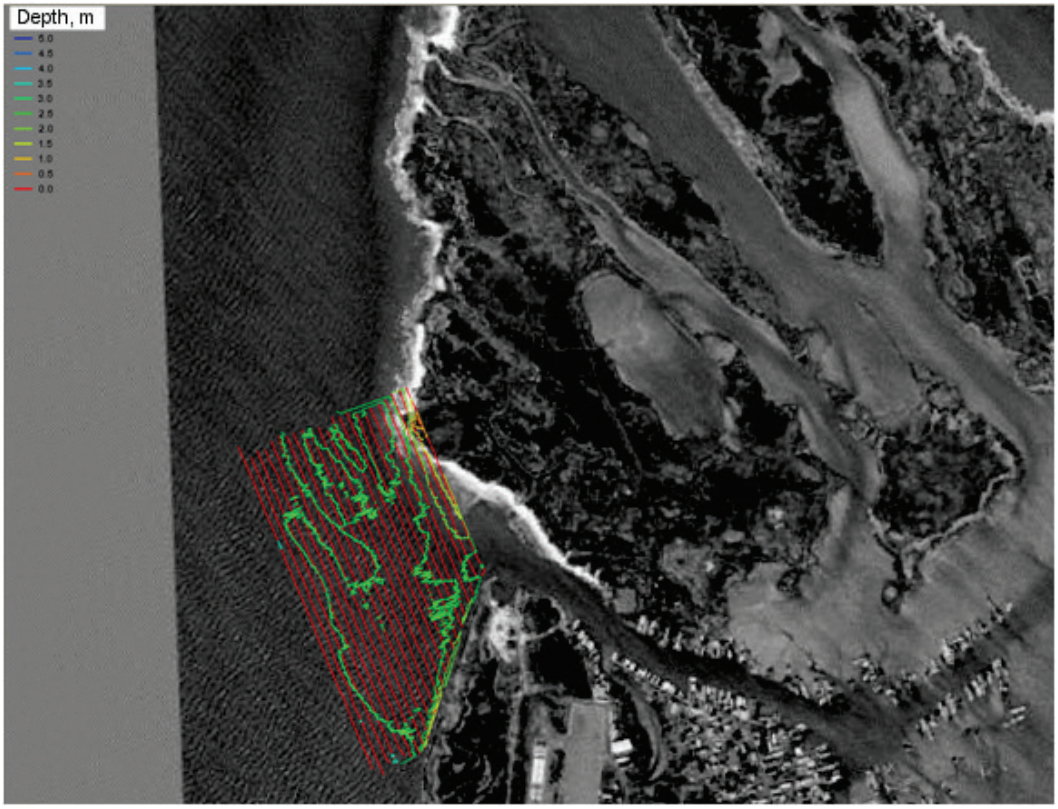

Figure 8. West channel and north shoreline depth contour lines (m, MTL); data locations shown as red points.

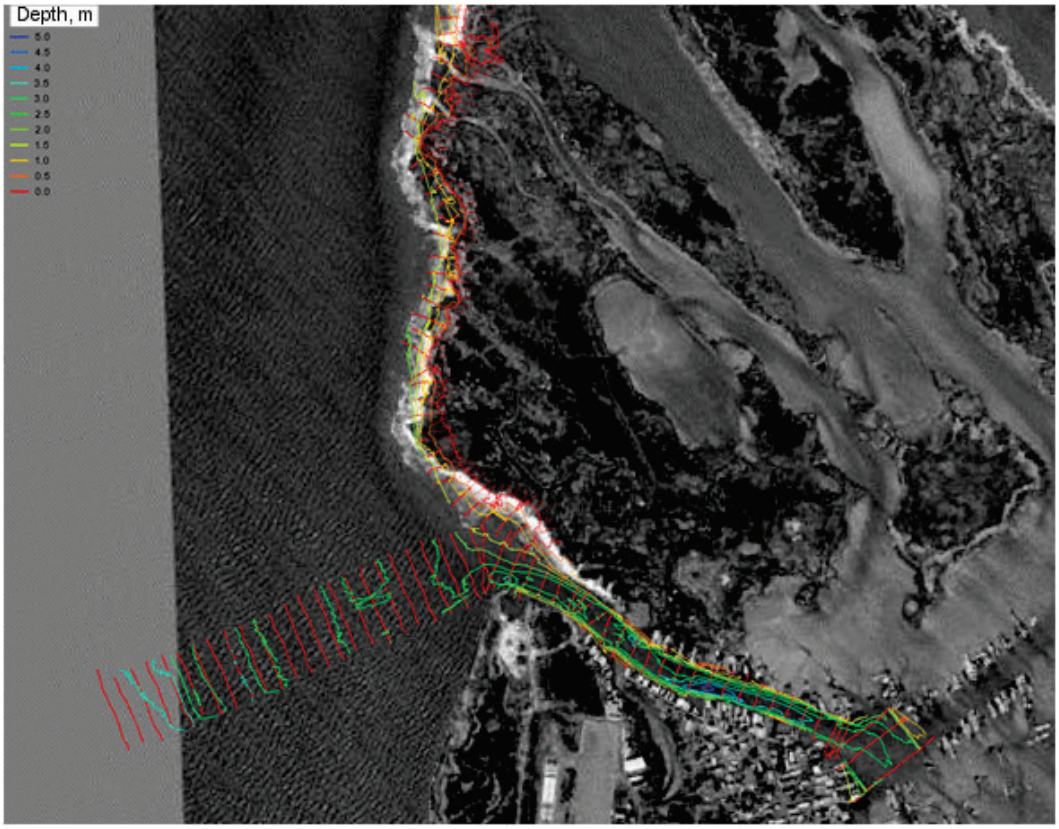

Figure 9. East channel depth contour lines (m, MTL); data locations shown as red points.

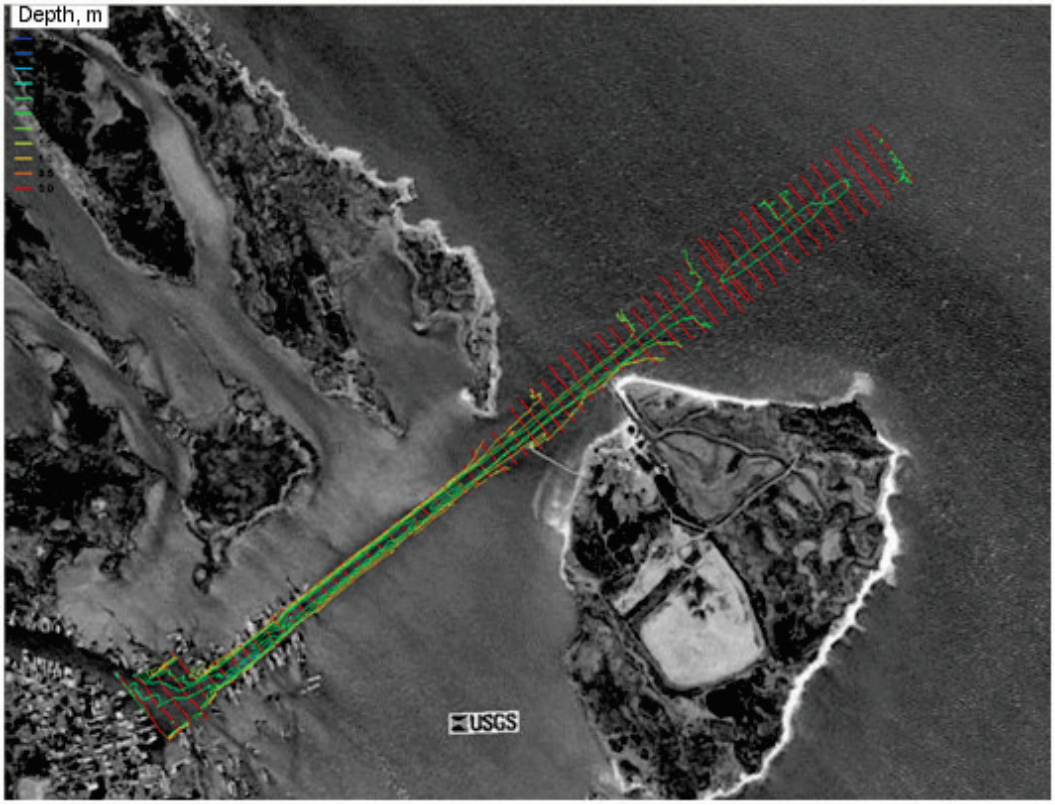

2.4 Model grids

Figures 10 and 11 show the CMS modeling domain for the Chesapeake Bay region and corresponding depth contours, respectively. This bay-wide large grid domain, approximately 60 mi by 180 mi (100km by 300 km), is referred to as the regional grid, which has a constant grid cell size of 1,600 ft by 1,600 ft (500 m by 500 m). The depths in this grid vary from 0 to 150 ft (0 to 45 m).

Figure 10. CMS regional grid modeling domain for this study. The small rectangle shows the location of the local grid for Tangier Island.

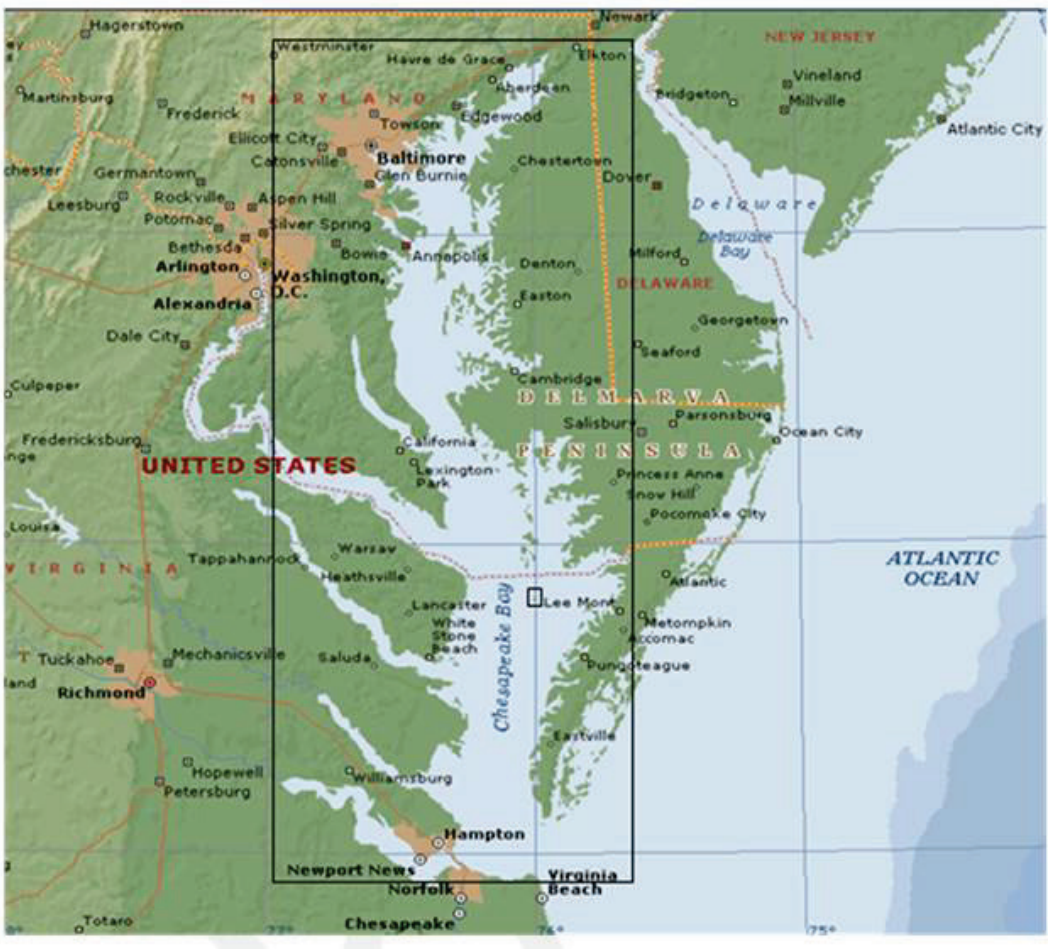

Figure 11. Depth contours (m, MTL) for the CMS Chesapeake Bay regional grid domain.

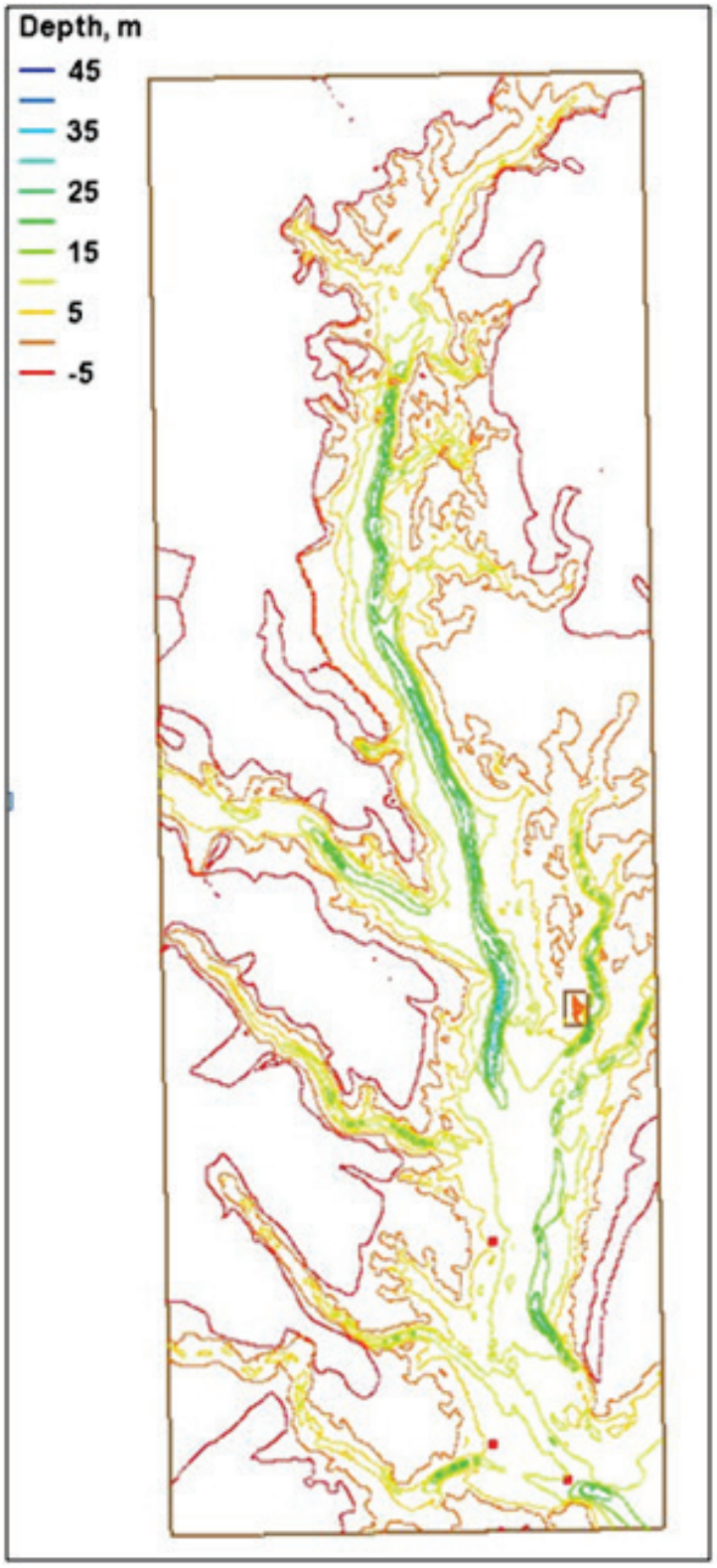

The CMS modeling includes a second domain, referred to as the local grid for Tangier Island, which is shown in Figures 10 to 12. This grid is more detailed and has a finer resolution of bathymetry to cover Tangier Island. The domain is approximately 3 mi by 4.4 mi (5 km by 7 km). The local grid cell size varies from 10 ft to 160 ft (3 m to 50 m).

Figure 12. Local grid depth contours (m, MTL) covering Tangier Island and vicinity.

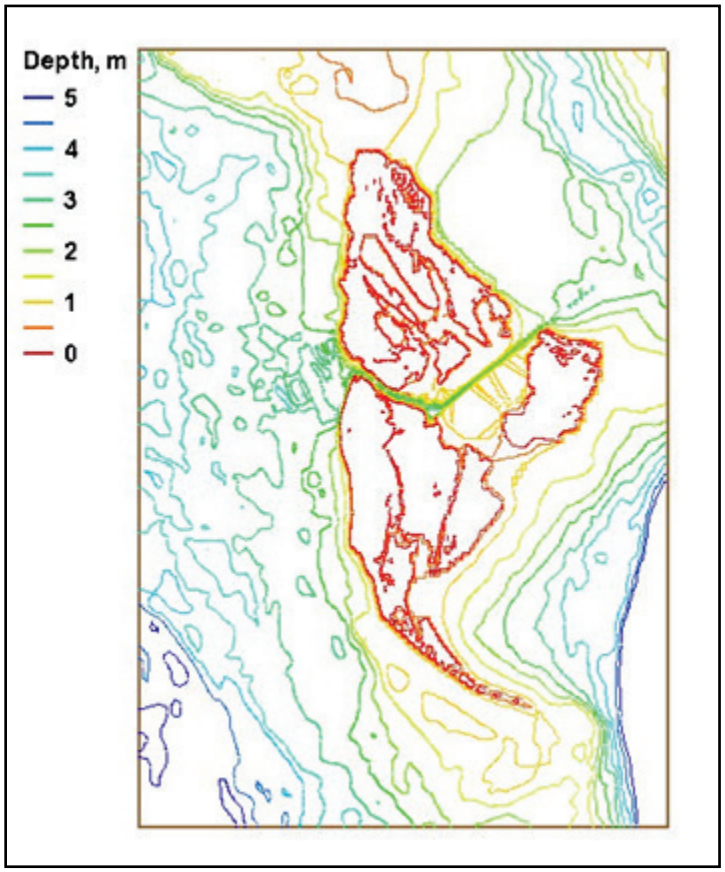

2.5 Existing channel and structural alternatives

Five alternatives and the existing channel geometry were investigated. All five alternatives have a breakwater system that includes a structure connecting to the north shoreline. Alternatives 3, 4, and 5 include an optional short structure (spur) joining to the south shoreline. The north structure is either a one-piece straight structure or a two-piece dogleg structure. Due to cost constraints, the District requested that the total length (linear foot) of structures in each alternative not exceed 650 ft (200 m).

The location, length, and orientation of structures used in the alternatives were determined in close consultation with the District. Because the goal

was to minimize wave-energy propagation into the canal, structures were positioned as close to the channel as possible at a safe (for navigation) distance of 164 ft to 328 ft (50 m to 100 m) from the channel edges. The geometry of each alternative was configured and sized according to these requirements. Data on the footprints of these alternatives are provided in Table 1. The information in Table 1 represents the location of the modeled alternatives. Subsequent to the modeling, adjustments were made to the position of the landward root of the north jetty for the purpose of selecting the best landward connection area for the jetty. The final recommended construction footprint coordinates are provided in Chapter 3.*

Table 1 Location (Footprint, State Plane, m, Virginia South 4502) of alternatives.

		Alt 1	Alt 2	Alt 3	Alt 4	Alt 5
North Jetty	Type	Straight	Dogleg	Dogleg	Dogleg	Straight
	Landward End Easting (m)	3720196	3720196	3720196	3720196	3720196
	Landward End Northing (m)	1169385	1169385	1169385	1169385	1169385
	Turning Point Easting (m)		3720161	3720161	3720161	
	Turning Point Northing (m)		1169306	1169306	1169306	
	Seaward End Easting (m)	3720161	3720089	3720089	3720089	3720161
	Seaward End Northing (m)	1169306	1169271	1169271	1169271	1169306
	Shore Segment Length (m)		86.4	86.4	86.4	
	Bay segment Length (m)		80.1	80.1	80.1	
	Tot Length (m)	86.4	166.5	166.5	166.5	86.4
South Spur Jetty	Type	None	None	Straight	Straight	Straight
	Landward End Easting (m)			3720203	3720206	3720206
	Landward End Northing (m)			1169209	1169220	1169220

* The final recommended construction footprint coordinates are located in Table 24, Chapter 3.

		Alt 1	Alt 2	Alt 3	Alt 4	Alt 5
	Seaward End Easting (m)			3720203	3720181	3720181
	Seaward End Northing (m)			1169249	1169251	1169251
	Length (m)			40	39.8	39.8

Figures 13-18 show the existing (without project) and five alternatives (with project), respectively. For all alternatives, the structures were represented in the numerical model with a crest elevation of 3.3 ft (1 m) and crest width of 13 ft (4 m). The west channel and vicinity depth ranges from 0 to 15 ft (0 to 5 m) and are color-contoured in the figures, and land elevations are white.

Figure 13. Existing west channel configuration and depth field (m, MTL).

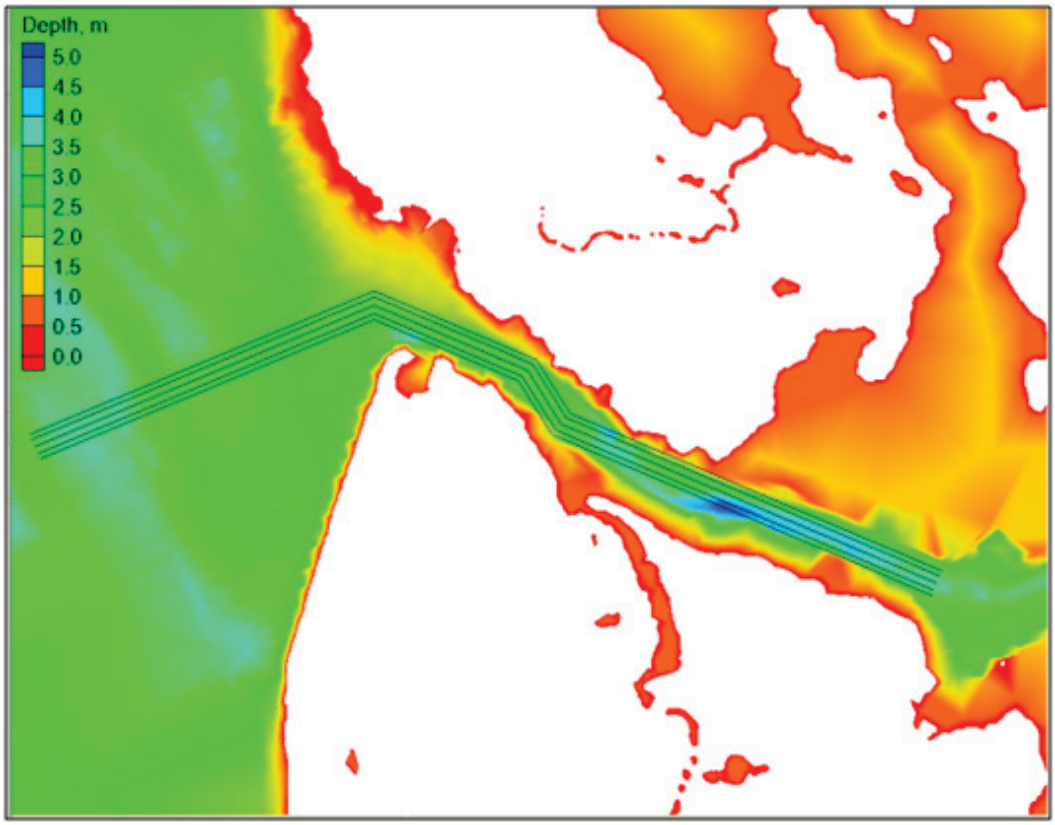

Figure 14 shows the Alternative 1 (Alt 1) channel configuration with a one-piece straight structure. The length, crest elevation, and crest width of the Alt 1 structure are 280 ft (85 m), 3.3 ft (1 m, MTL) and 13 ft (4 m), respectively.

Figure 14. Alt 1 with channel and structure configuration.

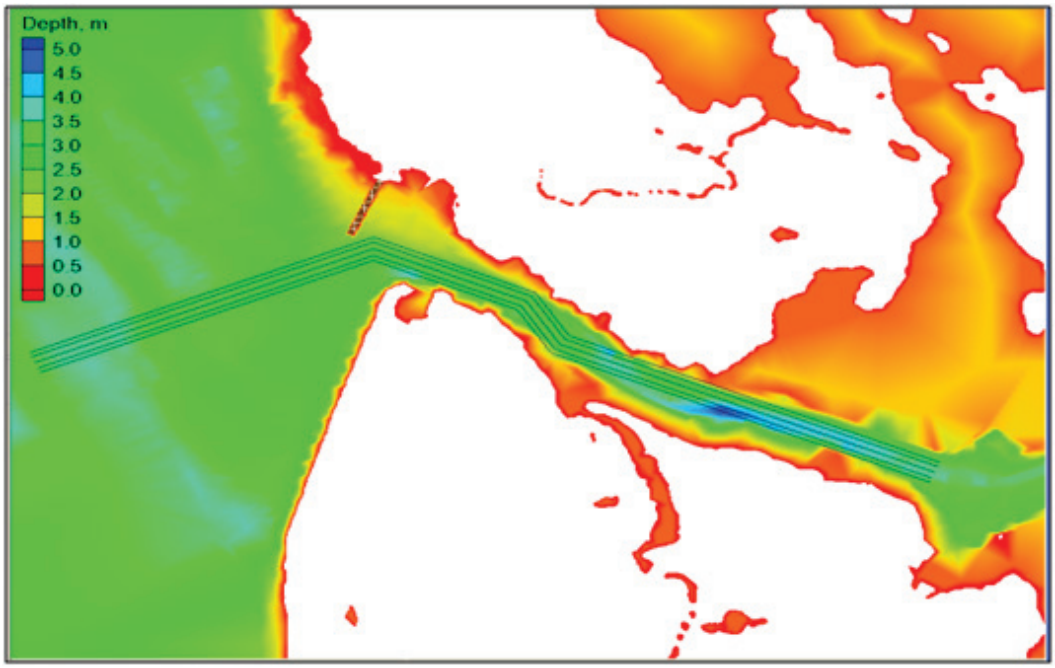

Alternative 2 (Alt 2) has a two-piece dogleg north structure (Figure 15). The total length, crest elevation, and crest width of the structure are 560 ft (170 m), 3.3 ft (1 m, MTL) and 13 ft (4 m), respectively.

Figure 15. Alt 2 with channel and structure modification.

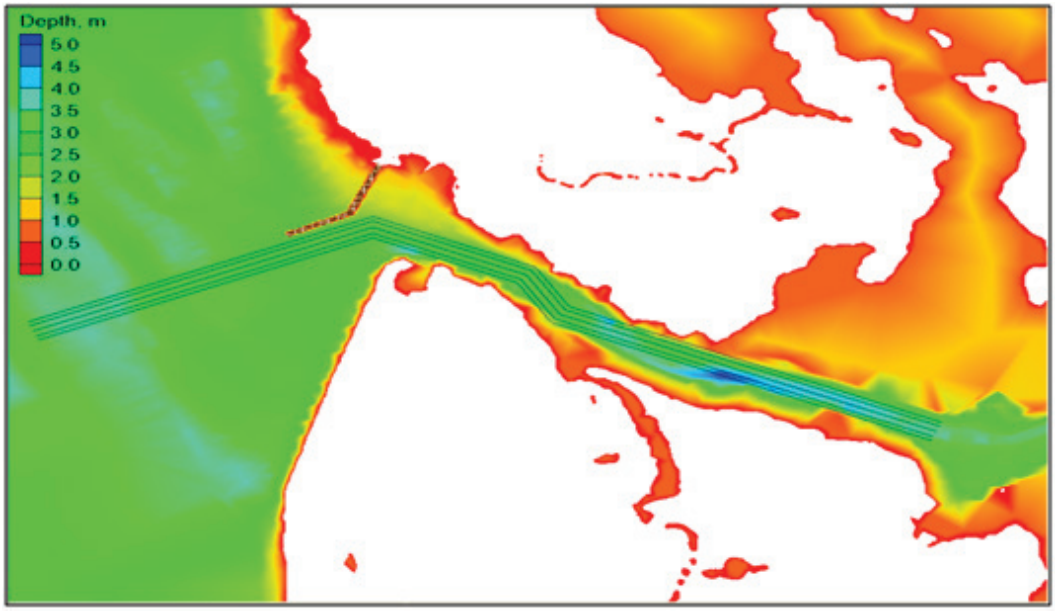

Alternative 3 (Alt 3) has a two-piece dogleg north structure and a straight south side spur structure pointing to north (Figure 16). Total length, crest

elevation, and crest width of Alt 3 north structure are 560 ft (170 m), 3.3 ft (1 m, MTL) and 13 ft (4 m), respectively. The south spur is 82 ft (25 m) long with its crest height and width the same as those of the north structure.

Figure 16. Alt 3 with channel and structure configuration.

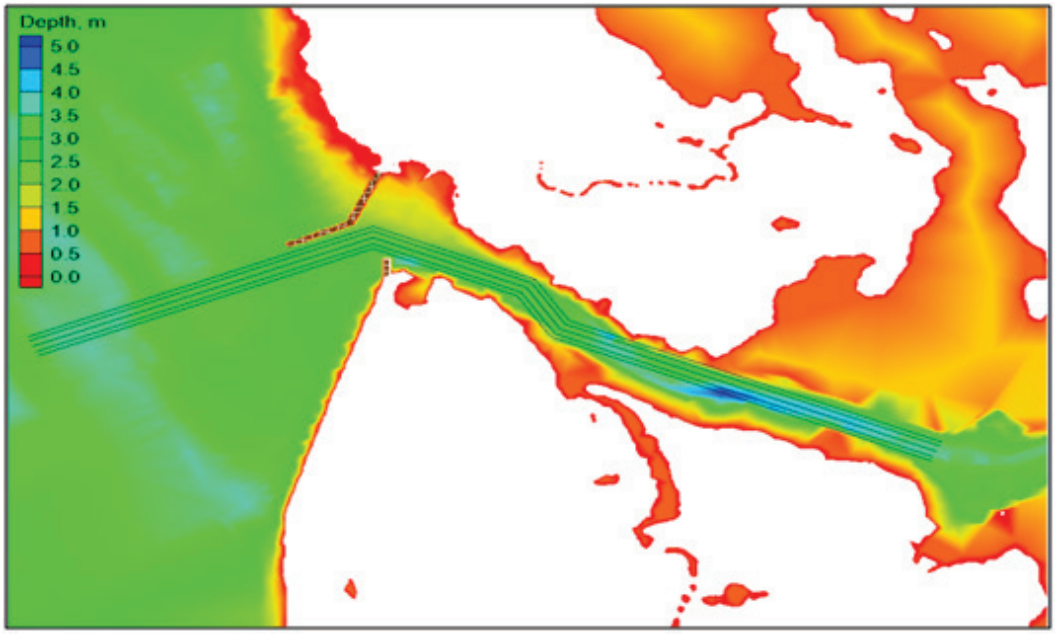

Alternative 4 (Alt 4) has a two-piece dogleg north structure and a straight south side spur structure pointing towards northwest (Figure 17). Total length, crest elevation, and crest width of Alt 4 north structure are 560 ft (170 m), 3.3 ft (1 m, MTL) and 13 ft (4 m), respectively. The south spur is 82 ft (25 m) long with its crest height and width the same as those of the north structure.

Alternative 5 (Alt 5) has a one-piece straight north structure and a straight south side spur structure pointing towards northwest, as shown in Figure 18. The length, crest elevation, and crest width of Alt 5 north structure are 280 ft (85 m), 3.3 ft (1 m, MTL) and 13 ft (4 m), respectively. The south spur is 82 ft (25 m) long with its crest height and width the same as those of the north structure.

Figure 17. Alt 4 with channel and structure configuration.

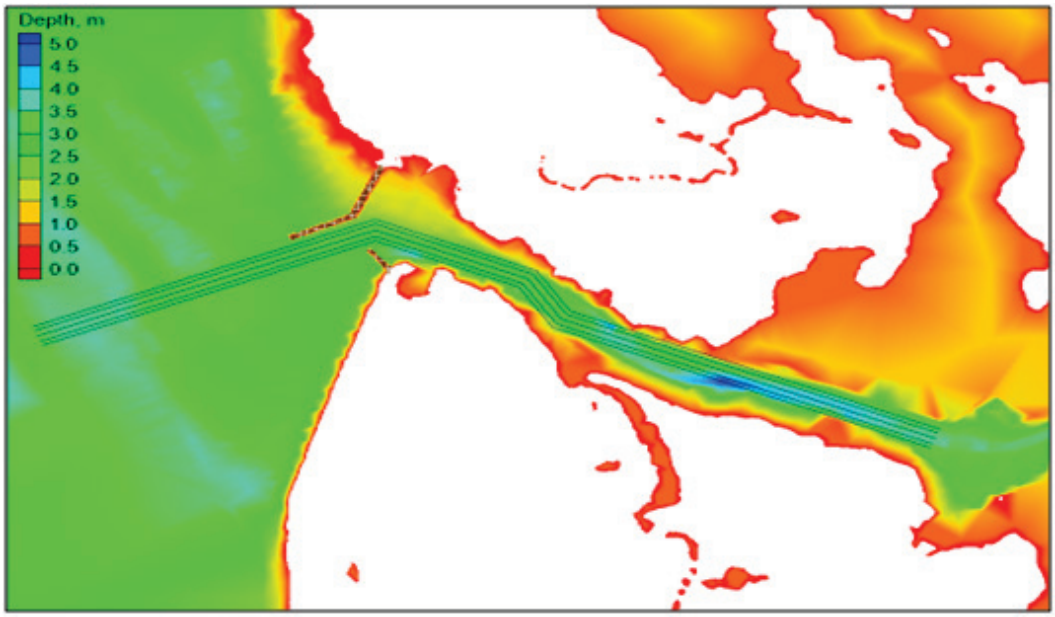

Figure 18. Alt 5 with channel and structure configuration.

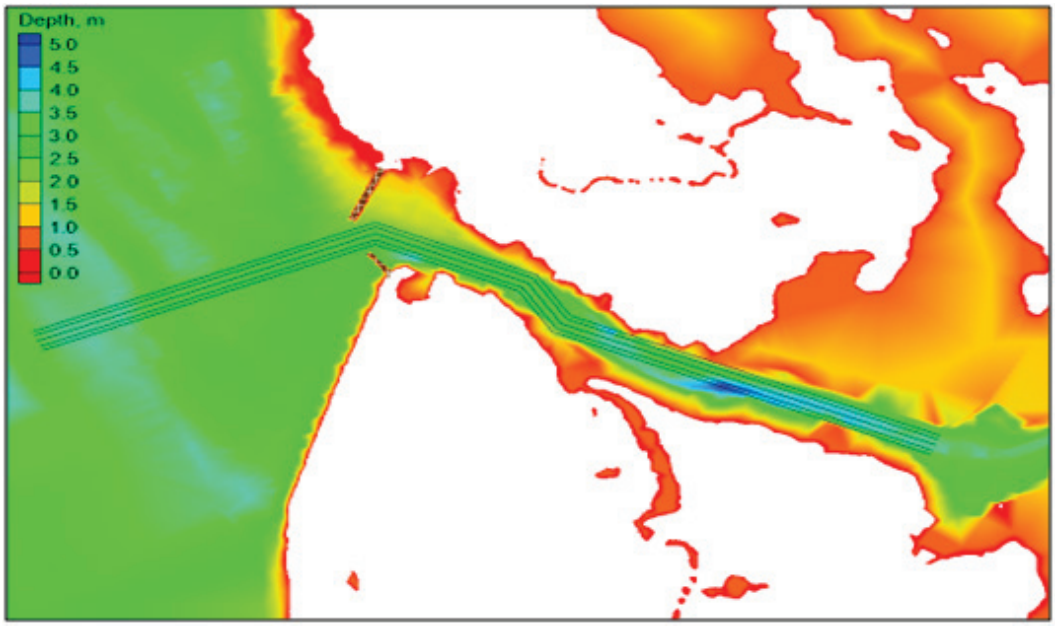

2.6 Forcing conditions

Winds, waves, and tidal conditions affecting Tangier Island change year to year, as well as seasonally. These forcings consist of metocean events including storms, northeasters, and hurricanes, which can impact the Chesapeake Bay and reach Tangier Island from all directions. As seen in Figure 19, the wind rose shows winds blowing from different directions during two years, 2011 and 2012, at NOAA station 8632837. The modeling effort

was designed to address both the survivability of the jetty during a 50 yr return period storm and also its effectiveness at reducing wave energy in the channel for much more common, less intense events.

Figure 19. Wind rose for years 2011 and 2012 at NOAA station 862837.

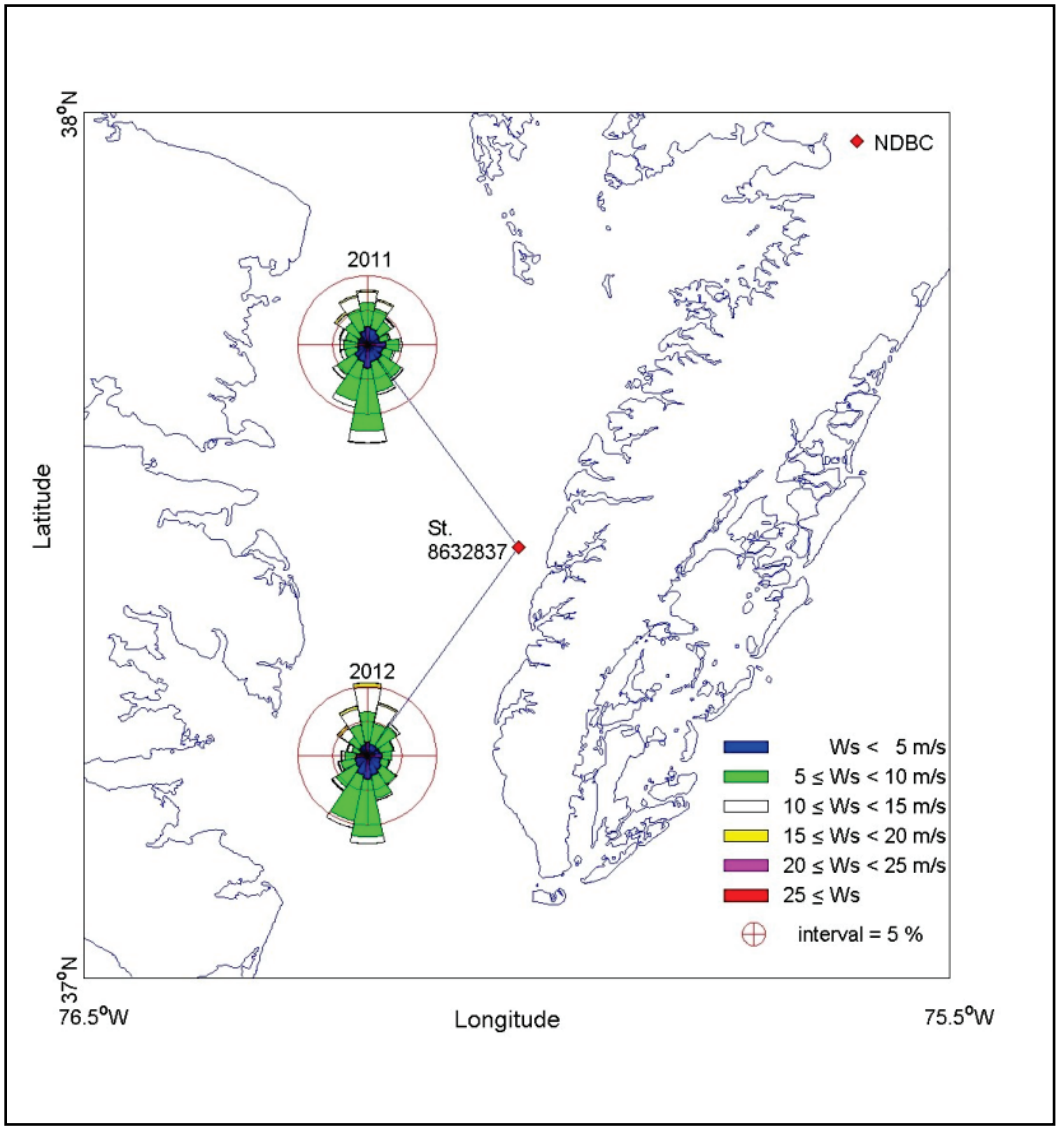

Table 2 lists the 50 yr wind and wave conditions simulated in the modeling for water levels (WL) equal to 0 and 5 ft (1.5 m). Winds and waves that affect the west channel are those approaching from the bay side, coming from all westerly directions from north to south. Note that in Table 2 the wind speed and water levels only appear once; these are constants.

Table 2. Wind, wave, and water level conditions simulated.

CASE	1 N	2 NNW	3 NW	4 WNW	5 W	6 WSW	7 SW	8 SSW	9 S
Wind speed (m/sec)					20				
Wind Dir (deg)	0	337.5	315	292.5	270	247.5	225	202.5	180
Water Level (m)					WL=0				
CASE	**10**	**11**	**12**	**13**	**14**	**15**	**16**	**17**	**18**
Wind speed (m/sec)					20				
Wind Dir (deg)	0	337.5	315	292.5	270	247.5	225	202.5	180
Water Level (m)					WL=1.5				

The half-plane sector from north to south is split up into nine bins (or sub-sectors), which are designated by case numbers 1 through 9 for 0 m water level, and 10 through 18 apply to the 1.5 m water level simulations. These counter-clockwise directions from N to S are 22.5 deg bins, representing incident winds and waves to Tangier Island from NNW, NW, WNW, W, WSW, SW, SSW, and S directions.

The 50 yr design wind speed of 45 mph (20 m/sec) is used in this study with two water levels, 0 and 5 ft (1.5 m), representing possible mean tide level (WL = 0 m) and high water level (WL = 1.5 m) conditions observed at and around the Tangier Island by NOAA coastal stations (Figure 20). The design wind speed is based on a previous study by Basco and Shin (1993) analyzing storms for 1945-1983 at Patuxent Naval Air Station. The storms include both tropical events and northeasters.

Figure 21 shows the example of the water level measurements for year 2012 recorded at three NOAA stations: 8571421 (Bishops Head, MD), 8636580 (Windmill Point, VA), and 8638863 (Bay Bridge Tunnel, VA). The maximum water level observed at Station 8638863 (Bay Bridge Tunnel) was about 5 ft (1.5 m). The high water level WL=1.5 m at the Tangier Island is based on previous numerical modeling of Hurricane Isabel for Chesapeake Bay (Demirbilek et al. 2005).

Figure 20. NOAA coastal stations.

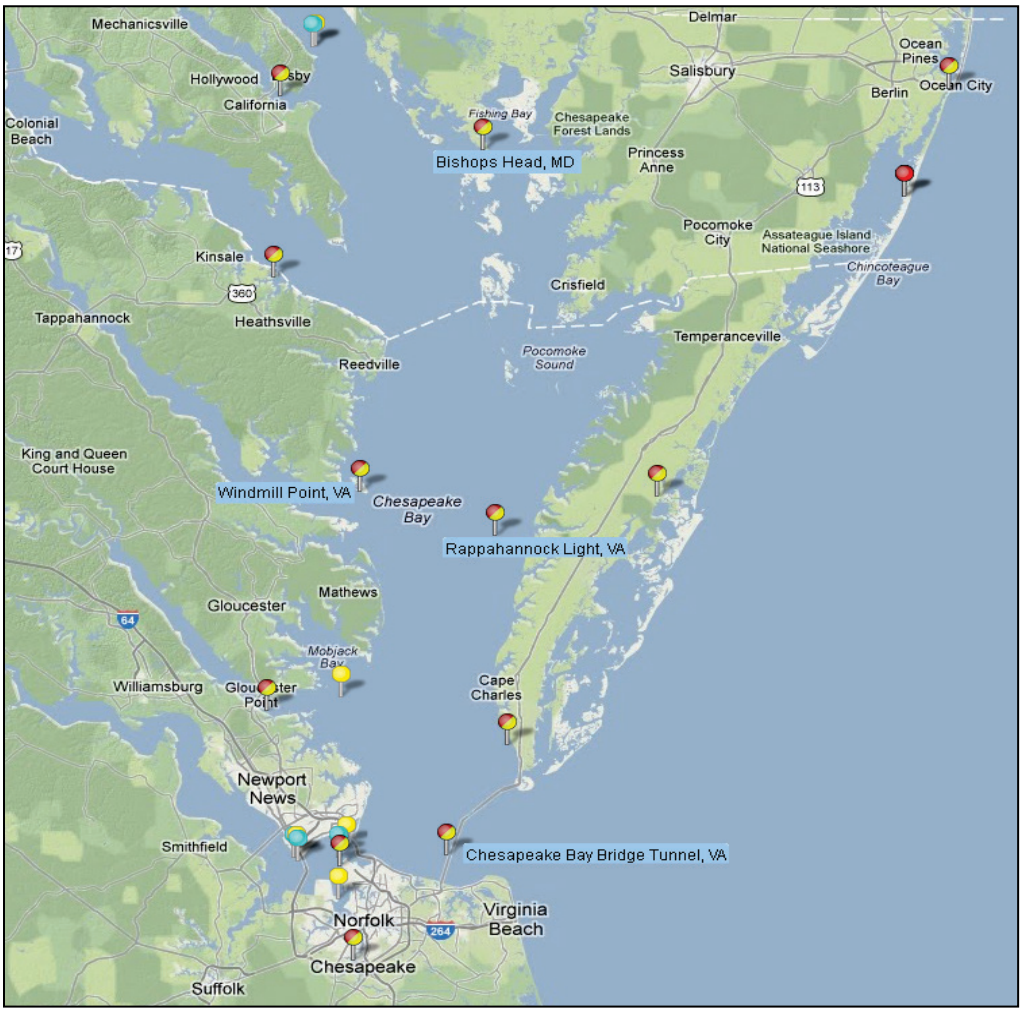

Figure 21. Water levels at Bishops Head, Windmill Point, and Bay Bridge Tunnel for 2012.

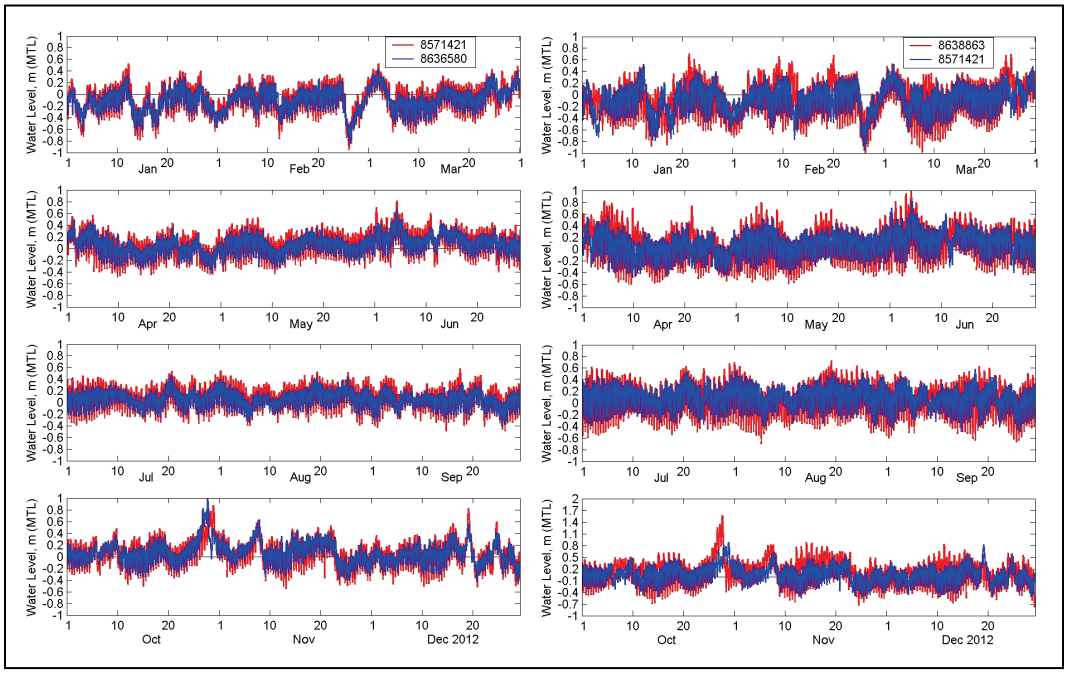

2.7 Save stations

Numerical model results have been extracted along three transact lines: the channel centerline, and along the north and south shorelines. Figure 22 shows the three transact lines. A total of 103 save stations were placed along the channel centerline, north and south shorelines, and around the perimeter of structures (Figure 23).

Figure 22. Transects (lines) where model results are extracted.

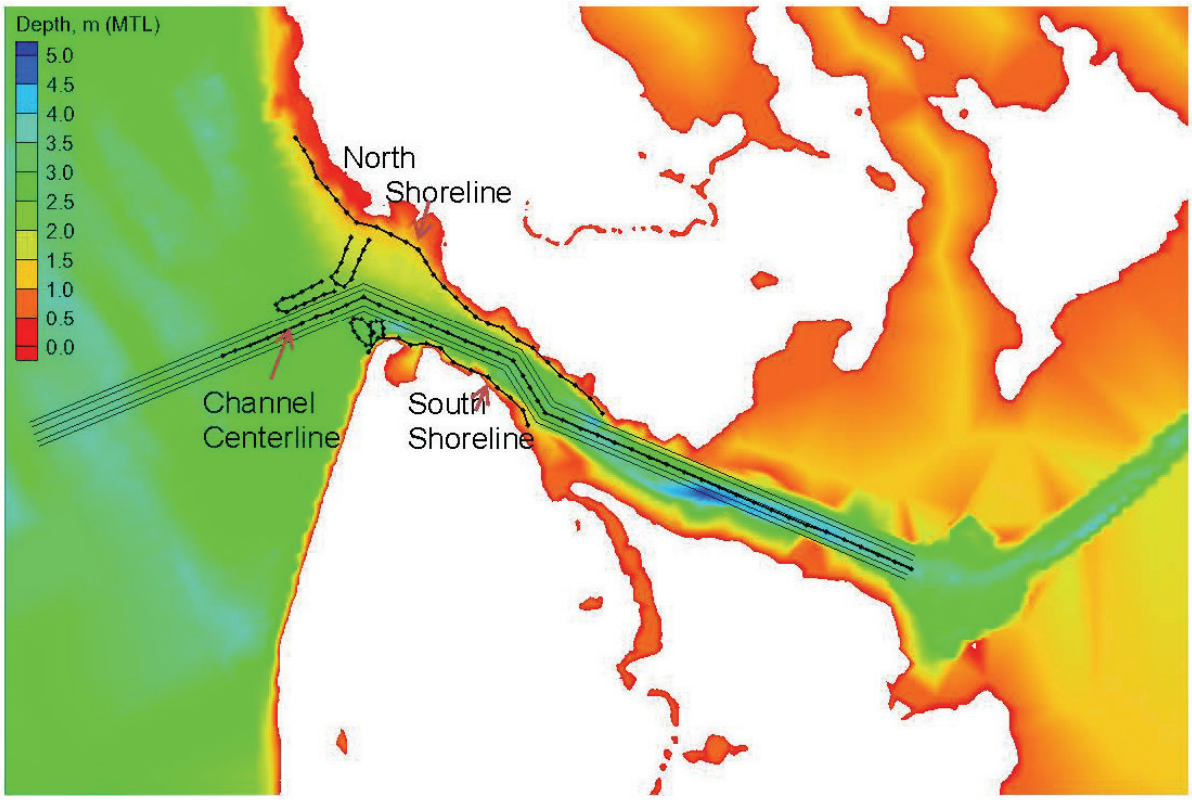

Figure 23. Point locations where model results are extracted.

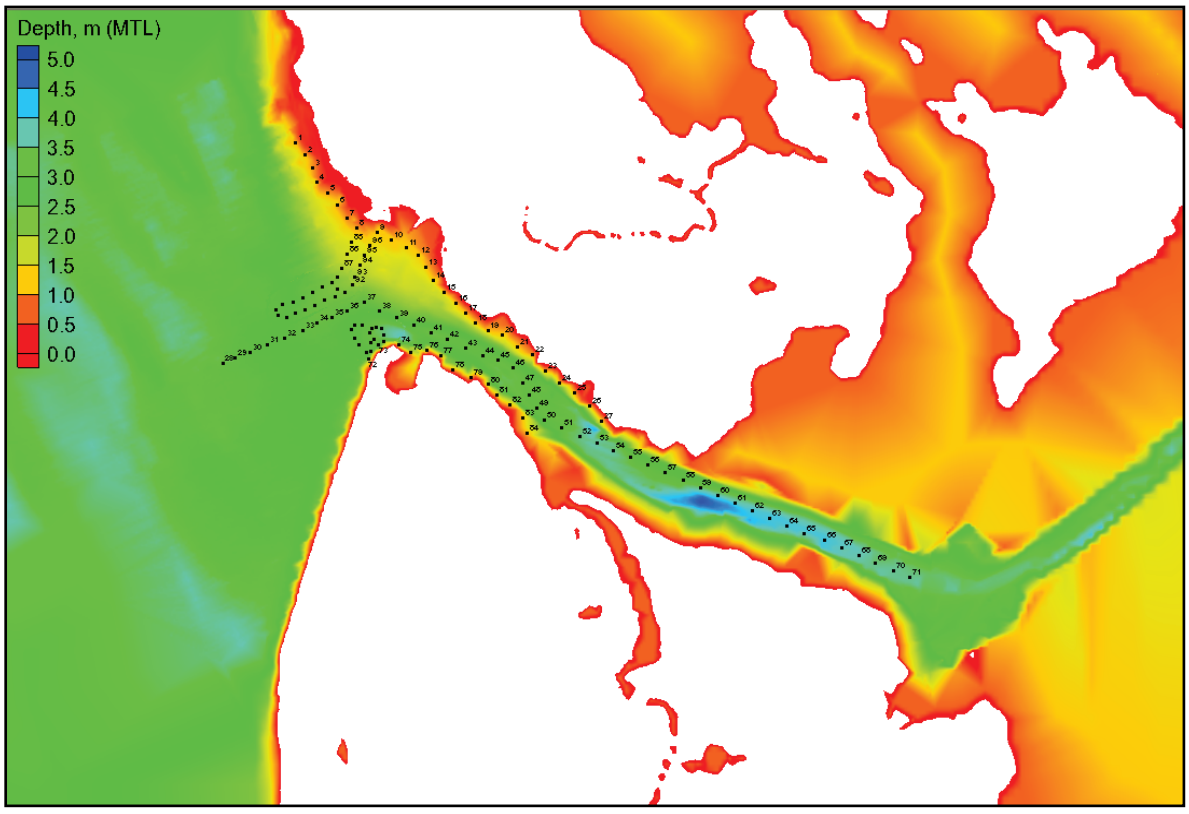

2.8 Idealized wind and water level simulations (waves without current)

Idealized wind and wave simulations were performed for nine wind directions listed in Table 2 and two water levels, 0 and 5 ft (0 and 1.5 m). The idealized wind conditions, representing the 50 yr return period, were used in the numerical simulations for the existing west channel without a structure (without project) and for five alternatives with structures (with project). The 50 yr wind condition was based on a previous study by Basco and Shin (1993). Details of existing and five alternative configurations are shown in Figures 13-18. First, the model simulations were conducted in the regional grid for waves and flow only, without sediment transport. The results from the regional simulations were provided as input to the local Tangier Island grid for wave, flow, and sediment transport calculations. Because the focus of the study was intended for structure design, the modeling was emphasized on waves and flow, not sediment transport results.

A total of 108 simulations (9 wind conditions x 2 water levels x 6 structure configurations) were performed to develop the spatially varying estimates of the winds, waves, water levels, and currents throughout the Chesapeake Bay. These simulations used the large regional grid. For example, Figure 24 shows the bay-wide wave-height fields calculated by models for two wind directions (wind speed of 45 mph or 20 m/sec blowing from NW and SW), and two water levels (0 and 5 ft or 1.5 m).

Figure 24. Examples of models of calculated wave heights in the Chesapeake Bay for the 50 yr design winds from NW and SW and two water levels.

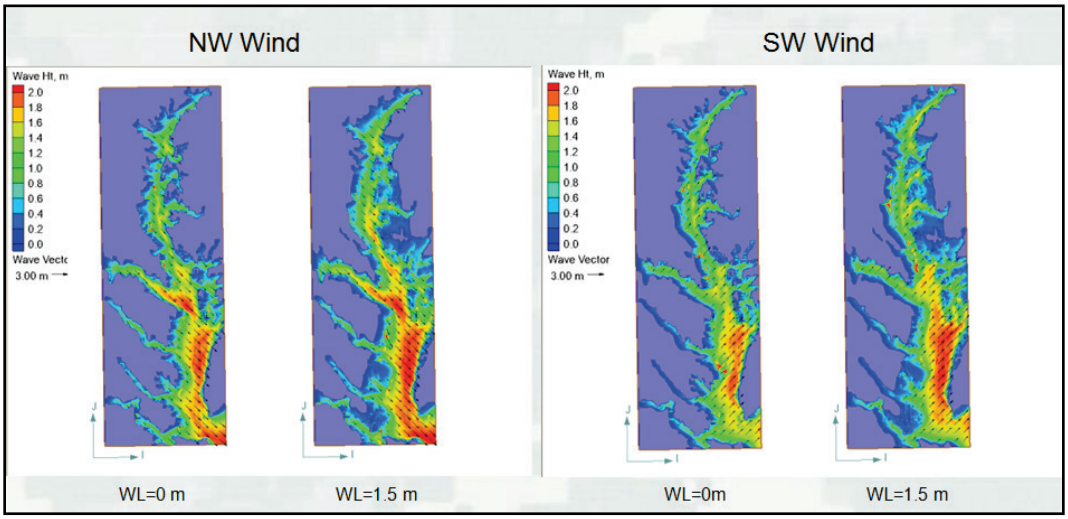

2.9 Relative comparison of alternatives

Results from the wind-wave simulations for the entire bay were used as input to the fine resolution local grid to develop the estimates of waves, flow, and water levels at the project site. A total of 108 simulations were conducted with the local grid. Numerical model results along the channel centerline were compared to determine which structural alternative provided the greatest wave-energy reduction in the west channel section of Tangier Island. Figures 25-28 show contour plots of calculated wave heights for existing, Alt 1, Alt 2, and Alt 3 using the 50 yr design conditions (e.g., 45 mph or 20 m/sec winds from NW and SW directions, and water levels of 0 m and 5 ft or 1.5 m). For the four configurations shown, these spatial variation plots display the change in the wave heights at the bayside entrance of the west channel. These color-coded plots show the extent of wave penetration into the canal, and also variation of wave heights occurring along the channel centerline and north and south shorelines.

Figure 25. Example of models of calculated wave heights in the west channel for the 50 yr design winds from NW and water level of 0 m.

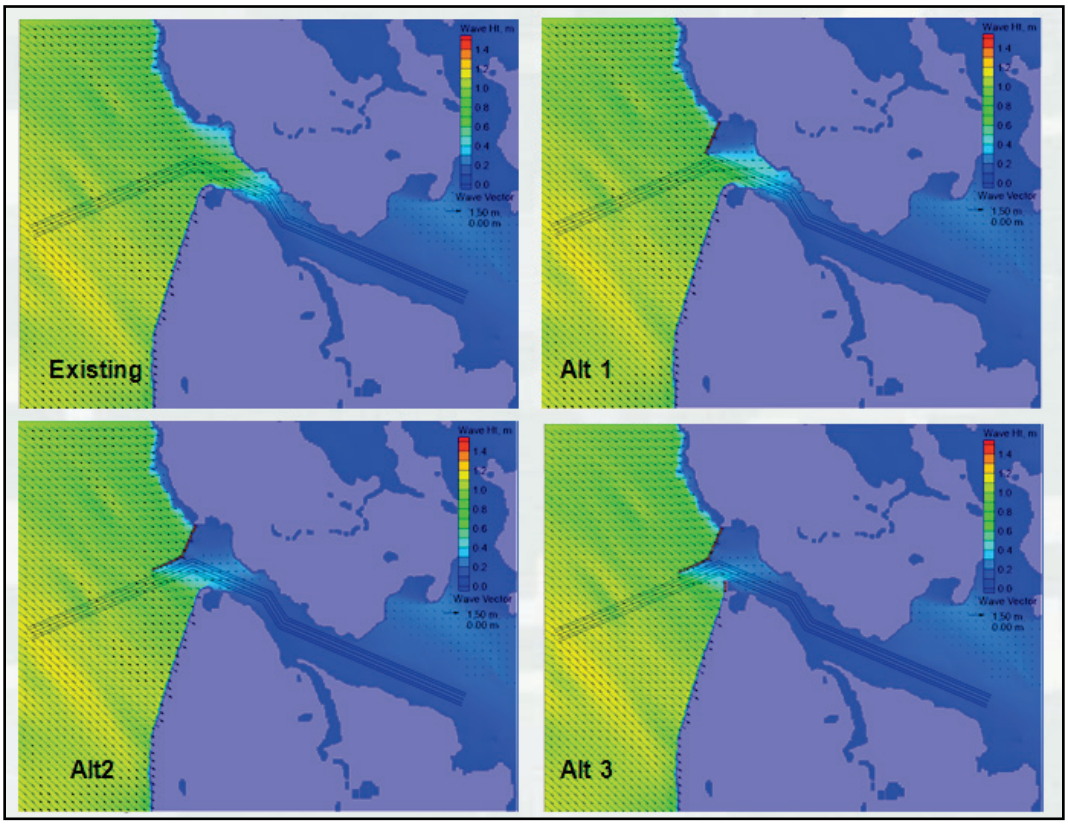

Figure 26. Examples of models of calculated wave heights in the west channel for the 50 yr design winds from SW and water level of 0 m.

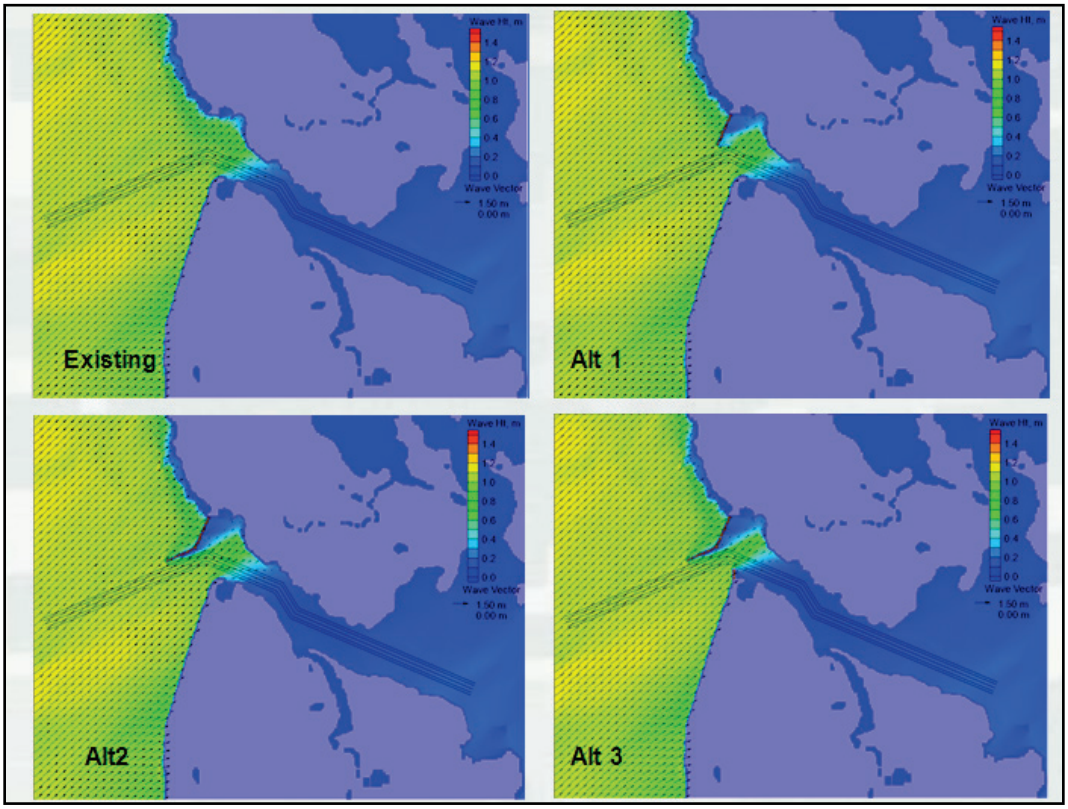

Figure 27. Examples of models of calculated wave heights in the west channel for the 50 yr design winds from NW and water level of 1.5 m.

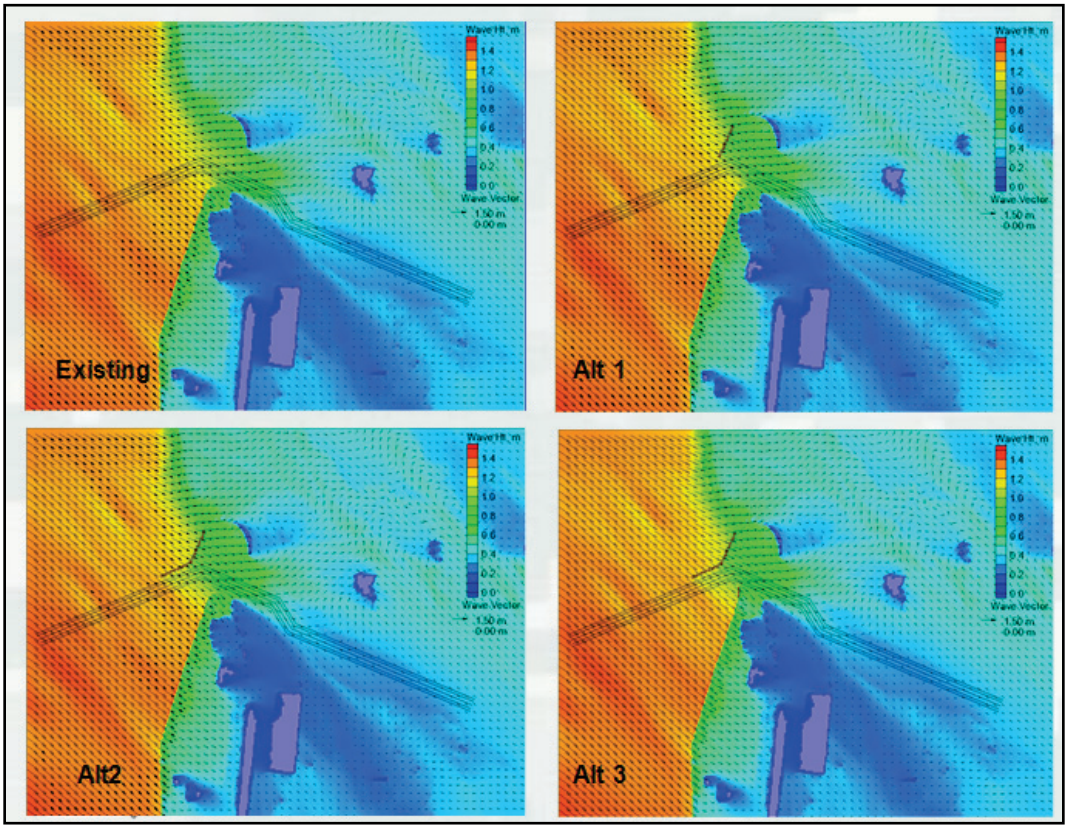

Figure 28. Examples of models of calculated wave heights in the west channel for the 50 yr design winds from SW and water level of 1.5 m.

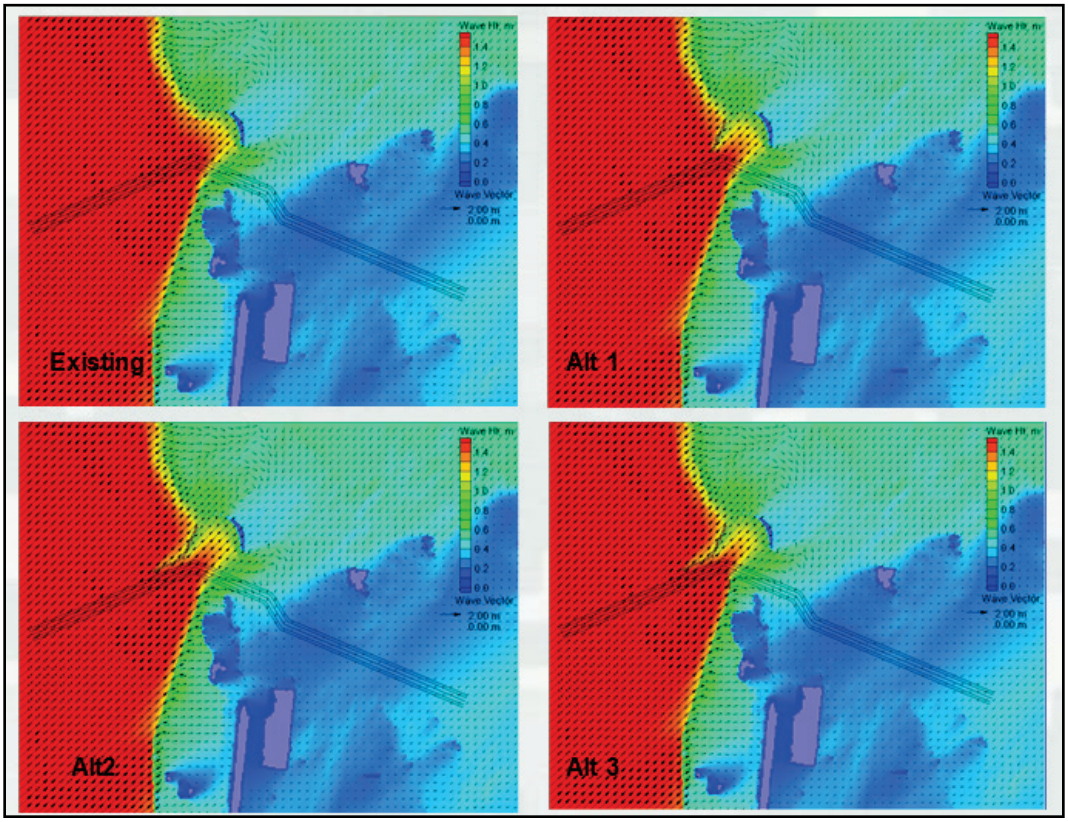

The wave-reduction analysis was performed for all simulations by comparison of the alternatives to the existing channel. Figures 29-34 show the comparison of wave-height variation along the channel centerline for NW, W, and SW directions. Figure 35 shows the example of calculated wave heights for Alt 4 along the channel centerline for 0 m water level and all directions.

Figure 29. Calculated wave heights in the west channel for 50 yr design winds from NW and water level of 0 m.

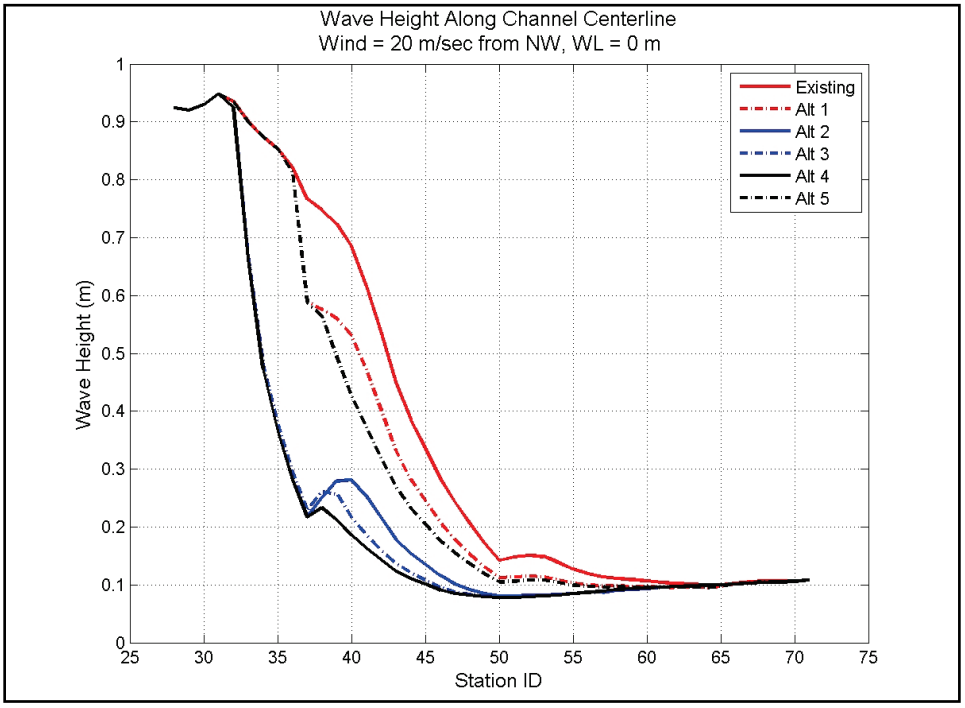

Figure 30. Calculated wave heights in the west channel centerline for 50 yr design winds from NW and water level of 1.5 m.

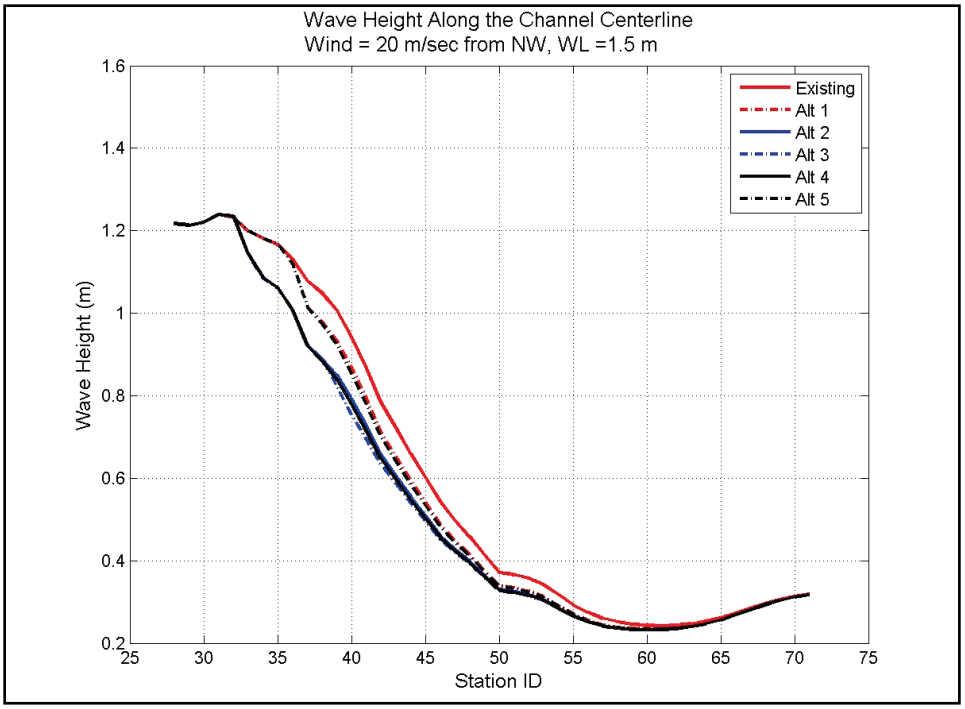

Figure 31. Calculated wave heights in the west channel for 50 yr design winds from W and water level of 0 m.

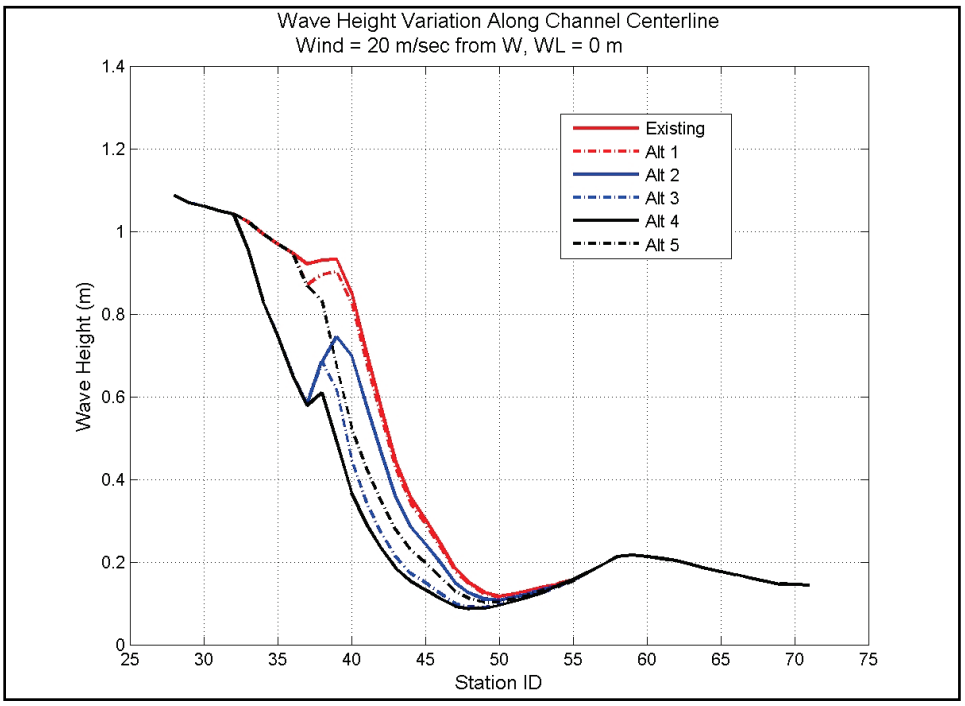

Figure 32. Calculated wave heights in the west channel centerline for 50 yr design winds from W and water level of 1.5 m.

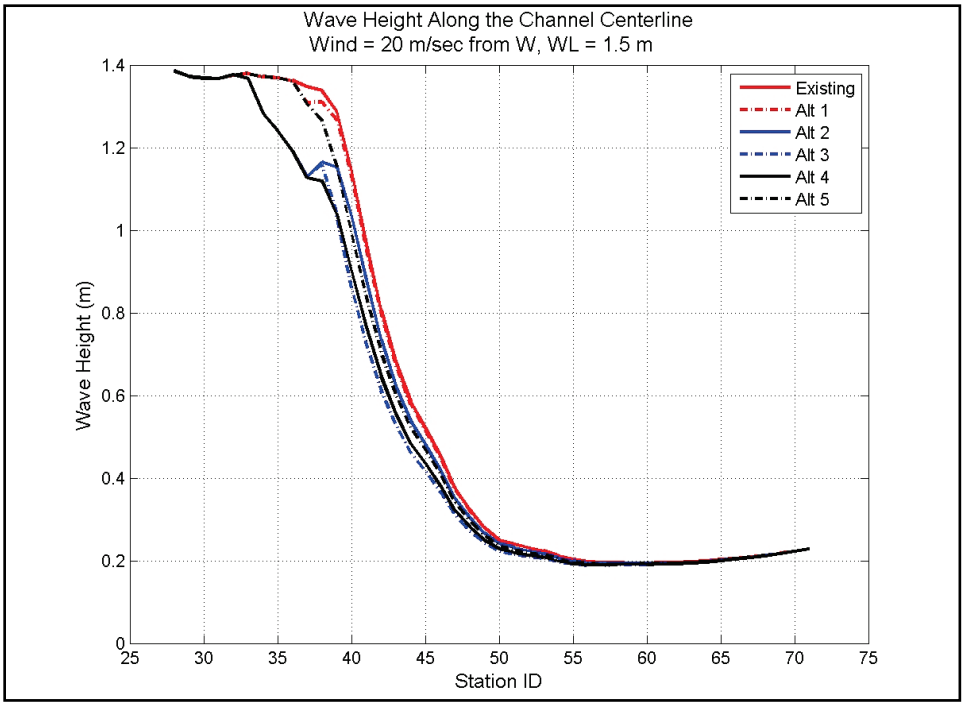

Figure 33. Calculated wave heights in the west channel centerline for 50 yr design winds from SW and water level of 0 m.

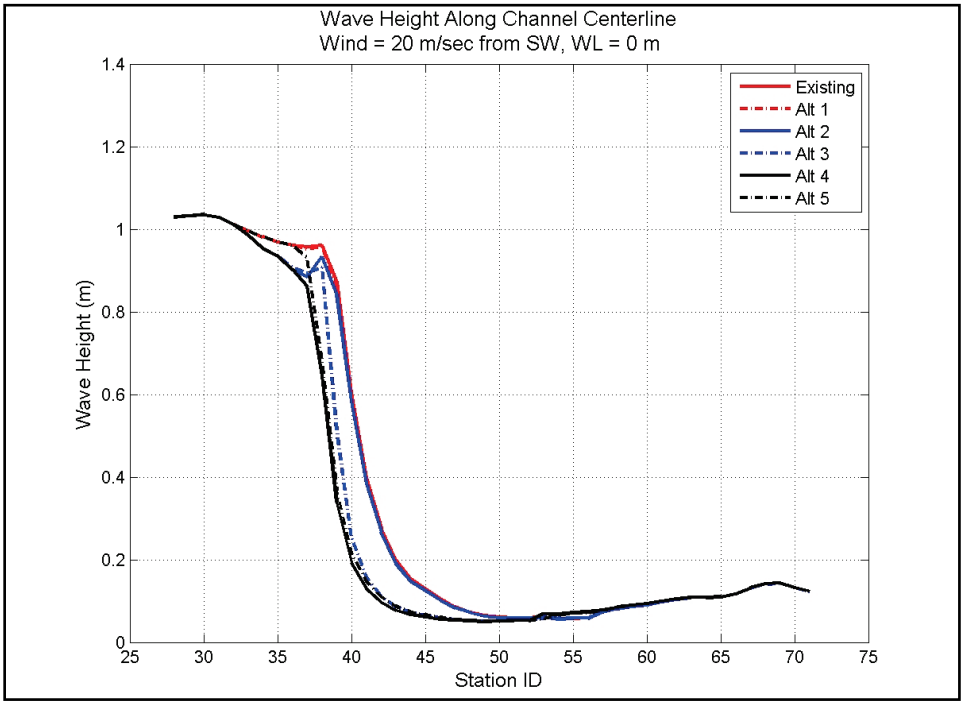

Figure 34. Calculated wave heights in the west channel centerline for 50 yr design winds from SW and water level of 1.5.

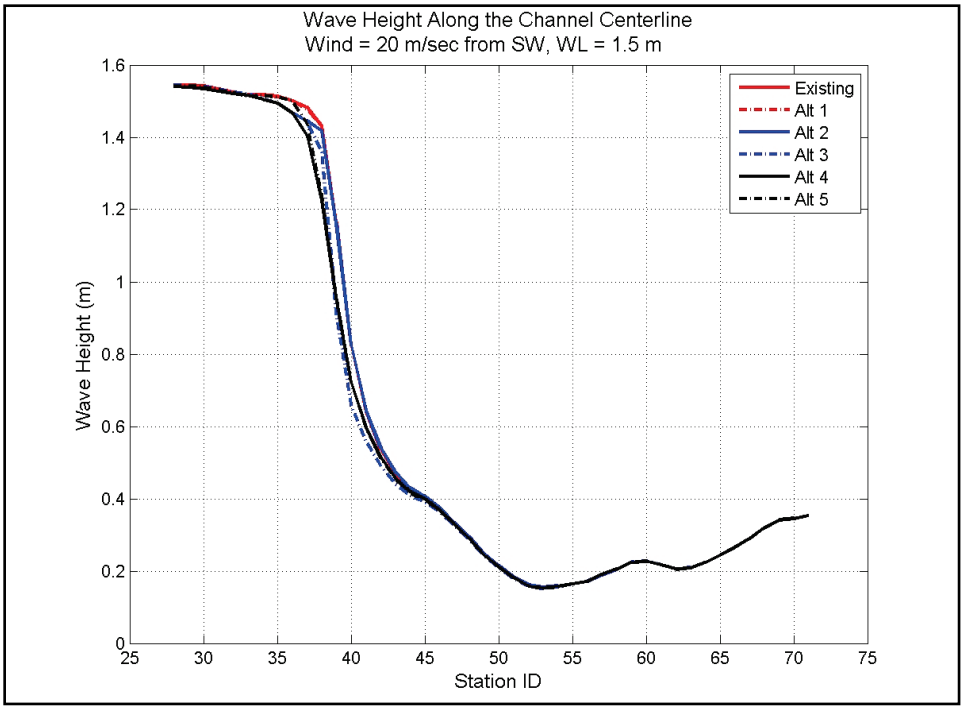

Figure 35. Calculated wave heights for Alt 4 along the west channel centerline for 50 yr design winds from six directions (NW, WNW, W, WSW, SW, and SSW) at water level of 0 m.

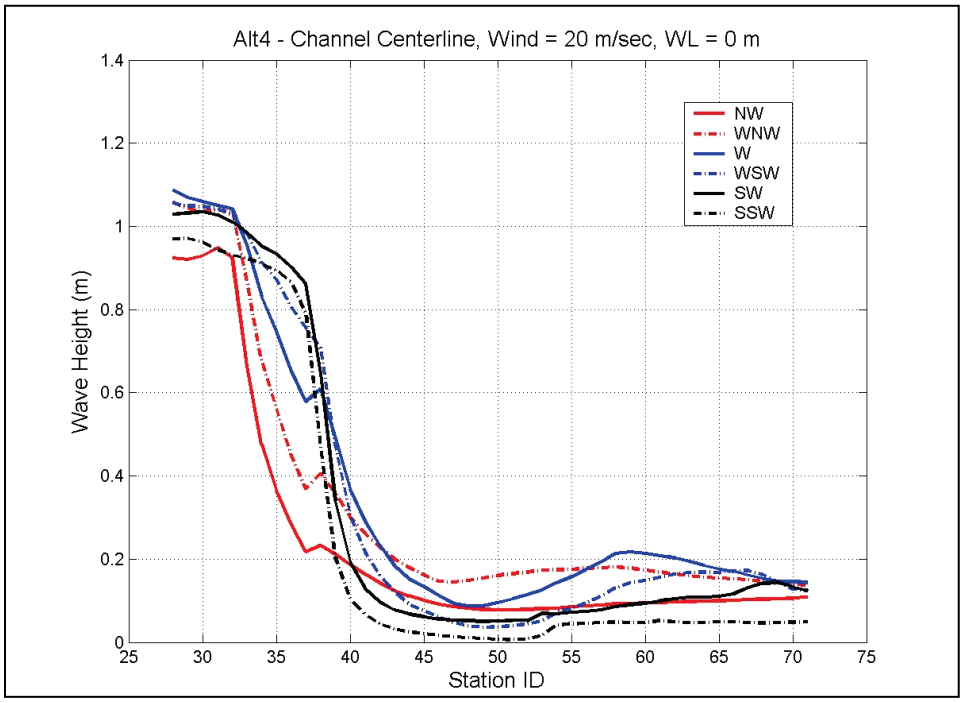

For all wind directions and two water levels investigated in this study, the analysis of wave-height reduction from five alternatives is based on the wave-height reduction factor calculated as the percentage of wave-height reduction to the wave heights in the existing channel without the project condition.

$$\left|\frac{\text{(Wave Height, Alternative) - (Wave Height, Existing Channel)}}{\text{(Wave Height, Existing Channel)}}\right| \times 100\%$$

For example, Figures 36 to 38 show the wave-height reduction factor along the channel centerline for Alternatives 1 to 5 and 50 yr design winds from directions of NW, W, SW, respectively, and WL = 0 m. Figures 39 to 41 show the wave-height reduction factor along the channel centerline for alternatives 1 to 5 and 50 yr design winds from NW, W, and SW, respectively, and WL = 1.5 m.

Figure 36. Calculated wave-height reduction for Alts 1-5 along the west channel centerline for 50 yr design winds from NW at water level of 0 m.

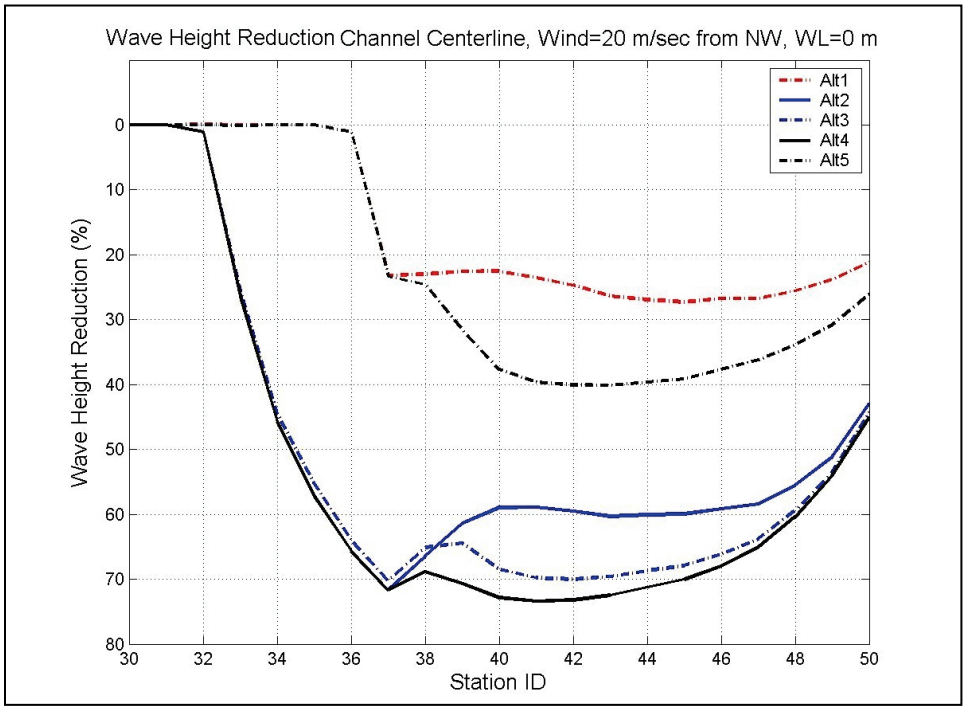

Figure 37. Calculated wave-height reduction for Alts 1-5 along the west channel centerline for 50 yr design winds from W at water level of 0 m.

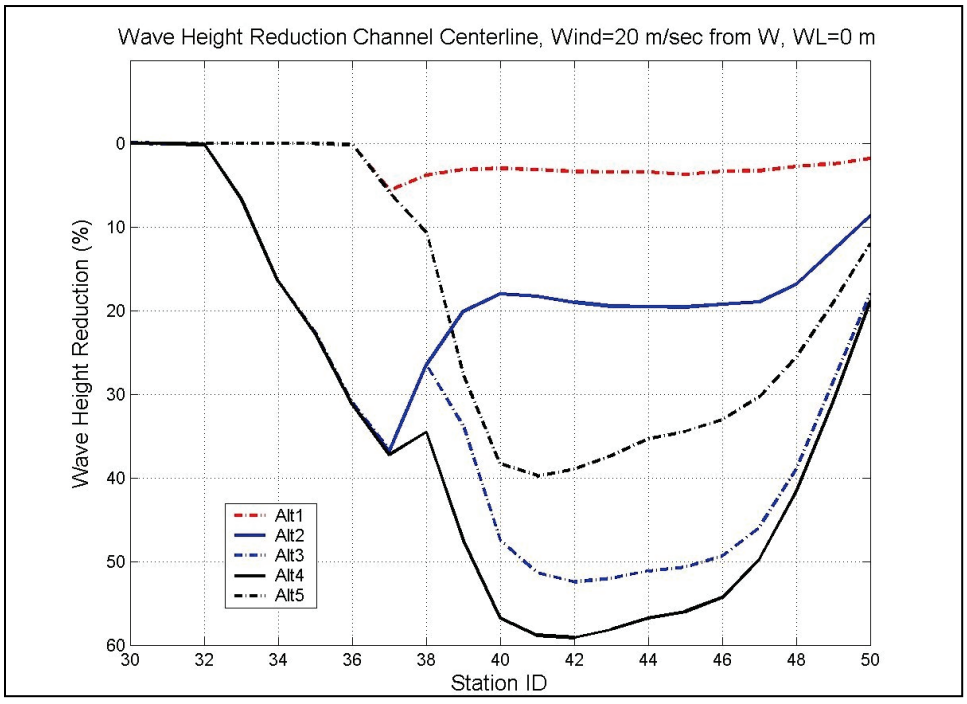

Figure 38. Calculated wave-height reduction for Alts 1-5 along the west channel centerline for 50 yr design winds from SW at water level of 0 m.

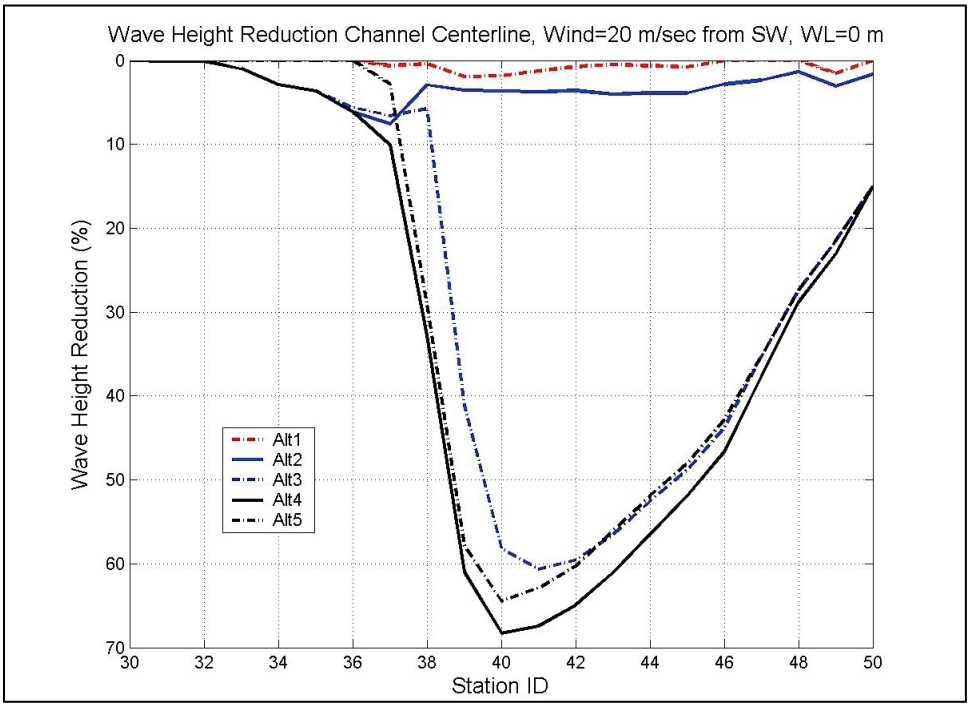

Figure 39. Calculated wave-height reduction for Alts 1-5 along the west channel centerline for 50 yr design winds form NW at water level of 1.5 m.

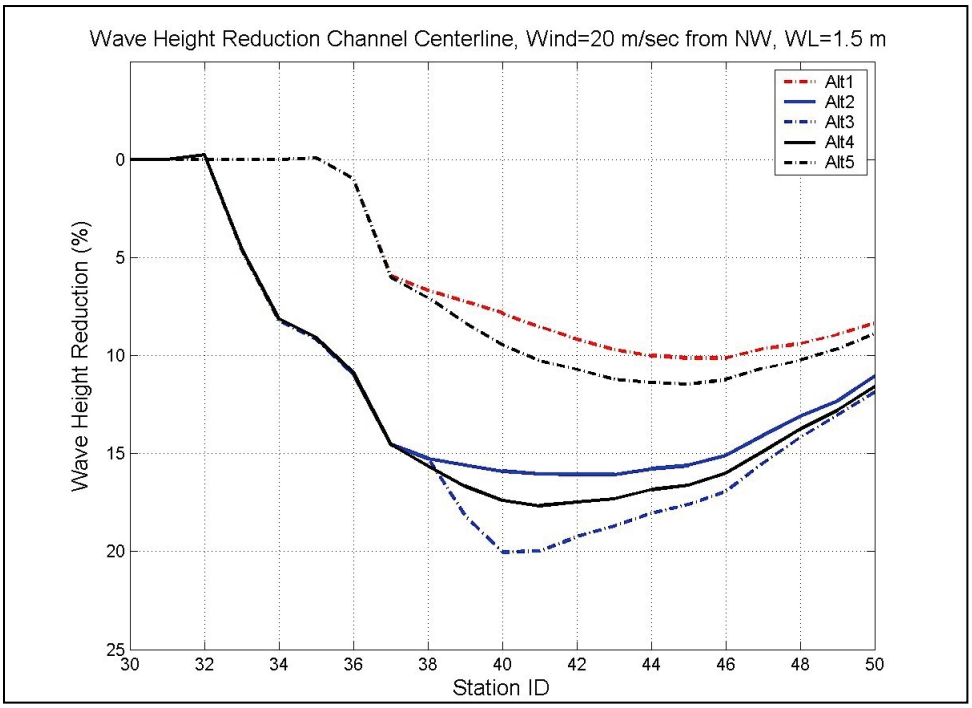

Figure 40. Calculated wave-height reduction for Alts 1-5 along the west channel centerline for 50 yr design winds from W at water level of 1.5 m.

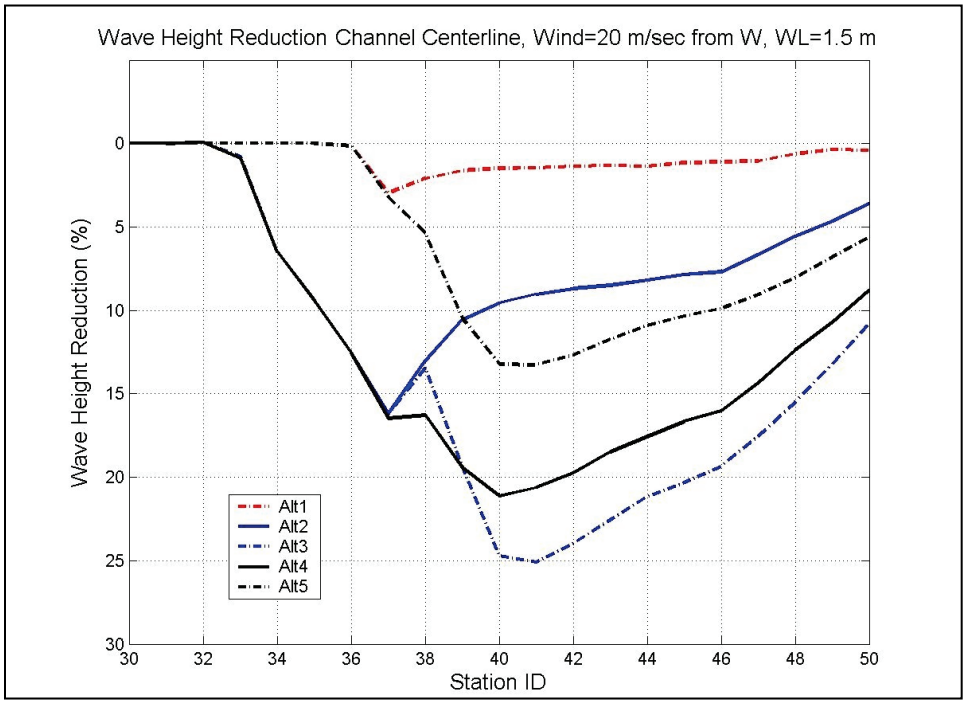

Figure 41. Calculated wave-height reduction for Alts 1-5 along the west channel centerline for 50 yr design winds from SW at water level of 1.5 m.

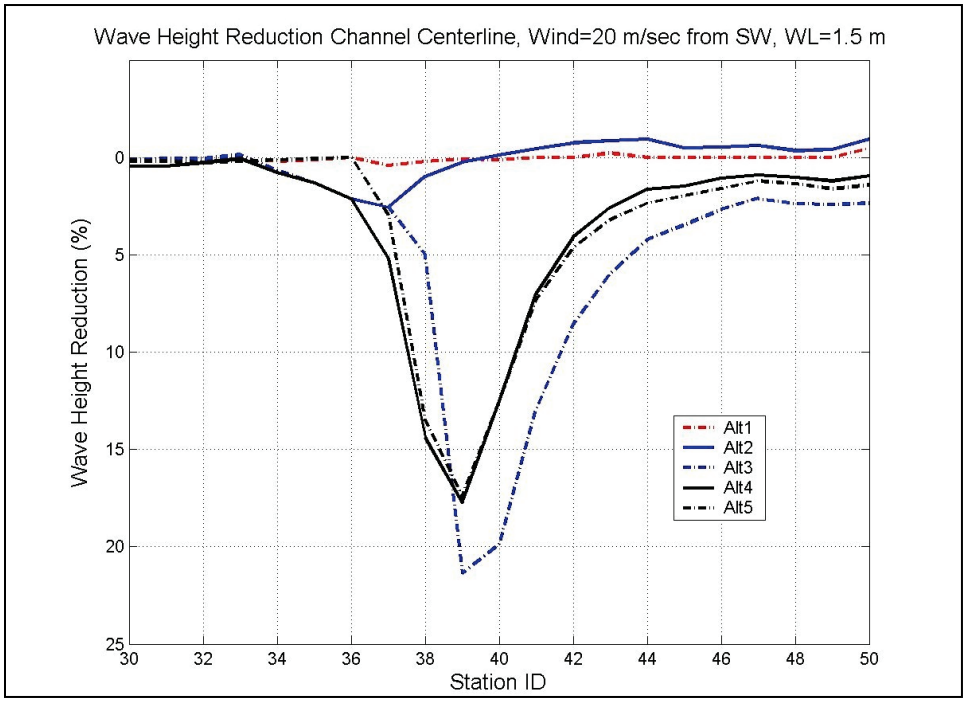

The corresponding wave-height variations along the north and south shorelines for the existing channel and five alternatives with design wind speeds from NW, W and SW at WL = 0 m are shown in Figures 42-47. Similarly, the wave-height variation along the north and south shorelines with design wind speeds from NW, W, and SW at WL = 1.5 m are shown in Figures 48-53. Among all alternatives, Alts 3 and 4 generally produced the largest wave-height reduction for WL = 0 m and 1.5 m, respectively, along the west channel centerline and along north and south shorelines. The high water (WL = 1.5 m) situation produces larger waves as compared to the lower water level (WL = 0 m). It must be emphasized that for high water level (WL=1.5 m), the structures used in the alternatives will be submerged, losing much of their effectiveness to intercept and reduce wave energy propagating into west and mid-sections of the channel. Under such extreme water level conditions, the wave-height reduction by alternatives cannot be used as a measure to rank the alternatives. Consequently, the ranking of alternatives is based on their performance (e.g., wave-height reduction factor) calculated for the WL = 0 m.

Figure 42. Calculated wave-heights along the north shoreline for 50 yr design winds from NW and water level of 0 m.

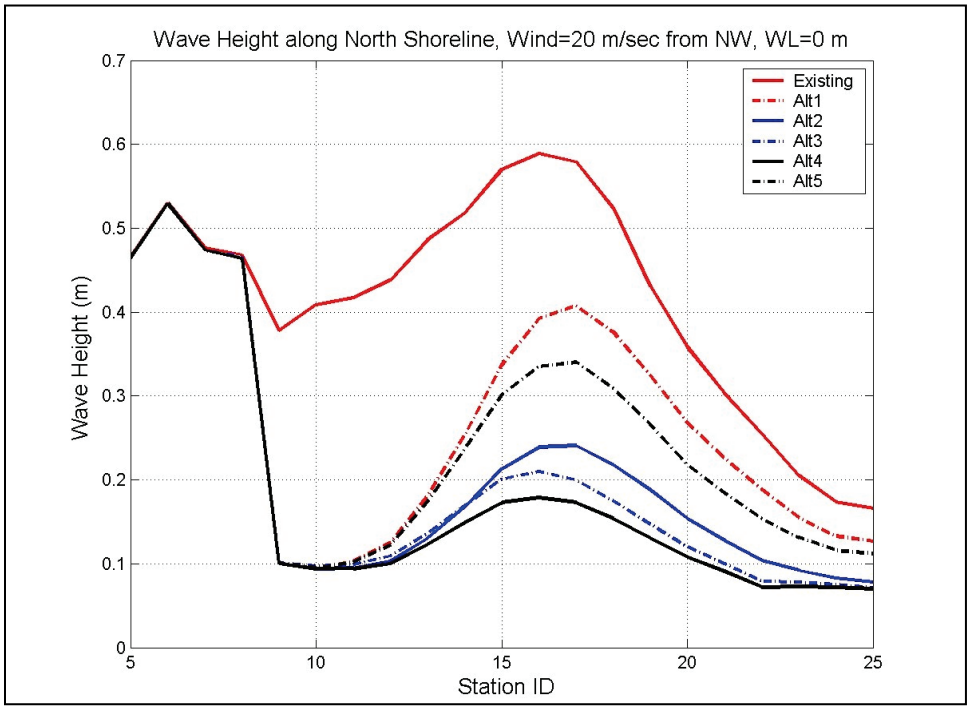

Figure 43. Calculated wave-heights along the north shoreline for 50 yr design winds from W and water level of 0 m.

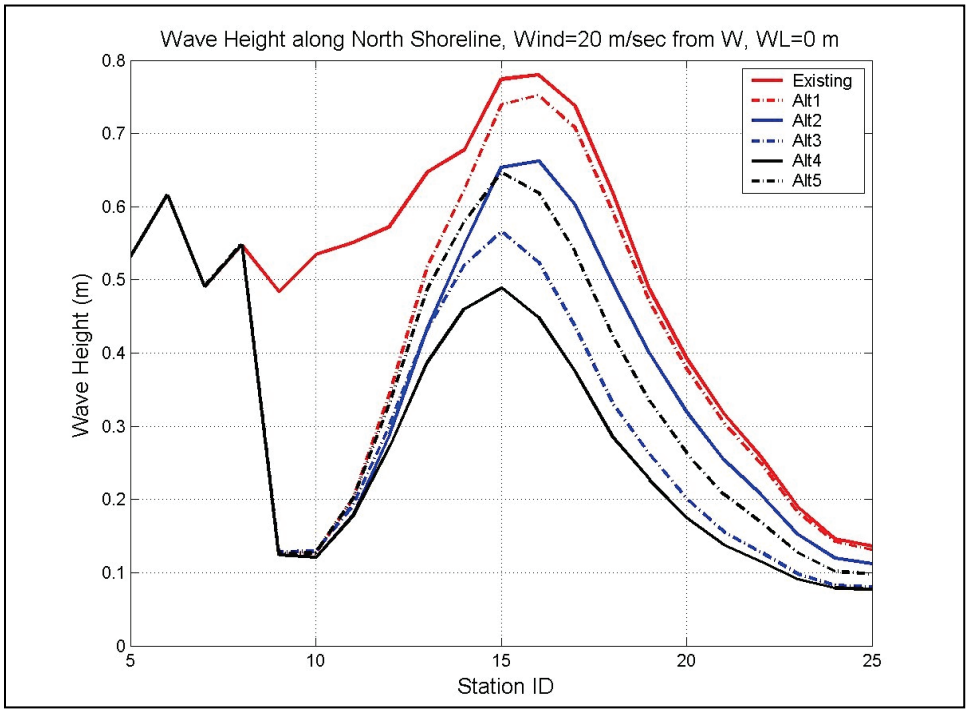

Figure 44. Calculated wave heights along the north shoreline for 50 yr design winds from SW and water level of 0 m.

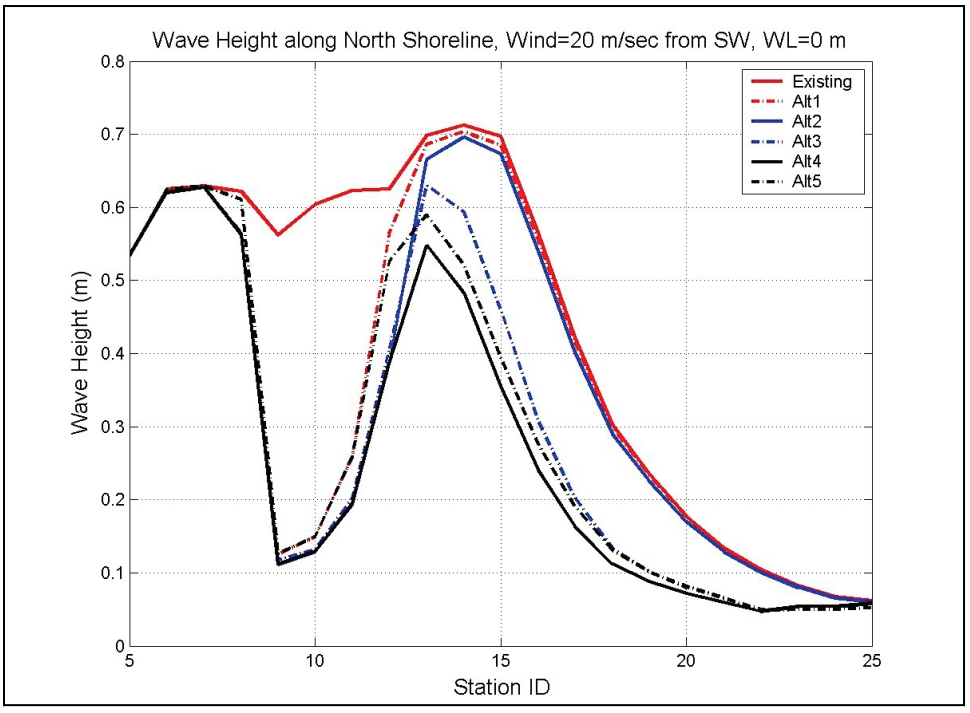

Figure 45. Calculated wave heights along the south shoreline for 50 yr design winds from NW and water level of 0 m.

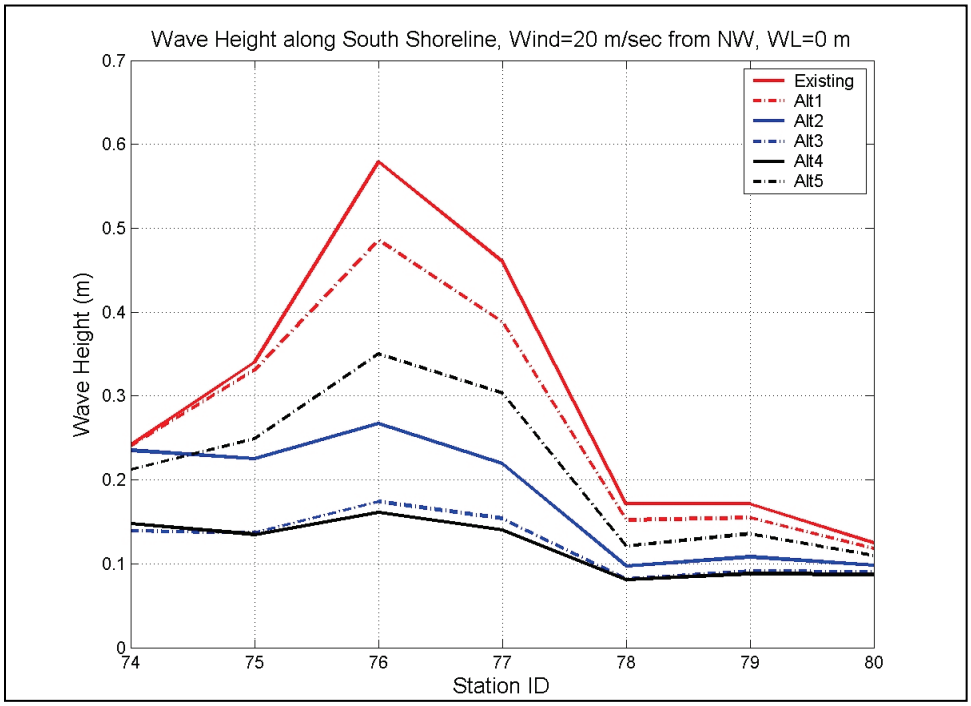

Figure 46. Calculated wave heights along the south shoreline for 50 yr design winds from W and water level of 0 m.

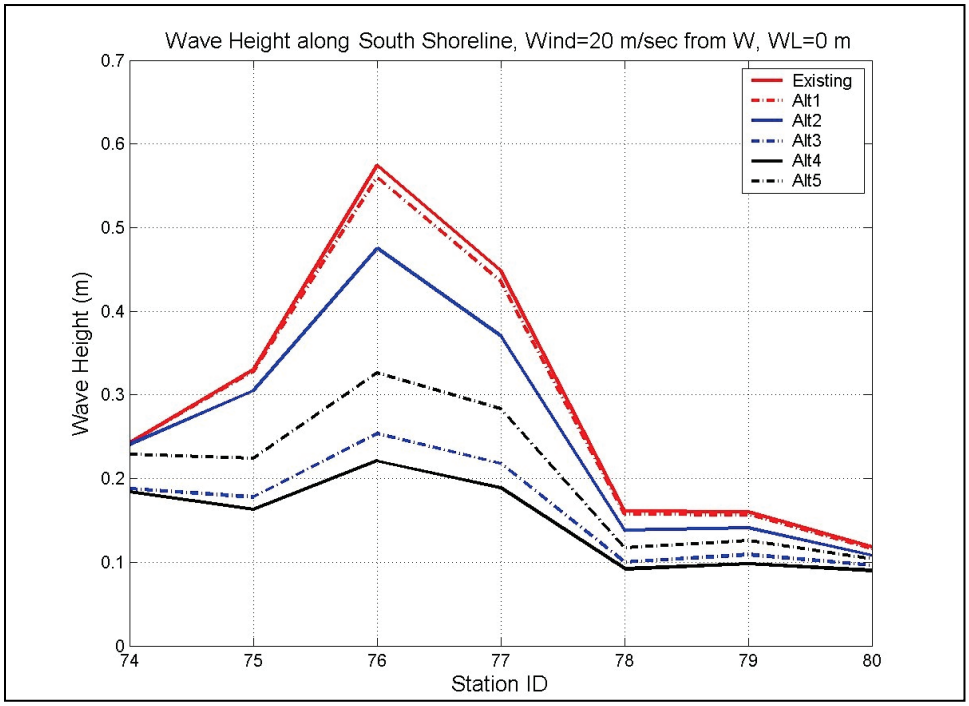

Figure 47. Calculated wave heights along the south shoreline for 50 yr design winds from SW and water level of 0 m.

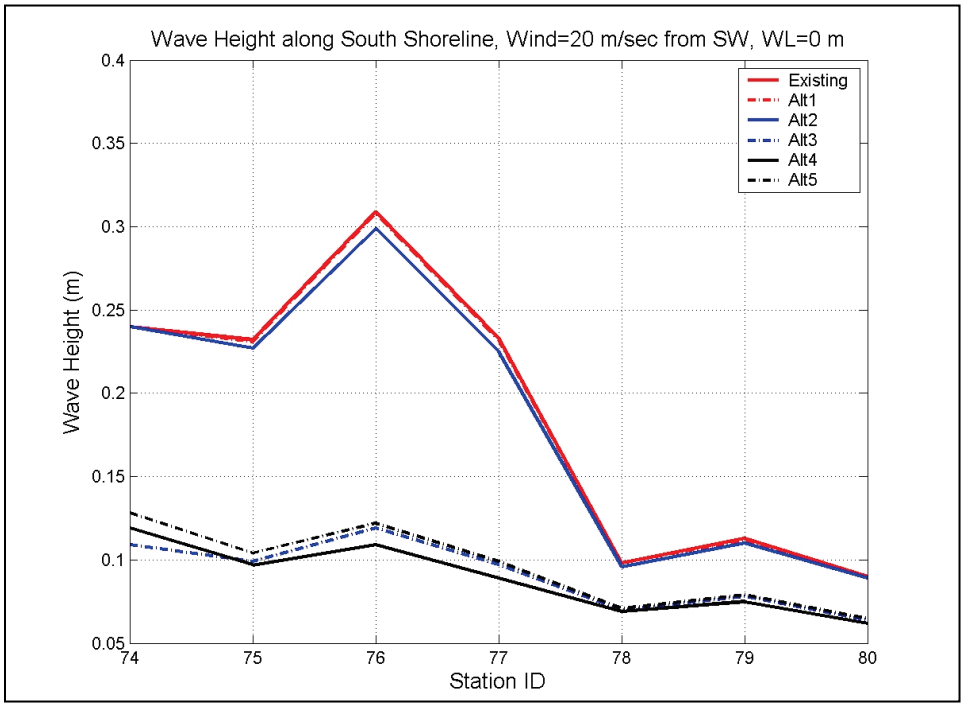

Figure 48. Calculated wave heights along the north shoreline for 50 yr design winds from NW and water level of 1.5 m.

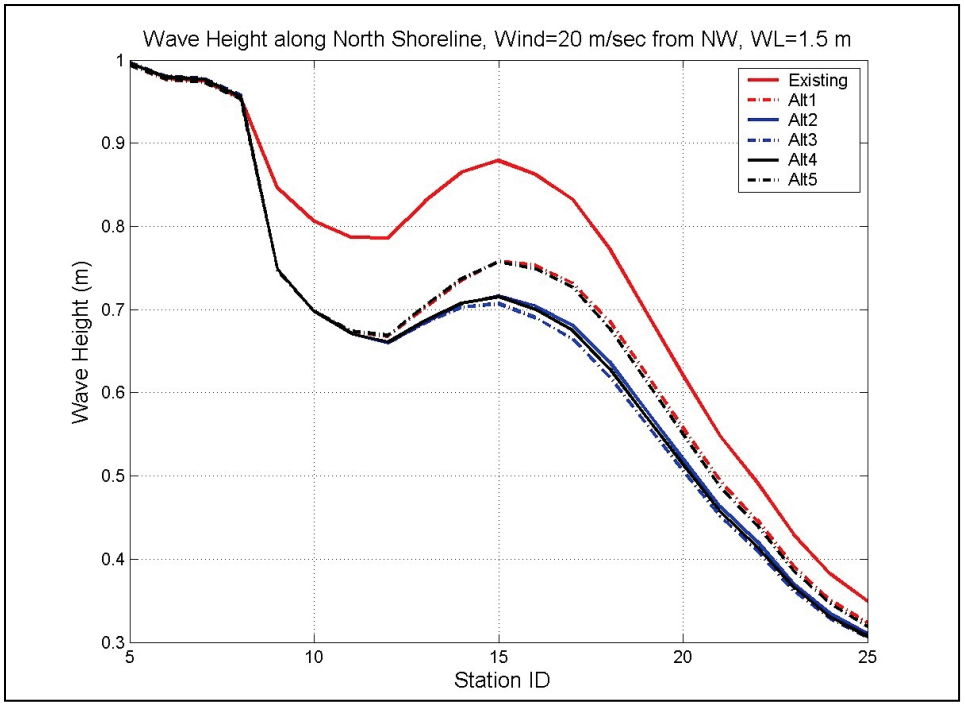

Figure 49. Calculated wave heights along the north shoreline for 50 yr design winds from W and water level of 1.5 m.

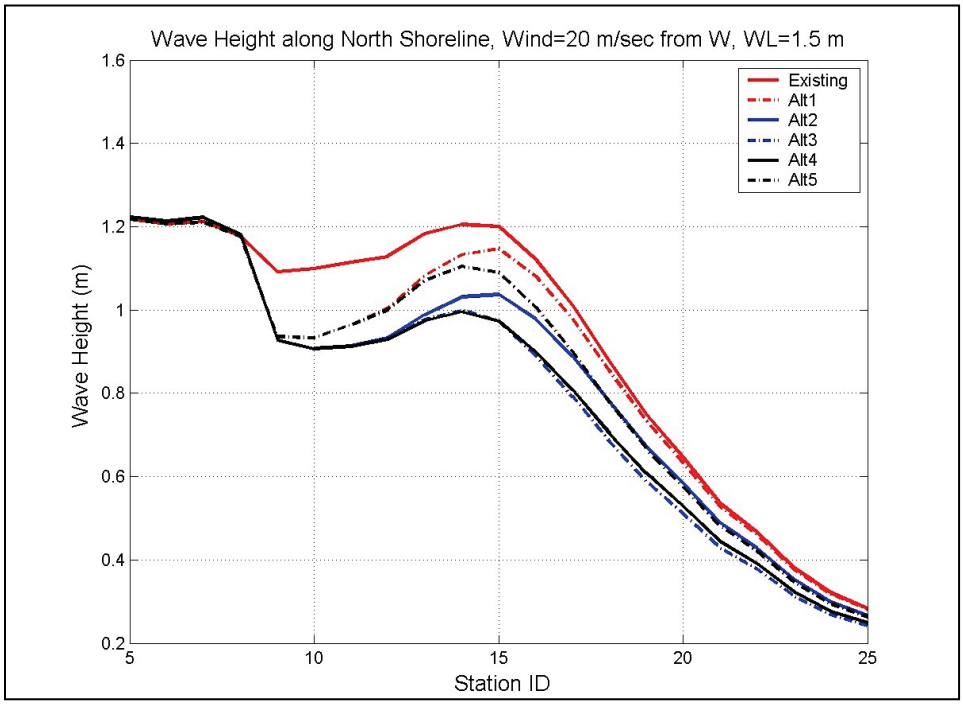

Figure 50. Calculated wave heights along the north shoreline for 50 yr design winds from SW and water level of 1.5 m.

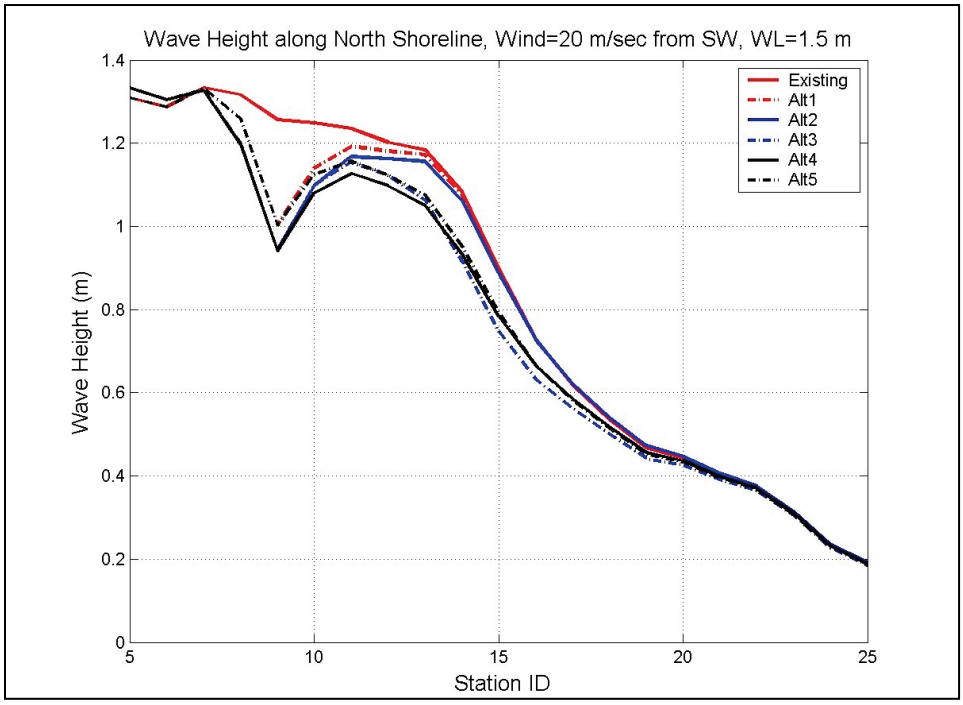

Figure 51. Calculated wave heights along the south shoreline for 50 yr design winds from NW and water level of 1.5 m.

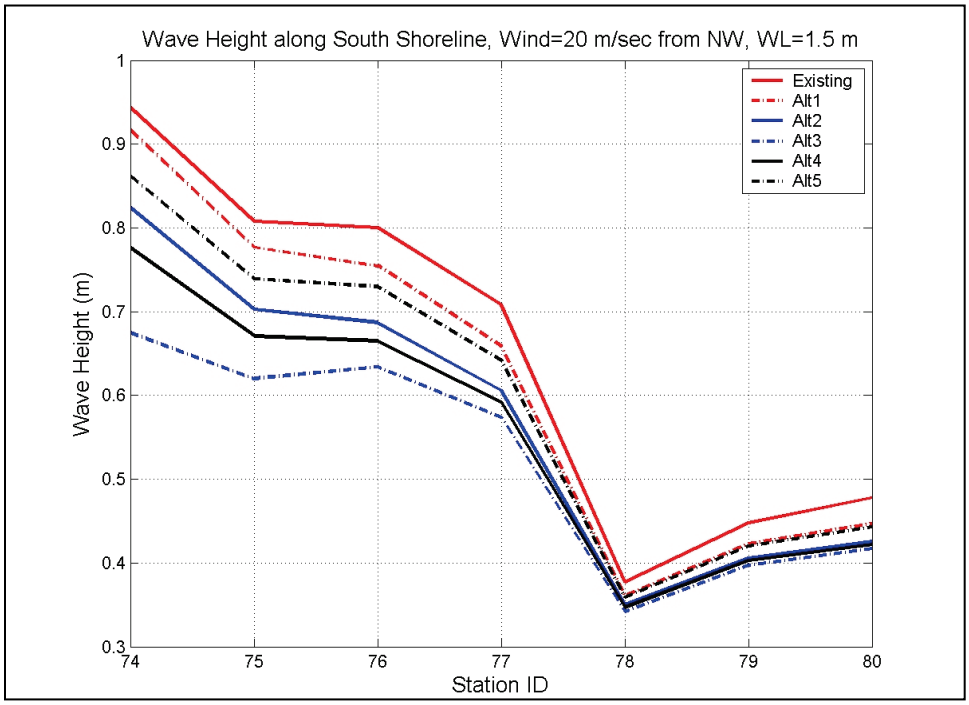

Figure 52. Calculated wave heights along the south shoreline for 50 yr design winds from W and water level of 1.5 m.

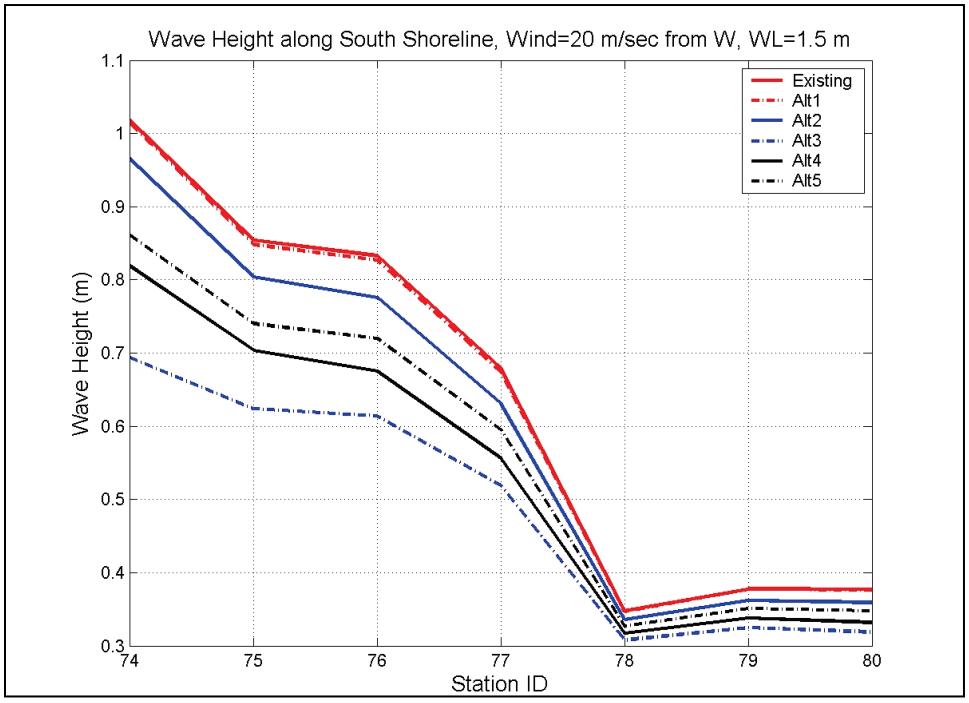

Figure 53. Calculated wave heights along the south shoreline for 50 yr design winds from SW and water level of 1.5 m.

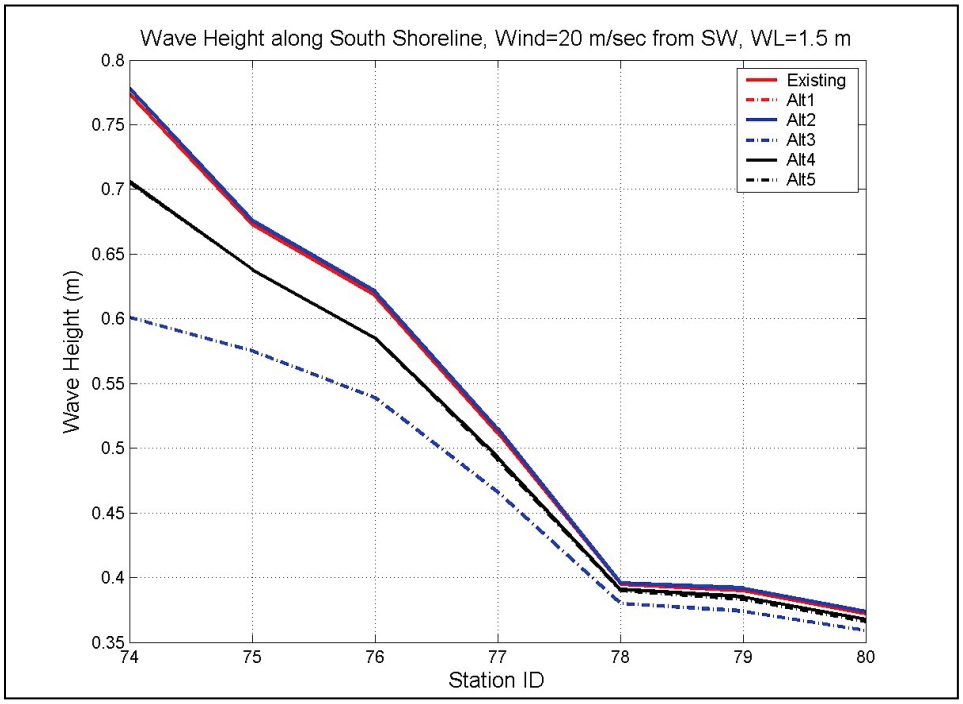

2.10 Hurricane Isabel simulations (waves with current)

A similar analysis of waves was performed using Hurricane Isabel winds for six channel configurations (existing and five alternatives). This was done to determine wave and water level estimates for a 50 yr hurricane event. Because the winds for Hurricane Isabel approached Chesapeake Bay from the east side and winds rotate counter-clockwise around the center (eye) of the hurricane, significant over-land drag reduction of wind speeds occurred, affecting the water level close to the land-water boundaries. The strong east-to-west winds associated with Hurricane Isabel produced elevated water levels along the west side of the bay and lowered the water level in the mid and east side of bay. As a consequence, although lower water levels occurred at and around Tangier Island during Isabel, this event was considered as a 50 yr hurricane for the entire bay. The wind and water-level pattern associated with Hurricane Isabel was simulated for 17-20 September 2003. As expected, model results indicated comparatively lower waves and water levels at Tangier Island than in the western portion of the bay. Figure 54 shows an example of the calculated wave-height field in the Chesapeake Bay (regional grid) and at Tangier Island (local grid) for the existing channel configuration during Isabel.

Figure 54. Example of calculated wave-height fields during Hurricane Isabel.

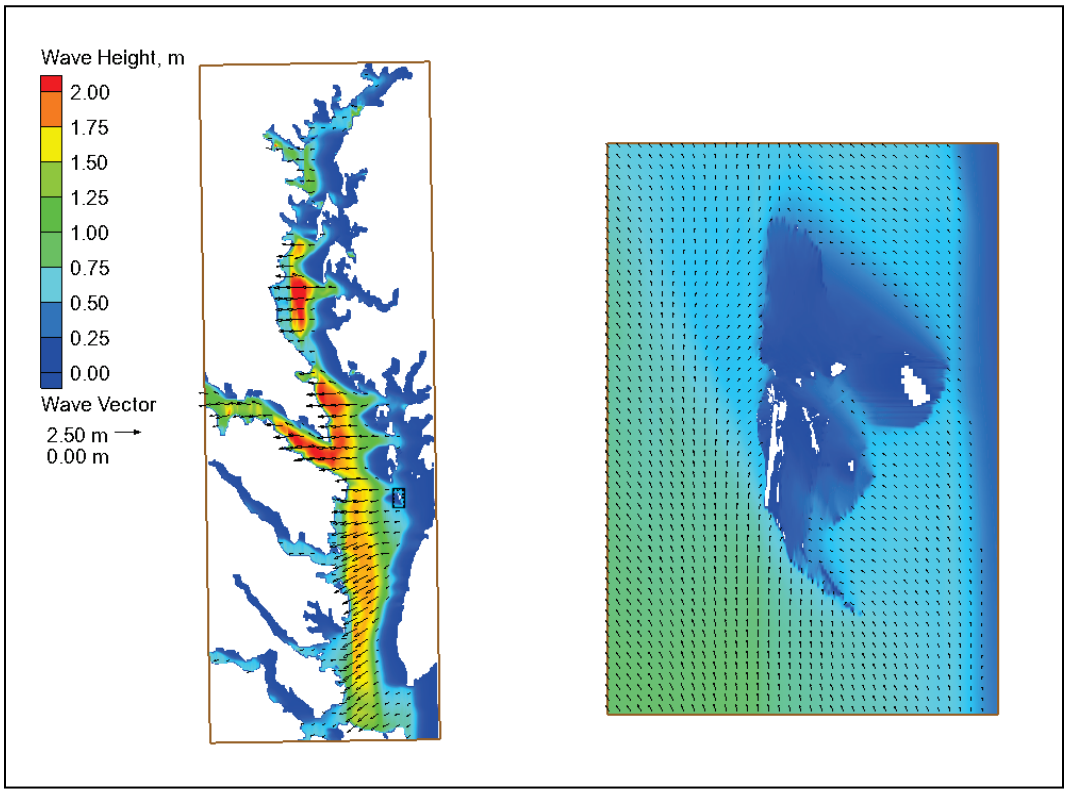

2.11 Estimates for structure design

Based on results described in the two previous sections, the structural lay-out of Alt 4 overall is more effective at reducing wave-energy propagation into the canal than the other alternatives for all conditions evaluated. Consequently, Alt 4 is the recommended structural lay-out for achieving the project goals. This recommendation is based on the performance of alternatives for WL = 0 m, defined as the wave-height reduction factor achieved along the channel centerline. However, it is noted that at the extreme high water level (WL=1.5 m, 5 ft), the structures evaluated are partially or fully submerged, diminishing their effectiveness to intercept and reduce wave energy penetrating into the west and mid-sections of the channel. Under such extreme water level conditions, wave-height reduction cannot be used as a measure to rank the alternatives. For purposes of completeness and future records, the ranking of alternatives is provided in this report for both water levels.

The calculated wave-height, period, direction, and water-level estimates at ten locations on the windward side of the north and south structures of Alt 4 and along north shoreline are shown in Figure 46. These stations are

marked in black squares in Figure 55 and are 4, 7, 10, 13, 85, 88, 99, 103, 118, and 121. Wave and water-level estimates at these stations are used in the structure design calculation and evaluation of wave effects to north shoreline. Calculated wave direction, height, and period estimates at these ten stations marked on Figure 55 are listed in Tables 3, 4, and 5 for two water levels (0 and 5 ft or 1.5 m). Wave direction is meteorological (e.g., direction waves coming from).

Figure 55. Ten selected locations (black squares) in Alt 4 where wave and water-level estimates are provided for design of structure and evaluation of wave effect to north shoreline.

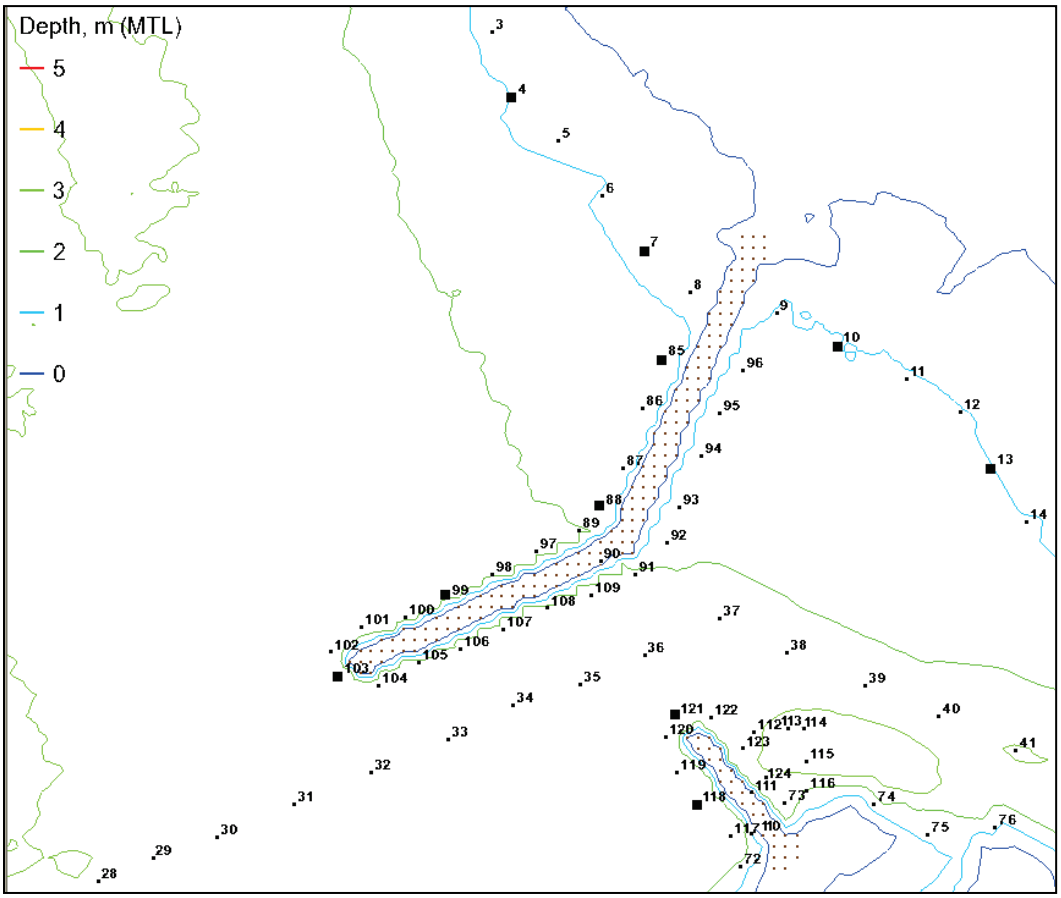

Table 3. Wave parameters for 50 yr design conditions (water level = 0 m).

Sta	Depth (m, MTL)	Wave Height (m)	Wave Period (sec)	Direction (deg)
4	0.93	0.81	5.4	250
7	0.7	0.63	5.4	237
10	1.0	0.26	5.4	259

Sta	Depth (m, MTL)	Wave Height (m)	Wave Period (sec)	Direction (deg)
13	1.0	0.64	5.4	233
85	1.27	0.7	5.4	266
88	1.88	0.9	5.4	285
99	2.35	1.02	5.4	288
103	2.64	1.06	5.4	287
118	2.65	0.98	5.4	233
121	2.56	0.97	5.4	232

Table 4. Wave parameters for 50 yr design conditions (water level = 1.5 m).

Sta	Depth (m, MTL)	Wave Height (m)	Wave Period (sec)	Direction (deg)
4	2.43	1.39	5.2	247
7	2.2	1.33	5.2	229
10	2.5	1.09	5.3	224
13	2.5	1.1	5.3	241
85	2.77	1.27	5.3	247
88	3.38	1.3	5.3	284
99	3.85	1.34	5.3	289
103	4.14	1.53	5.3	230
118	4.15	1.47	5.3	230
121	4.06	1.47	5.3	229

Table 5. Wave parameters for Hurricane Isabel.

Sta	Depth (m, MTL)	Wave Height (m)	Wave Period (sec)	Direction (deg)
4	0.93	0.47	2.6	36
7	0.7	0.41	2.7	25
10	1.0	0.27	2.7	42
13	1.0	0.28	2.7	32

Sta	Depth (m, MTL)	Wave Height (m)	Wave Period (sec)	Direction (deg)
85	1.27	0.38	2.7	16
88	1.88	0.32	2.7	6
99	2.35	0.32	2.7	3
103	2.64	0.6	2.4	44
118	2.65	0.44	2.7	29
121	2.56	0.41	2.7	43

Table 6 presents the average of wave-height reduction factors at WL = 0 m along the west channel centerline from Sta 30 to 50 for each of five alternatives. Tables 7 and 8 present the average wave-height reduction factors at WL = 0 m along the north shoreline (Sta 5 to 25) and along south shoreline (Sta 74 to 80), respectively for Alts 1 to 5. The average of wave-height reduction factor is provided for nine cases (wind directions from N, NNW, NW, WNW, W, WSW, SW, SSW, and S) and average of cases of all nine wind directions for each alternative. Overall, the wave reduction for Alt 4 was greater than other alternatives for WL = 0 m.

Tables 9 to 11 presents the average of wave-height reduction factor at WL = 1.5 m along the west channel centerline, north shoreline, and south shoreline, respectively. In this higher water-level scenario (WL = 5 ft or 1.5 m), the average wave reduction is less for all alternatives, about 25 percent less as compared to existing channel configuration (without project). The average wave reduction for Alt 3 was greater than other alternatives. However, as discussed earlier, ranking of alternatives is based on the low water results (WL = 0.0 m) because at high water the structures are underwater. Therefore, Alt 4 is the recommended alternative.

Table 6. Average of wave-height reduction factors along west channel centerline (Sta 30 to 50) for Alts 1-5 at WL = 0 m.

Wind Dir	Alt 1	Alt 2	Alt 3	Alt 4	Alt 5
N	20.3	53.9	57.4	56.5	27.3
NNW	21.5	51.9	55.0	56.7	28.6
NW	16.4	48.6	52.0	54.0	22.9

Wind Dir	Alt 1	Alt 2	Alt 3	Alt 4	Alt 5
WNW	5.6	31.2	38.5	40.7	14.4
W	2.2	16.7	31.4	35.1	18.5
WSW	1.1	7.7	30.9	36.1	27.1
SW	0.5	2.9	26.0	30.4	27.4
SSW	0.1	2.8	38.2	43.9	38.4
S	0.2	2.1	25.7	30.6	28.1
Average	7.5	24.2	39.5	42.7	25.9

Table 7. Average of wave-height reduction factors along north shoreline (Sta 5 to 25) for Alts 1-5 at WL = 0 m.

Wind Dir	Alt 1	Alt 2	Alt 3	Alt 4	Alt 5
N	38.4	57.5	61.6	61.2	44.9
NNW	39.6	55.9	59.0	60.5	46.2
NW	34.2	51.3	54.6	56.9	40.4
WNW	23.0	40.3	47.2	50.4	31.4
W	15.3	24.8	37.8	42.3	29.3
WSW	12.3	17.3	35.6	40.6	34.4
SW	11.2	15.5	37.2	40.6	36.9
SSW	10.8	15.7	40.5	46.9	40.8
S	11.4	20.0	45.6	50.9	42.1
Average	21.8	33.1	46.6	50.0	38.5

Table 8. Average of wave-height reduction factors along south shoreline (Sta 74 to 80) for Alts 1-5 at WL = 0 m.

Wind Dir	Alt 1	Alt 2	Alt 3	Alt 4	Alt 5
N	18.3	56.3	74.0	63.6	35.8
NNW	16.6	48.4	65.7	65.6	35.3
NW	8.7	34.9	52.2	53.2	24.9

Wind Dir	Alt 1	Alt 2	Alt 3	Alt 4	Alt 5
WNW	2.4	17.4	36.7	40.3	17.3
W	1.6	11.0	37.7	42.7	25.4
WSW	0.7	4.4	41.6	45.9	36.5
SW	0.3	2.1	45.7	47.1	43.6
SSW	0	2.1	65.1	68.6	61.1
S	0	1.2	59.6	63.6	59.5
Average	5.4	20.0	53.1	54.5	37.7

Table 9. Average of wave-height reduction factors along west channel centerline (Sta 30 to 50) for Alts 1-5 at WL = 1.5 m.

Wind Dir	Alt 1	Alt 2	Alt 3	Alt 4	Alt 5
N	1.9	8.0	8.9	8.9	2.8
NNW	5.8	11.0	12.2	11.7	6.4
NW	5.8	11.4	12.7	12.0	6.5
WNW	2.9	10.4	13.4	12.3	5.2
W	0.9	7.1	13.9	12.3	6.2
WSW	0.1	1.6	8.6	6.7	5.1
SW	0.1	0.1	4.8	3.7	3.5
SSW	0.7	0.1	3.9	2.6	2.9
S	0.0	0.2	1.6	2.1	2.0
Average	2.0	5.5	8.9	8.0	4.5

Table 10. Average of wave-height reduction factors along north shoreline (Sta 5 to 25) for Alts 1-5 at WL = 1.5 m.

Wind Dir	Alt 1	Alt 2	Alt 3	Alt 4	Alt 5
N	6.2	9.5	10.0	10.0	6.7
NNW	9.8	13.0	13.8	13.4	10.2
NW	9.5	12.6	13.6	13.0	10.0

Wind Dir	Alt 1	Alt 2	Alt 3	Alt 4	Alt 5
WNW	7.3	12.0	14.1	13.4	8.9
W	4.4	9.7	15.0	13.9	8.6
WSW	2.5	4.4	10.5	9.2	7.0
SW	1.9	2.5	7.2	6.1	5.4
SSW	2.7	3.1	7.2	5.9	5.2
S	3.6	5.7	7.3	8.1	5.7
Average	5.3	8.1	11.0	10.3	7.5

Table 11. Average of wave-height reduction factors along south shoreline (Sta 74 to 80) for Alts 1-5 at WL = 1.5 m.

Wind Dir	Alt 1	Alt 2	Alt 3	Alt 4	Alt 5
N	0.7	8.9	13.0	12.4	4.2
NNW	4.7	11.8	16.3	14.0	7.1
NW	5.1	11.7	17.8	14.0	7.7
WNW	1.8	9.1	19.6	14.6	7.7
W	0.5	5.3	21.4	15.1	10.8
WSW	0.0	0.3	15.1	8.2	7.8
SW	0.0	0.0	10.0	3.8	4.0
SSW	0.5	0.0	8.0	2.2	2.6
S	0.0	0.0	2.0	1.5	1.5
Average	1.5	5.2	13.7	9.5	5.9

2.12 Single-parameter representative wave-reduction rating

Ranking of alternatives based on a single number is not recommended, but may be useful for preliminary analysis. As discussed earlier, alternatives are ranked based on the wave-reduction factors calculated at the low water level (WS = 0.0 m). The bottom line in Tables 6, 7, and 8 give the wave-reduction factor for each alternative averaged over the nine wind direction cases for the channel centerline, north shoreline, and south shore-

line, respectively. By averaging the results for the centerline and north and south shoreline, we can obtain a single number on which to base a preliminary ranking of each alternative. By this method, we obtain the representative wave-reduction ratings given in Table 12. Again, Alt 4 has the highest representative wave reduction.

Table 12. Representative wave-reduction ratings for Alt 1-5.

Alternative	Alt 1	Alt 2	Alt 3	Alt 4	Alt 5
Ave Wave Reduction (%)	11.6	25.8	46.4	49.1	34.0

2.13 Channel sedimentation issues

A detailed sediment-transport component was not deemed necessary in the scope of the modeling study. Consequently, changes in the sedimentation patterns caused by the construction of alternative 4 were not considered warranted for two reasons. First, the dogleg shape of the Alt 4 northern jetty is expected to trap the southward longshore transport moving along the western side of Tangier Island, blocking sediments from entering the channel. Second, both tidally driven and wave-driven currents in the channel are below the threshold for the initiation of sediment motion. Therefore, a detailed examination of sediment transport and local scouring potential along the structures was not considered in this study.

It is noted that the CMS development of sediment transport is continuing. Consequently, modeling estimates for flow and sediment transport if used in the final design should be validated either with field data or compared to estimates obtained from other two- or three-dimensional hydrodynamic models. Because of the absence of field data at Tangier Island, the flow and sediment modeling results presented in this report are qualitative and were not used in the relative comparison of alternatives.

However, the CENAO dredges the boat channel on a regular basis. The proposed construction may affect the overall sedimentation pattern in the vicinity of the structures and throughout the channel reaches of Tangier Island. This required modeling of sediment transport. The CMS was used to simulate the sediment transport for Hurricane Isabel. The purpose of the sediment simulation was to provide a quick view of potential shoaling and erosion areas from a 50 yr tropical storm (Hurricane Isabel). It was

by no means to model long-term morphology evolution at Tangier Island and channel reaches. For this reason, a constant sediment median size of 0.15 mm was specified in the three-day simulation of Hurricane Isabel, because modeling of fines, mud, and cohesive sediments was not available in CMS at the time of this study.

Figure 56 shows the calculated spatially varying sediment accretion and erosion field for the existing west channel configuration (without project) in the 3-day simulation of Hurricane Isabel. There is apparent sediment deposition immediately outside the west entrance channel and bottom erosion inside the west entrance channel. Figures 57 to 61 show the calculated erosion and deposition fields for Alts 1 to 5, respectively, in the three-day simulation of Isabel. The result of calculated morphology change for Alts 1, 2, and 5 indicates sediment can be scoured in the channel near the tip of the breakwater and trapped inside the west entrance channel during large storms. There is more bottom erosion between north breakwater and south spur structure in Alts 3 and 4. The eroded sediment is carried by stronger currents into the bay. Accordingly, the sediment deposition is insignificant inside the west channel entrance.

Figure 56. Calculated sediment accretion and erosion field for the existing west channel configuration in three-day simulation of Hurricane Isabel.

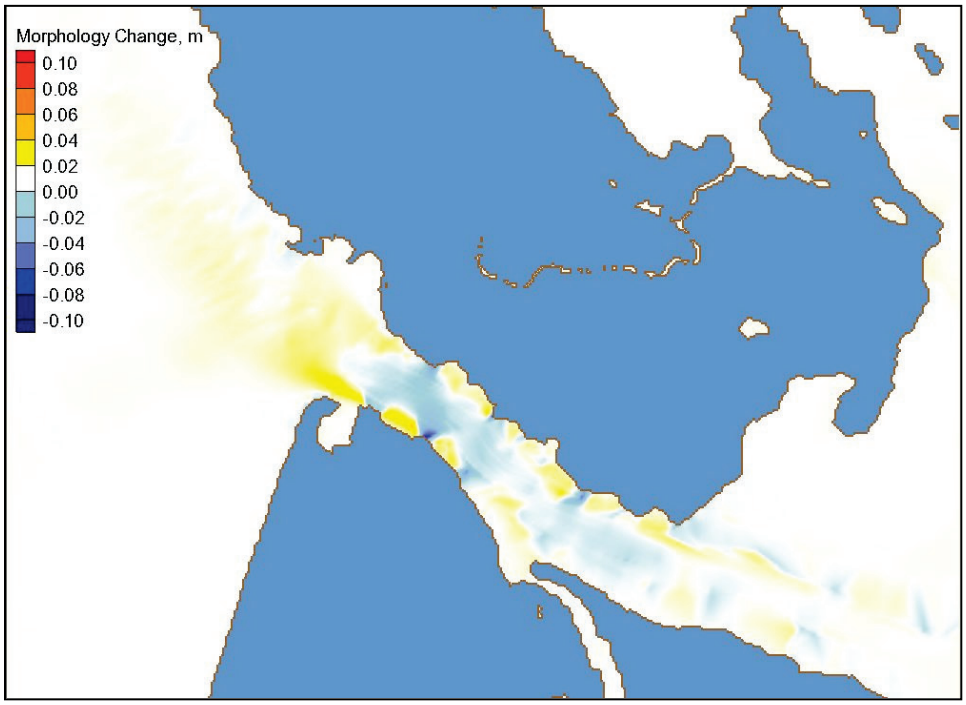

Figure 57. Calculated sediment accretion and erosion field for Alt 1 in three-day simulation of Hurricane Isabel.

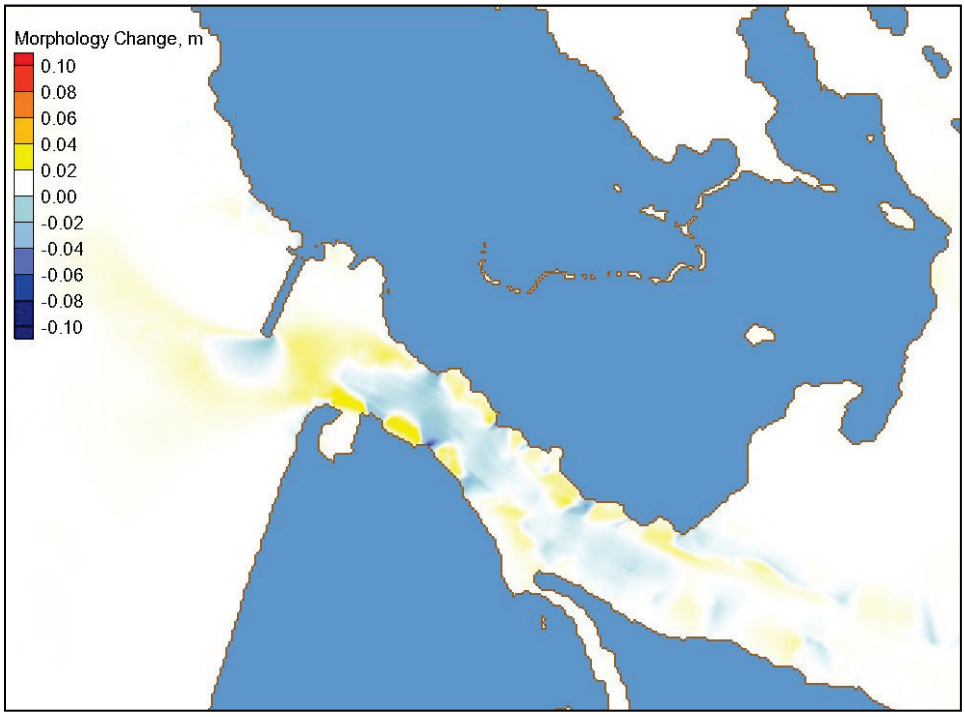

Figure 58. Calculated sediment accretion and erosion for Alt 2 in three-day simulation of Hurricane Isabel.

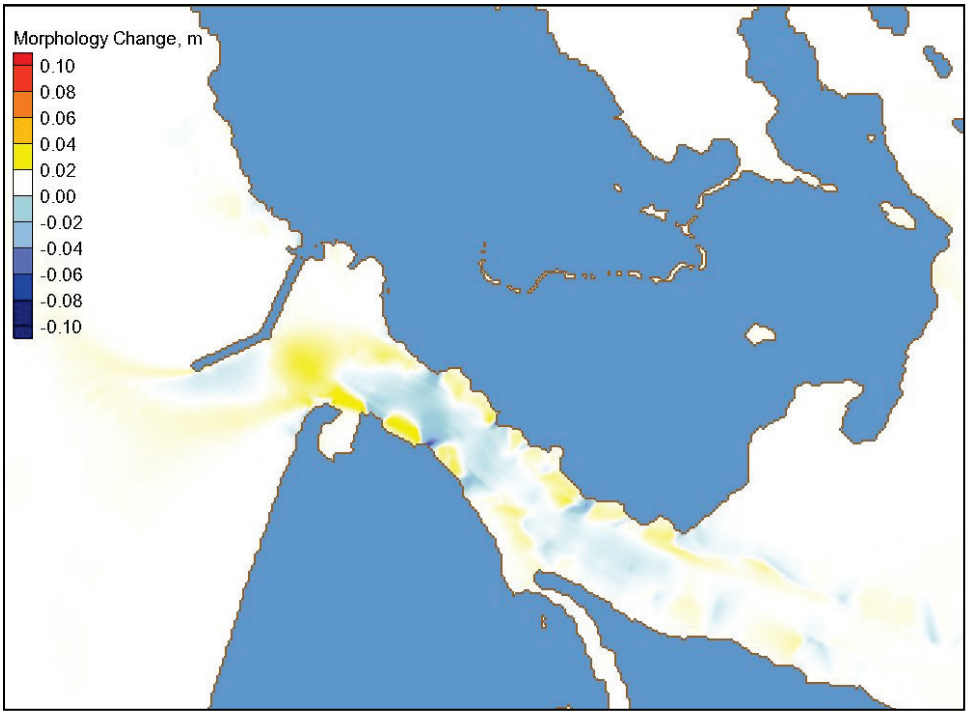

Figure 59. Calculated sediment accretion and erosion field for Alt 3 in three-day simulation of Hurricane Isabel.

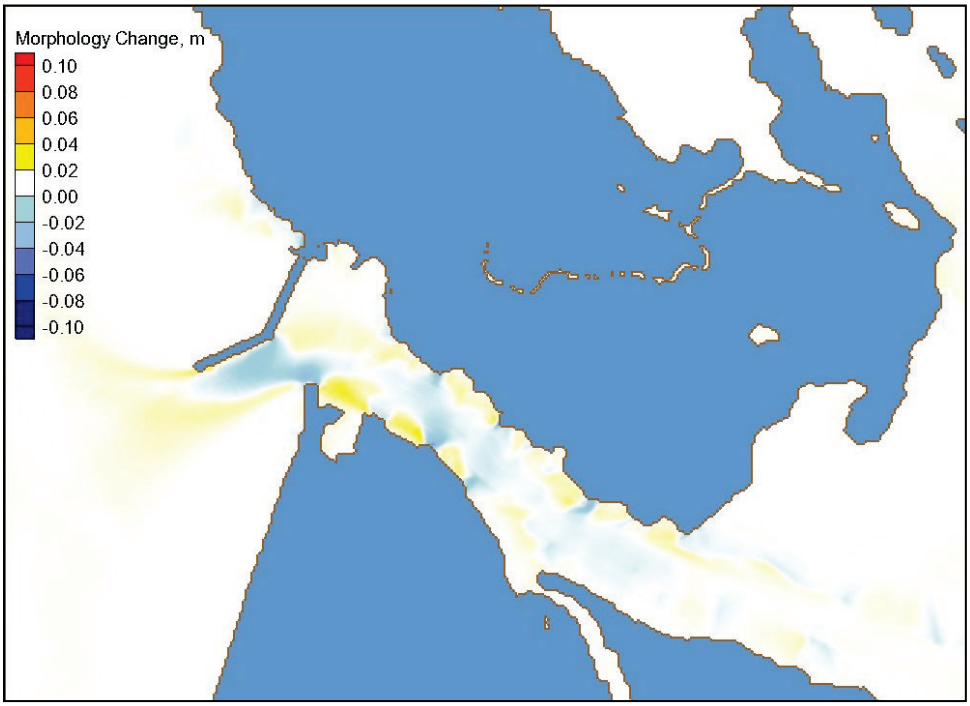

Figure 60. Calculated sediment accretion and erosion field for Alt 4 in three-day simulation of Hurricane Isabel.

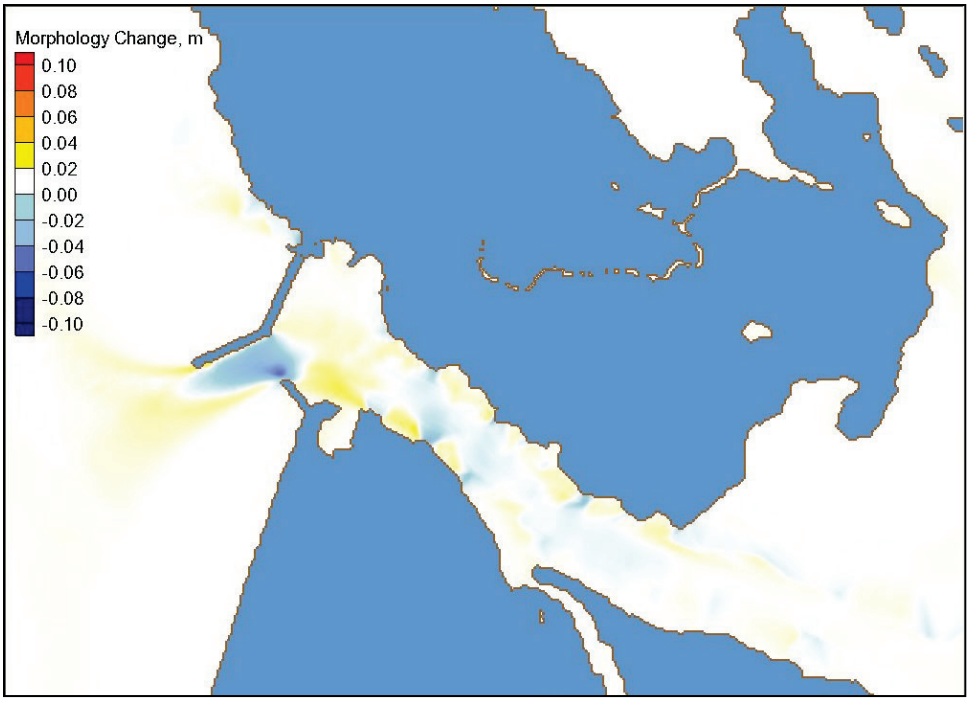

Figure 61. Calculated sediment accretion and erosion field for Alt 5 in three-day simulation of Hurricane Isabel.

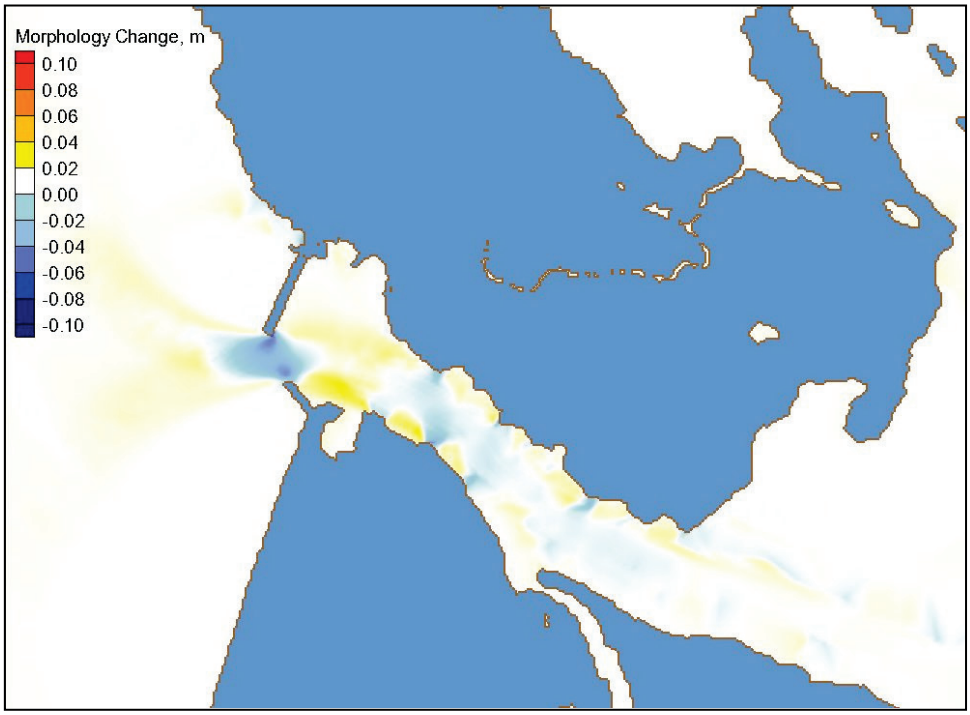

Overall, sediment transport results for the existing channel configuration and all five alternatives were similar with an insignificant morphology change (magnitude of either erosion or deposition less than 2 in. or 0.05 m). As the structure is intended to reduce wave energy in the channel, the current could increase and scour channel near structures. Some additional settling of suspended sediments could occur away from the channel due to reduced wave currents. Based on model results for the 50-year, return-interval event, Hurricane Isabel (three-day simulation), the depth-averaged current magnitude is less than 3 ft/sec (1 m/sec) in the channel and the maximum channel depth change is less than 2 in. (0.05 m). No significant effect of structure on channel sedimentation and channel infilling was apparent for the Hurricane Isabel simulation.

3 Structural Design Calculations

3.1 Selection of design wave and water level

For design purposes, the storm with a statistical return period of 50 years was recommended by CHL and agreed to by CENAO. Wave heights and wave periods for the 50 yr event were presented in the preceding chapter. Although the tidal range is small in the area of Tangier Island, a significant storm surge is expected during the design event. As related in the previous chapter, a water-level rise of 1.5 m (5 ft) was selected to include tidal fluctuations, storm surge, and wave setup.

The basic design of the structures will therefore be based on the wave height and wave period of a storm with a return period of 50 yrs, with a still-water level of 1.5 m (5 ft). The recommended design will then be examined under the conditions presented during Hurricane Isabel, and examined again using the same wave heights and periods (50 yr storm) but with increased water levels due to sea level rise.

At the request of CENAO, all calculations have been converted to American Customary units in this section. A table of conversions is included at the beginning of this report to assist in conversion back to SI units if desired.

3.2 Stability equations

3.2.1 Stable seaside armor size

Stable armor stone size is computed here based on 50-year return period wave and water-level conditions given in the previous sections. The Hudson equation is well known and has been used for years to determine armor stability (Hudson 1959; Shore Protection Manual 1984). The equation in stability number form is given by

$$N_s = \frac{H_{1/10}}{\Delta D_{n50}} = (K_D \cot\theta)^{1/3} \quad (1)$$

In Equation 1, $H_{1/10}$ is the average height of the highest 10 percent of waves. $\Delta = S_r - 1$, where S_r is immersed specific gravity of the armor

stone; that is: $S_r = \rho_r/\rho_w$, where ρ_r = density of armor stone and ρ_w = density of water at the project site. D_{n50} is nominal stone size defined as $D_{n50} = (M_{50}/\rho_r)^{1/3}$ where M_{50} = median mass of armor stone. K_D is an empirical coefficient and $\cot\theta$ is the structure's seaward slope. K_D takes into account all parameters not in the equation. The Hudson equation was originally developed for monochromatic waves, and use of the equation with irregular wave height statistics has been discussed by many authors. The most common application of the equation utilizes $H_{1/10}$ for depth-limited wave conditions with the depth-limited breaker height limited to 0.78*depth. Values published for K_D in the *Shore Protection Manual* (1984) are appropriate. The Hudson equation design assumes damage based on eroded volume of $D\%$ = 0 to 5.

In this report, seaside armor stability is computed based on more recent guidance published in Melby and Kobayashi (2011). The maximum wave-momentum flux is highly nonlinear for nonlinear waves (steep waves in shallow water). This corresponds to the case where armor stability is at its minimum. Melby and Hughes (2004) described a non-linear wave momentum flux using a numerical Fourier solution. The resulting approximate relation was found to be

$$\left(\frac{M_F}{\rho_w g h^2}\right)_{\max} = A_0\left(\frac{h}{gT_m^2}\right)^{-A_1}$$

$$A_0 = 0.639\left(\frac{H_{m0}}{h}\right)^{2.026} \tag{2}$$

$$A_1 = 0.180\left(\frac{H_{m0}}{h}\right)^{-0.391}$$

where M_f is the momentum flux, g is acceleration of gravity, h is local water depth, T_m is mean wave period, and H_{mo} is wave height of the zeroth moment of the wave energy spectrum. A nonlinear approximation for momentum flux is important because stability is at its minimum when the incident wave is the most nonlinear.

Two stability equations resulted from the fit to data using Equation 2. The recommended equations for stability are

$$N_m = \frac{1}{a_m}\left(\frac{S}{K_s\sqrt{N_z}}\right)^{0.2} \tag{3}$$

and

$$N_m = \left(\frac{(M_F/\gamma_w h^2)_{\max}}{\Delta}\right)^{1/2}\frac{h}{D_{n50}} \tag{4}$$

where for plunging waves

$$a_m = \frac{1}{5P^{0.18}\sqrt{\cot\theta}} \qquad s_m \geq s_{mc} \tag{5}$$

and for surging waves

$$a_m = \frac{s_m^{P/3}}{5P^{0.18}(\cot\theta)^{0.5-P}s_m^{-P/3}} \qquad s_m < s_{mc} \tag{6}$$

and

$$s_m = H_{m0}/L_{m,} \qquad s_{mc} = -0.0035\cot\theta + 0.028 \tag{7}$$

Solving for the stable stone size yields

$$D_{n50} = ha_m\left(\frac{S}{K_s\sqrt{N_z}}\right)^{-1/5}\left(\frac{(M_F/\gamma_w h^2)_{\max}}{\Delta}\right)^{1/2} \tag{8}$$

In Equations 3 through 8: Nm is the momentum flux stability number, P = notional permeability of the structure, S = Ae/(Dn50)2 = normalized eroded area, Ae = eroded area, and Nz = storm duration/Tm. S and Ae are illustrated in Figure 62. Ks = 1.3 is an empirical parameter to account for accelerated damage that occurs with constant wave conditions, γw is the specific weight of water, θ is the seaside structure slope, sm is the local wave steepness and smc is critical wave steepness. Damage levels given by S = 1 to 3 represent the start of damage and correspond to Hudson's D% = 0 to 5 percent.

Figure 62. Illustration of damage parameters.

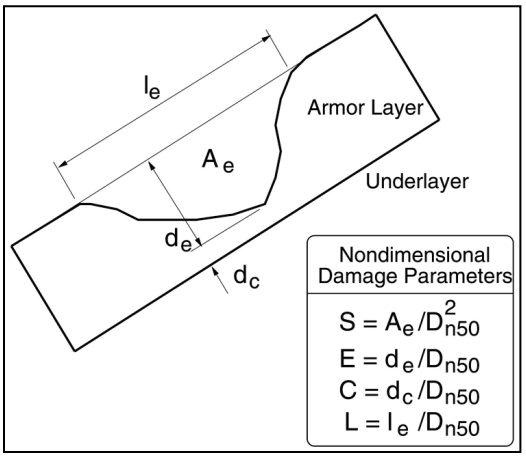

For an impermeable dike, P = 0.1. For a traditional multi-layer breakwater, P = 0.4 – 0.6. For the Tangier Island jetty, a somewhat porous core would be desirable to allow some flow through the structure to improve leeside circulation ($P = 0.6$), but may not be economically feasible. Use of small core material that effectively restricts transmission would give a permeability of $P = 0.4$. In the absence of more detailed information, a value of $P = 0.5$ is selected for this study.

3.2.2 Stable leeside armor stone

Stability equations were given by Van Gent and Pozueta (2004) for leeside stability. Melby (2009) revised these equations to be in a similar form to the seaside equations as follows

$$D_{n50} = a_{ls}\left(\frac{S_{ls}}{K_{ls}\sqrt{N_z}}\right)^{-1/r}\left(\frac{u_{1\%}T_{m-1,0}}{125\sqrt{\Delta}}\right) \tag{9}$$

$$a_{ls} = (\cot\phi)^{-2.5/r}[1 + 10\cdot\exp(-R_{c-rear}/H_s)]^{1/r} \tag{10}$$

where S_{ls} is the leeside damage, K_{ls} and r are empirical fit parameters, with $r = 6$ for constant wave conditions, $u_{1\%}$ = maximum crest velocity exceeded by 1% of the waves, $T_{m\text{-}1,0} = m_{-1}/m_0$ of incident spectrum, $T_{m\text{-}1,0} \sim T_p/1.1$ for a JONSWAP incident wave spectrum, cot φ = leeside slope, $R_{c\text{-}rear}$ = freeboard of leeside edge of crest, $H_s = H_{m0}$ of incident wave spectrum, and $(D_n)_{ls}$ and Δ_{ls} are the nominal stone size and density parameter for the leeside armor, respectively. A leeside stability number, N_{ls}, is introduced where

$$N_{ls} = \left(\frac{u_{1\%} T_{m-1,0}}{125 (D_n \sqrt{\Delta})_{ls}} \right) = \frac{1}{a_{ls}} \left(\frac{S_{ls}}{K_{ls} \sqrt{N_z}} \right)^{1/r} \tag{11}$$

Then the single-storm leeside damage for constant wave conditions can be expressed as

$$S_{ls} = K_{ls} \sqrt{N_z} \left(a_{ls} N_{ls} \right)^r \tag{12}$$

The n^{th} moment of the incident wave-energy density spectrum is given by

$$m_n = \int_0^\infty f^n S(f) df \tag{13}$$

The crest velocity exceeded by 1 percent of the waves is given by

$$\frac{u_{1\%}}{\sqrt{g H_s}} = \frac{1.7 (\gamma_{f-C})^{0.5} \left(\frac{z_{1\%} - R_c}{\gamma_f H_s} \right)^{0.5}}{\left(1 + 0.1 \frac{B_c}{H_s} \right)} \tag{14}$$

where $\gamma_{f\text{-}C}$ = friction factor on crest, γ_f = friction factor on seaward slope, R_c = freeboard of seaside crest, B_c = breakwater crest width, and $z_{1\%}$ = run-up exceeded by 1 percent of waves. The friction coefficients and run-up can be computed by Equations 15 and 16, respectively.

$$\gamma_f = \gamma_{f-C} = \begin{cases} 0.55 & \xi_{s,-1} \le 2 \\ 0.05625 * (\xi_{s,-1} - 2) + 0.55 & 2 < \xi_{s,-1} < 10 \\ 1.0 & \xi_{s,-1} \ge 10 \end{cases} \tag{15}$$

$$\frac{z_{1\%}}{\gamma H_s} = \begin{cases} c_0 \xi_{s,-1} & for\ \xi_{s,-1} \le p \\ c_1 - c_2 / \xi_{s,-1} & for\ \xi_{s,-1} > p \end{cases}$$

$$\frac{z_{1\%}}{\gamma H_s} = \begin{cases} c_0 \xi_{s,-1} & for\ \xi_{s,-1} \le p \\ c_1 - c_2 / \xi_{s,-1} & for\ \xi_{s,-1} > p \end{cases} \tag{16}$$

Here $c_2 = 0.25\ c_1^2/c_0$, $p = 0.5\ c_1/c_0$, and $\gamma = \gamma_f \gamma_\beta$ = reduction factor for roughness and angular wave attack, with $\gamma_\beta = 1.0$ for normally incident

waves. The Iribarren parameter based on the first negative moment wave period is

$$\xi_{s,-1} = \frac{\tan\theta}{\sqrt{\frac{H_s}{L_{m-1,0}}}} \tag{17}$$

where

$$L_{m-1,0} = \frac{gT_{m-1,0}^2}{2\pi} \tag{18}$$

and $c_0 = 1.45$ and $c_1 = 5.1$ for $z_{1\%}$. So, for the Tangier Island jetties, Equation 16 becomes

$$\frac{z_{1\%}}{H_s} = \begin{cases} 1.45\xi_{s,-1} & for\ \xi_{s,-1} \le 1.76 \\ 5.10 - 4.485/\xi_{s,-1} & for\ \xi_{s,-1} > 1.76 \end{cases} \tag{19}$$

An illustration of seaside damage on a rubble mound structure is shown in Figure 63, indicated by numbers 1 and 2. Condition 1 illustrates damage initiation that occurs as armor is displaced near the still water line but has not extended into the filter layers. Condition 2 illustrates extensive damage over the entire active zone of the seaward side extending into the filter layers and even into the core and crest. Herein, we assume that once seaside damage reaches Condition 2, the structure has no capacity and will breach during the storm that caused it to be in Condition 2.

Figure 63. Illustration of damage on a rubble-mound structure (CEM).

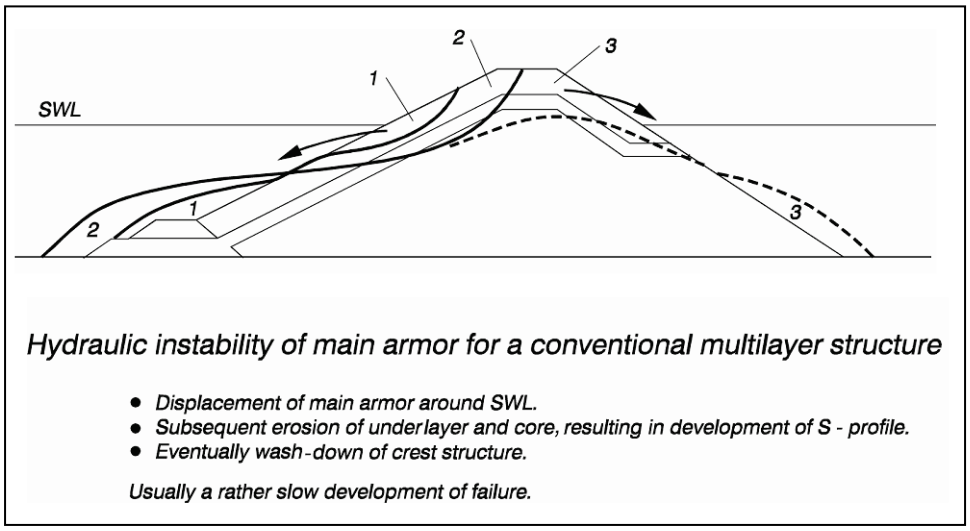

Leeside damage is illustrated in Figure 64. Damage begins on the rear crest and erodes seaward through the crest.

Figure 64. Illustration of leeside erosion of a rubble-mound breakwater cross-section (CEM).

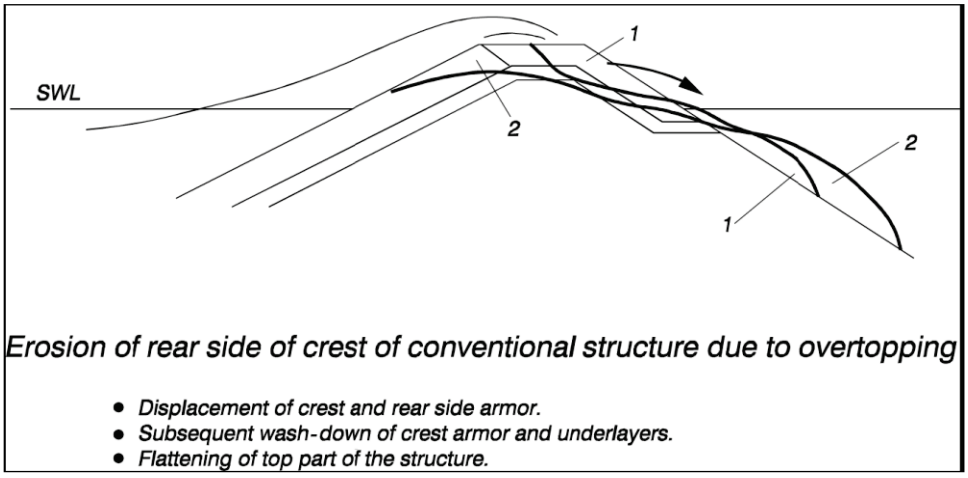

3.3 Design structure

3.3.1 Assumptions

Incident-wave direction is not included in the stability equations; therefore, it is assumed that waves are approaching normal to the structure.

Because the wave climate is relatively mild, structure side slopes of 1:2 (vertical: horizontal) were selected. A crest width of three armor stones was chosen as a minimum structure size. As will be seen below, stable

stone sizes have a nominal diameter of approximately 2 ft, so a crest width of 6 ft was used in the initial computations.

In the absence of detailed information on stone that will be used, a specific weight of 165 pcf was assumed for the calculations. Zero damage $S = 2$ was assumed.

3.3.2 Calculations

Wave run-up on a rubble-mound structure is typically on the order of 1.5 to 1.6 times the incident-wave height. Selecting a design height that includes storm surge plus a freeboard of 1.5 times the design wave height will yield some overtopping by the larger waves, but it will be minimal. Reducing the height of the structure to storm surge plus design wave height will obviously result in increased overtopping, but is probably justifiable because ships are not expected to be using the channel in the midst of a 50 yr storm. For the initial design calculations, structure heights of storm surge plus 0.5, 1.0, and 1.5 times the design wave height were considered.

Using the equations 1 through 19, above, and the assumptions given above in this section, stable armor stone sizes were calculated for each of the save points presented in Figure 55, above. Tables 13, 14, and 15 present the calculated stone weights and transmitted wave heights for freeboards of storm surge plus one-half wave height, storm surge plus one wave height, and storm surge plus 1.5 times the design wave height, respectively.

Table 13. Stable stone weights and transmitted wave height for crest elevation of storm surge plus one-half the design wave height.

Station	Storm Water Level, MTL (ft)	Depth, MTL (ft)	Design Wave Ht (ft)	Design Wave Period (sec)	Freeboard (ft)	Sea-side Armor Diam (ft)	Sea-side Armor Weight (tons)	Lee-side Armor Diam (ft)	Lee-side armor weight (tons)	Trans Coef	Trans Wave Height (ft)
85	5.00	4.17	4.17	5.3	2.08	1.49	0.27	2.12	0.78	0.24	1.00
88	5.00	6.17	4.27	5.3	2.13	1.53	0.30	2.14	0.81	0.24	1.03
99	5.00	7.71	4.40	5.3	2.20	1.58	0.33	2.16	0.84	0.24	1.06
103	5.00	8.66	5.02	5.3	2.51	1.77	0.46	2.28	0.98	0.25	1.24
118	5.00	8.69	4.82	5.3	2.41	1.71	0.42	2.25	0.93	0.25	1.18
121	5.00	8.40	4.82	5.3	2.41	1.71	0.41	2.25	0.93	0.25	1.18

Table 14. Stable stone weights and transmitted wave heights for crest elevation of storm surge plus one design wave height.

Station	Storm Water Level, MTL (ft)	Depth, MTL (ft)	Design Wave Ht (ft)	Design Wave Period (sec)	Free-board (ft)	Sea-side Armor Diam (ft)	Sea-side Armor Weight (tons)	Lee-side Armor Diam (ft)	Lee-side armor weight (tons)	Trans Coef	Trans Wave Height (ft)
85	5.00	4.17	4.17	5.3	4.17	1.49	0.27	1.50	0.28	0.00	0.00
88	5.00	6.17	4.27	5.3	4.27	1.53	0.30	1.51	0.29	0.00	0.00
99	5.00	7.71	4.40	5.3	4.40	1.58	0.33	1.52	0.29	0.00	0.00
103	5.00	8.66	5.02	5.3	5.02	1.77	0.46	1.57	0.32	0.00	0.00
118	5.00	8.69	4.82	5.3	4.82	1.71	0.42	1.56	0.31	0.00	0.00
121	5.00	8.40	4.82	5.3	4.82	1.71	0.41	1.56	0.31	0.00	0.00

Table 15. Stable stone weights and transmitted wave heights for crest elevation of storm surge plus 1.5 times the design wave height.

Station	Storm Water Level, MTL (ft)	Depth, MTL (ft)	Design Wave Ht (ft)	Design Wave Period (sec)	Free-board (ft)	Sea-side Armor Diam (ft)	Sea-side Armor Weight (tons)	Lee-side Armor Diam (ft)	Lee-side armor weight (tons)	Trans Coef	Trans Wave Height (ft)
85	5.00	4.17	4.17	5.3	6.25	1.49	0.27	0.73	0.03	0.00	0.00
88	5.00	6.17	4.27	5.3	6.40	1.53	0.30	0.72	0.03	0.00	0.00
99	5.00	7.71	4.40	5.3	6.59	1.58	0.33	0.70	0.03	0.00	0.00
103	5.00	8.66	5.02	5.3	7.53	1.77	0.46	0.59	0.02	0.00	0.00
118	5.00	8.69	4.82	5.3	7.23	1.71	0.42	0.63	0.02	0.00	0.00
121	5.00	8.40	4.82	5.3	7.23	1.71	0.41	0.63	0.02	0.00	0.00

3.3.3 Analysis

Changing the crest elevation does not change the stable armor stone size on the seaside of the structure, but it significantly affects the leeside armor stone. With the crest elevation at still water level (SWL=storm surge = +5 ft MTL) plus one-half wave height (Table 13), the armor stone on the lee side of the jetties are more than twice as large as on the sea side. With the crest at SWL plus a full wave height, stable armor stones on the sea side and lee side are roughly the same size.

Run-up calculations (not shown) indicate that if the crest is at SWL plus one wave height (Table 14), the run-up elevation will be higher than the crest so there will be some overtopping of the seaside of the jetty. However, there is essentially no transmission indicating that the volume of water overtopping the seaside crest is small. Because there is effectively zero transmission, a higher crest elevation is not needed.

During Hurricane Isabel, water piled up along the western shore of the bay, so water levels, wave heights, and wave periods were all lower than for the design 50 yr storm (Table 5). The hurricane is therefore discounted from the calculations.

Selected options at this point are a structure with a crest elevation of SWL plus one-half wave height or a higher-crested structure with a crest elevation of SWL plus one wave height. The lower-crested structure has some transmission and requires armor stone on the leeside more than twice as large as the higher-crested structure. The higher-crested structure has no transmission and smaller armor stone, but is 2- to 2-1/2-ft higher.

There are three reaches of the jetties to be considered: the shore-attached reach of the main jetty, the dogleg extending to the head of the main jetty, and the spur jetty. Each of these reaches will be considered by examining a cross-section at save stations 85, 99, and 118, respectively.

The cross-section is considered based on a core plus underlayers, covered by two layers of armor stone. For simplicity, the volume of the underlayers will be included with the core volume. Crest width is three armor stones. If the leeside armor stones are different from the seaside armor stones, the crest width is based on one smaller stone and two larger stones, regardless of whether the larger stones are on the seaside or leeside.

In Figure 65, a(ss) and a(ls) are nominal diameters of the seaside armor stone and leeside armor stone, respectively. Armor(1) is the cross-sectional area of the seaside armor, Armor(3) is the cross-sectional area of the leeside armor, and the area of Armor(2) is divided into one-third seaside armor and two-thirds leeside armor.

Figure 65. Idealized cross-section of jetty.

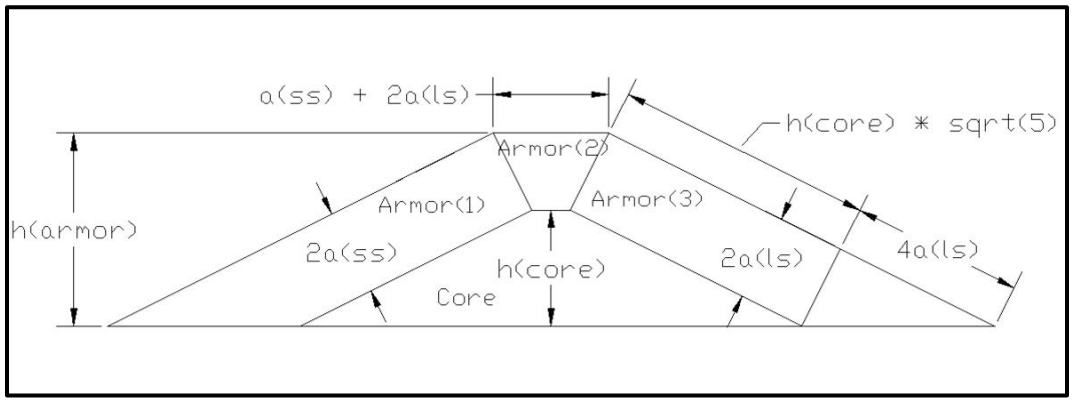

The dogleg extending to the seaward end of the main jetty (represented by save station 99) is exposed to waves both from the north and south. Although the 50 yr design storm shows waves approaching from 289 deg, it is possible for either side of the jetty to be the seaside or leeside, depending on actual wave angle of approach. Therefore, both sides of the jetty must be armored with the larger of the seaside or leeside armor stone.

Cross-sectional areas for the seaside armor stone, leeside armor stone, and core are shown in Table 16 for each of the three sections of jetty and at the two different crest elevations.

Table 16. Cross-sectional areas of armor stone and core.

Sta	Jetty Height (ft)	Seaside Stone Diam (ft)	Leeside Stone Diam (ft)	Total Area Seaside Armor (ft^2)	Total Area Leeside Armor (ft^2)	Total Area Armor Stone (ft^2)	Area of Core + Underlayers (ft^2)
Crest elevation = SWL + 0.5*wave height							
88	11.3	1.53	2.14	62.4	95.4	157.8	70.6
99	14.9	2.16	2.16	126.7	132.6	259.3	150.7
118	16.1	1.71	2.25	106.0	148.2	254.3	172.2
Crest elevation = SWL + 1.0*wave height							

Sta	Jetty Height (ft)	Seaside Stone Diam (ft)	Leeside Stone Diam (ft)	Total Area Seaside Armor (ft^2)	Total Area Leeside Armor (ft^2)	Total Area Armor Stone (ft^2)	Area of Core + Underlayers (ft^2)
88	13.3	1.53	1.51	82.6	84.3	166.9	131.9
99	17.1	1.58	1.58	111.6	114.8	226.4	231.1
118	18.5	1.71	1.56	132.5	123.4	255.9	278.8

There is surprisingly little difference in total area of armor stone for either the low-crested structure or the higher-crested structure due to the difference in size of the armor stone. The low-crested structure requires a larger armor stone size on the leeward side which means the two layers of armor stone will be thicker, which offsets the greater height of the higher-crested structure. The real difference is in the area of the core, where the higher-crested structure is significantly larger.

Although the core stone is typically significantly less expensive than the armor stone, and less expensive to place, it appears that the low-crested structure will be the less expensive of the two options. For this preliminary design, the structure crest will therefore be placed at SWL with storm surge, plus one-half the incident wave height.

The stability equations of Melby and Kobayashi (2011) and Melby (2009) presented above for the seaside and leeside armor, respectively, do not consider the jetty heads. In the Hudson equation (Equation 1), the stability coefficient K_D for jetty trunks with breaking waves and two layers of armor stone is 2.0, while for jetty heads with a 1:2 slope the recommended coefficient (two layers of armor and breaking waves) is 1.6 (Shore Protection Manual 1984), resulting in a 25 percent increase in stone size. In the absence of other guidance, armor stone sizes on the jetty heads (Stations 103 and 121) will be calculated in the same manner as on the jetty trunks, and then increased by 25 percent.

The basic features of the preliminary design are listed below in Table 17. As a reference, stone weights as calculated by the Hudson equation (Equation 1) are also included.

Table 17. Crest elevation and armor stone size for preliminary structure design.

Station	Depth MTL (ft)	Crest Elev MTL (ft)	Weight Seaside Armor W(50) (tons)	Weight Leeside Armor W(50) (tons)	Hudson Eqn W(50) (tons)
85	4.17	7.08	0.27	0.78	0.78
88	6.17	7.13	0.30	0.81	0.83
99	7.71	7.20	0.33	0.84	0.91
103	8.66	7.51	0.57	1.22	1.70
118	8.69	7.41	0.42	0.93	1.21
121	8.40	7.41	0.52	1.17	1.51

In general, Table 17 calls for a crest elevation of 7.1 ft MTL on the first reach of the main jetty, with seaside armor stone of 0.30 tons and leeside armor stone of 0.81 tons. The dogleg of the main jetty has a crest elevation of 7.2 ft MTL. Because either side of the dogleg could be the leeside depending on the direction of the storm, both sides of the dogleg are armored with 0.84-ton armor stone. The head of the main jetty has a crest elevation of 7.5 ft MTL and is armored with 1.22-ton armor stone.

The spur jetty is built to a crest elevation of 7.4 ft MTL. The trunk of the spur is armored with 0.42-ton stone on the seaside and 0.93-ton stone on the leeside. The head of the spur is armored with 0.52-ton stone on the seaside and 1.17-ton stone on the lee side.

3.4 Low-crested jetty

The calculations presented in the preceding sections developed a design for a traditional jetty with minimal transmission (transmitted wave heights about 1 ft) with minimal damage during a 50 yr storm event. However, the design storm assumed a water level of + 5 ft MTL. At that water elevation, much of the island where the north jetty is located will be inundated and there is little point in having a jetty extend higher than the surrounding land mass. A low-crested structure is therefore considered.

In Chapter 2 of this report, a crest elevation of 1 m (3.3 ft) was assumed when calculating the amount of wave-energy reduction for the different alternatives. This section will therefore consider the design of the jetties

with a crest elevation of 3.3 ft above MTL. Wave heights at the proposed structure locations for Alternative 4 were determined for water levels of 0.0 ft and 5.0 ft. For water levels between these two depths, a simple linear interpolation is used to estimate the wave heights.

The critical depth for design of the jetty is a water level near the crest of the jetty because the waves will be larger than at lower water levels and the overtopping will be directly impacting the jetty. At higher water levels, more of the energy passes over the structure. The equations presented above were therefore used to determine the required stone sizes for a water level of 3 ft. The results are given below in Table 18. As before, stone sizes on the jetty heads have been increased by 25 percent.

At the design flood level, this structure will be submerged and wave heights will be larger. Therefore, the armor stone weights were calculated for a submerged structure. As the water depth over a structure increases, the effects of waves on the structure decrease. However, in this case as the water level increases the wave heights increase. Therefore, two water levels were considered: the maximum design water level of +5 ft and a water level of +3.3 ft (crest elevation).

Table 18. Armor stone size for low-crested structure design.

Station	Depth MTL (ft)	Crest Elev MTL (ft)	Wave Height (ft)	Weight Seaside Armor W(50) (tons)	Weight Leeside Armor W(50) (tons)	Transmission Coefficient	Transmitted Wave Height (ft)
85	4.17	3.3	3.4	0.16	1.10	0.40	1.35
88	6.17	3.3	3.7	0.21	1.27	0.40	1.51
99	7.71	3.3	4.0	0.25	1.40	0.41	1.62
103	8.66	3.3	4.4	0.41	2.04	0.41	1.83
118	8.69	3.3	4.2	0.29	1.51	0.41	1.72
121	8.40	3.3	4.2	0.35	1.88	0.41	1.71

Unfortunately, there has been only limited research on armor layer stability of submerged structures. CIRIA et al (2007) presents results from Vidal et al. (1995) for stability of submerged structures. Nominal stone diameter, D_{n50}, is calculated by the equation

$$\frac{H_s}{\Delta D_{n50}} = A + B\frac{R_c}{D_{n50}} + C\left(\frac{R_c}{D_{n50}}\right)^2 \quad (20)$$

where R_c is the distance from the structure crest to still water level and is negative for submerged structures, and A, B, and C are coefficients that vary with the level of damage and the section of the structure. For the initiation of damage, the coefficients are given below in Table 19.

Table 19. Coefficients for initiation of damage in Equation 20 (from Vidal et al. 1995 as presented in CIRIA et al. 2007).

Segment	A	B	C
Front slope	1.831	-0.245	0.0119
Crest	1.652	0.0182	0.159
Back slope	2.575	-0.54	0.115
Total section	1.544	-0.23	0.053

The coefficients given in Table 19 were based on structures with seaside and leeside slopes of 1:1.5, but otherwise the proposed jetties generally fall within the range of parameters tested. Results of the calculations are shown below in Table 20 for a water level of 3.3 ft and Table 21 for a water level of 5.0 ft. As before, wave heights for the water level of 3.3 ft were determined by linear interpolation of the wave heights given for water levels of 0.0 and 5.0 ft, and stone sizes on the heads of the jetties were increased by 25 percent.

Table 20. Armor stone weights for submerged structures with water level at +3.3 ft and crest elevation at +3.3 ft.

Station	Wave Height H_s (ft)	Seaside Armor Wt (ton)	Crest Armor Wt (ton)	Leeside Armor Wt (ton)	Total Section Armor Wt (ton)
85	3.53	0.15	0.20	0.05	0.25
88	3.82	0.19	0.26	0.07	0.32
99	4.04	0.23	0.31	0.08	0.38
103	4.50	0.38	0.52	0.14	0.64
118	4.28	0.27	0.36	0.10	0.44
121	4.27	0.33	0.45	0.12	0.55

Table 21. Armor stone weights for submerged structures with water level at +5.0 ft and crest elevation at +3.3 ft.

Station	Wave Height H_s (ft)	Seaside Armor Wt (ton)	Crest Armor Wt (ton)	Leeside Armor Wt (ton)	Total Section Armor Wt (ton)
85	4.17	0.15	0.22	0.06	0.20
88	4.27	0.16	0.24	0.06	0.22
99	4.40	0.18	0.27	0.07	0.25
103	5.02	0.36	0.55	0.10	0.52
118	4.82	0.25	0.38	0.08	0.36
121	4.82	0.31	0.48	0.09	0.45

The results of the submerged structure analysis confirm that the armor stone weights presented in Table 18 for the low-crested jetty should be stable at all design water levels considered. However, the submerged structure analysis suggests that the leeside armor stone determined in the low-crested analysis are overly conservative. The design equations (Equations 1 through 19) were not developed for such low-crested structures. The crest elevation will not affect the seaside armor stone calculations, but the leeside armor weights do not appear reasonable. However, the leeside of the crest is the most vulnerable section of the armor for a heavily overtopped structure.

Obviously the low-crested structure will not provide the same level of protection during the design storm as would the higher-crested structure presented earlier. To illustrate the difference in levels of protection, Figures 66 and 67 show the wave fields during the design storm with water level at +5 ft for a structure with a crest elevation of 3.3 ft (Figure 66) and a structure high enough to block all overtopping (Figure 67). Waves in this example are from the southwest. There is little difference on the west side of the structures, but the higher structure clearly provides more protection on the lee side.

Figure 66. Wave field for structures with crest elevation of 3.3 ft, water level at 5.0 ft.

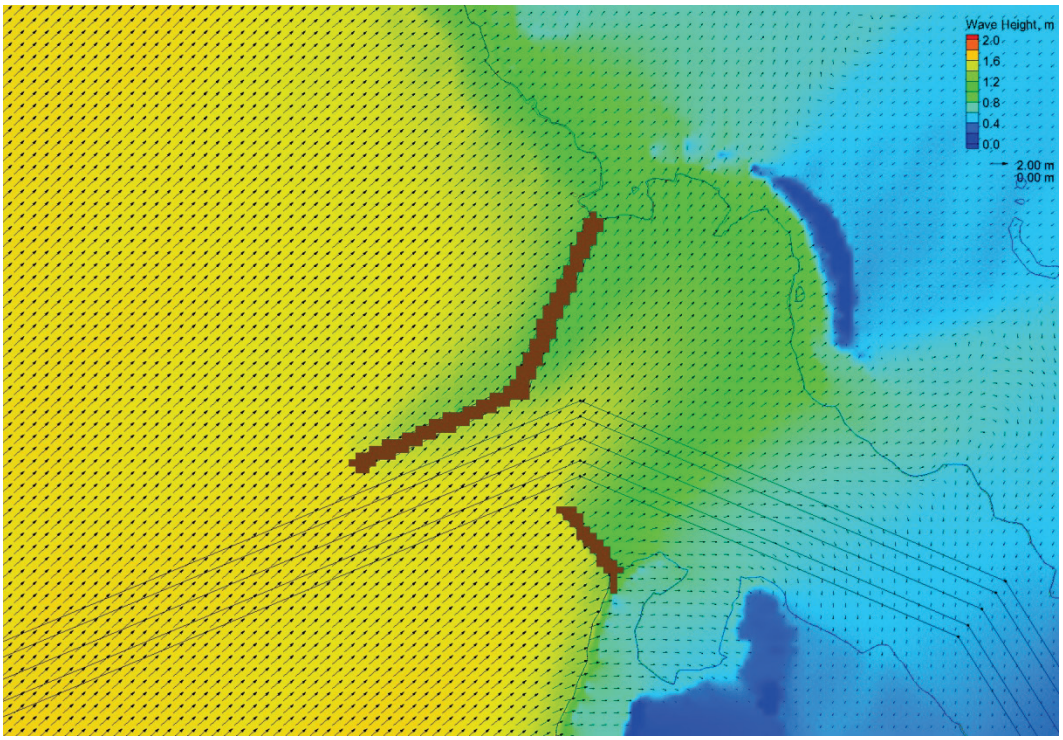

Figure 67. Wave field for structures with crest elevations sufficiently high to block all overtopping.

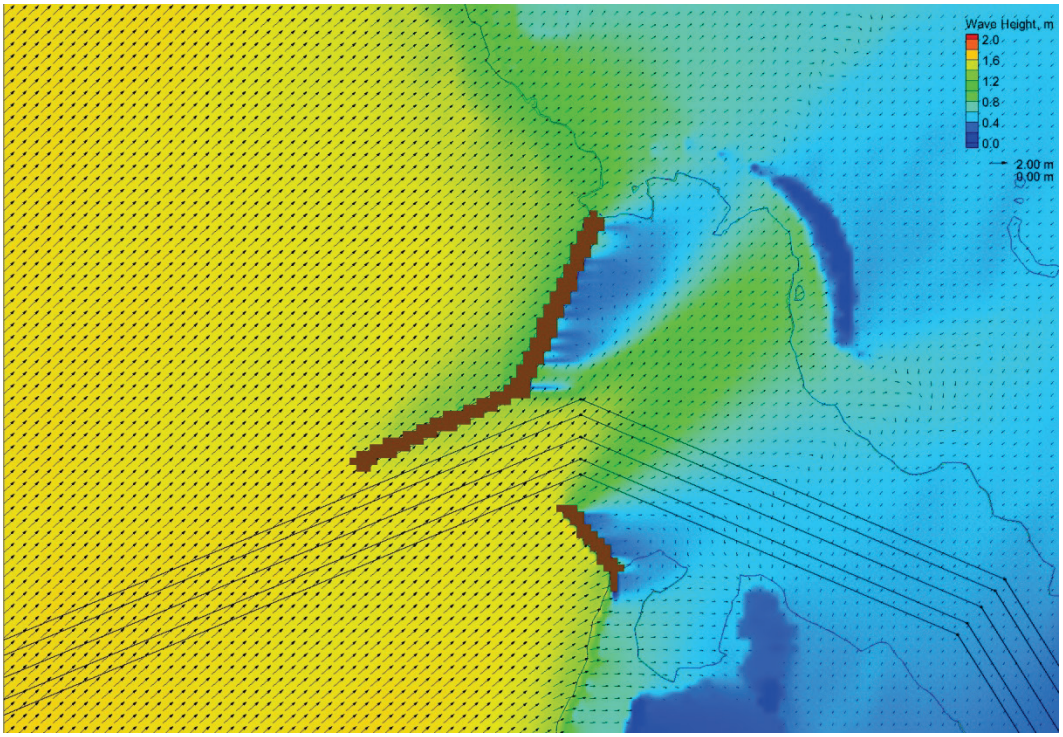

3.5 Tangier Island revetment

A rock revetment protects the shoreline along the west side of Tangier Island, running from the vicinity of the proposed spur jetty south, along the airport's runway (Figure 68). The revetment has performed satisfactorily, although there is evidence that some of the stones have moved. A letter dated 29 July 1986 from Norfolk District chief of the engineering division (Jack Starr) to the Coastal Engineering Research Center (Thomas Richardson), discusses what appears to be the final design of the revetment. The document calls for armor stone ranging in weight from 600 to 1,000 lbs with 75 percent greater than 750 lbs. Although it cannot be positively stated that this document represents the design of the as-built structure, the design would yield a W_{50} of at least 800 lbs (0.4 tons). This weight is surprisingly consistent with the 0.42 ton seaside armor weight for the spur jetty (Sta. 118) given in Table 17.

Figure 68. North end of revetment along the west side of Tangier Island.

3.6 Jetty response with sea level rise

The effects of sea level rise (SLR) on the performance and stability of the jetties were considered using four different SLR trends (USACE 2011) as follows:

1. No SLR
2. NRC-I
3. NRC-II
4. NRC-III

SLR in meters is computed using the equation

$$E(t_2) - E(t_1) = 0.0017(t_2 - t_1) + b(t_2^2 - t_1^2) \quad (21)$$

where t_2 and t_1 are times in years from a reference of 1992, t_2-t_1 is the time from 2013 and $E(t_2)$-$E(t_1)$ is the difference in water levels since 2013. The coefficient b is the only difference between the curves and is 2.71e-5, 7.00e-5, and 1.13e-4 for NRC-I, NRC-II, and NRC-III, respectively. The SLR rise scenarios, converted to feet, are shown in Figure 69.

Comparing Figure 60 to the results of Church and White (2011) and Houston (2012), the NRC-II prediction corresponds to a probability of occurrence of 0.05 while the NRC-I prediction is roughly a probability of excedance of 0.6. Boon et al. (2010) report that the current sea-level rise in the Chesapeake Bay area is about 1.8 mm/yr, which corresponds to a rise of 0.3 ft over 50 yrs. So the NRC-I prediction is a reasonable approximation of the most likely sea-level rise scenario and the NRC-II is reasonable as an upper bound at this time.

However, Boon et al. (2010) also report a subsidence in the Chesapeake Bay area of about -4 mm/yr, which corresponds to an increase in depth of 0.65 ft over 50 yrs.

Figure 69. Sea-level rise based on NRC-I, NRC-II, and NRC-III.

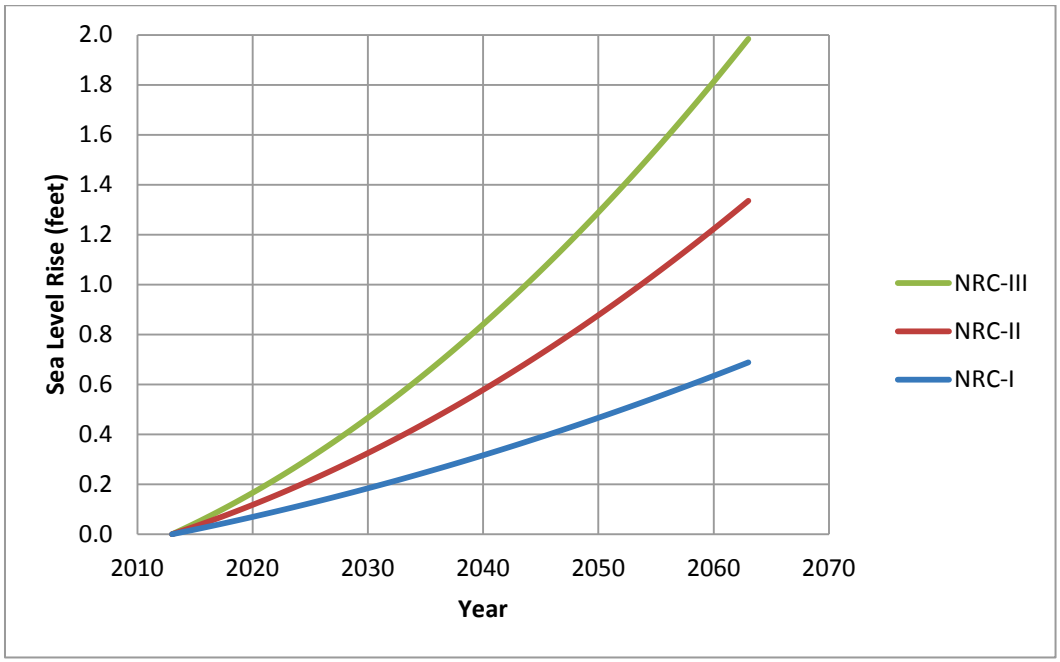

Although the design waves at the sites of the proposed Tangier Island jetties are not depth-limited, increased water depths will allow larger waves to reach the project site. However, the numerical models used in Chapter 2 of this report were not re-run with the higher water levels to determine the wave heights that would reach the structures. Instead, the design wave conditions presented in Table 4 were used with the structure freeboard reduced by the sea-level rise and the subsidence. Taking the NRC-I sea level rise as a most likely case, and adding 0.65 ft for subsidence, depth at the structure will increase by 1.34 ft in 50 yrs. Assuming the NRC-II as the upper bound of the expected sea-level rise, and adding 0.65 ft for subsidence, the depth at the structure could increase by as much as 2 ft in 50 yrs.

If depth at the structure increases, the jetty freeboard is reduced by the same amount. The seaside armor stone calculations are not affected by the freeboard, but the leeside armor stones will be unstable if the freeboard is reduced. Table 22 lists the stable leeside armor stone sizes at each of the save stations if the depth increases by 1.34 ft (NRC-I plus subsidence) or 2.0 ft (NRC-II plus subsidence). Jetty head stone weights have been increased by 25%.

The transmitted wave heights will increase if the freeboard decreases. Table 22 also lists the calculated transmitted wave heights for the design storm if the depth at the structure were to increase by 1.34 ft or 2.0 ft.

If the transmitted wave heights are considered unacceptable with the possibility of sea-level rise and subsidence, Table 23 lists leeside armor stone weights and transmitted wave heights for an initial crest elevation of one design wave height plus storm surge.

3.7 Local subsidence

The subsidence discussed above refers to the general subsidence of the Chesapeake Bay. It does not address local subsidence caused by the weight of the jetty compressing the underlying soil. Borings taken at the proposed jetty location indicate local subsidence should be expected. Design jetty crest elevation will need to be increased in order to have the desired crest elevation after the structure has settled. The geotechnical investigation necessary to determine the amount of local subsidence is being conducted at the same time as this study; thus, CENAO and CHL have agreed that CENAO will modify the final design to include local subsidence. Therefore, the design presented here is considered preliminary.

Table 22. Stable leeside armor stone required for crest elevation of storm surge plus one-half design wave height if depth increases by 1.34 ft (NRC-I plus subsidence) or 2.0 ft (NRC-II plus subsidence).

Station	Depth, MTL (ft)	Free-board, MTL (ft)	Weight Leeside Armor W(50) (tons)	Trans Wave Ht (ft)	Depth MTL (ft)	Free-board, MTL (ft)	Weight Leeside Armor W(50) (tons)	Trans Wave Ht (ft)	Depth, MTL (ft)	Free-board, MTL (ft)	Weight Leeside Armor W(50) (tons)	Trans Wave Ht (ft)
	No change in depth				Depth increases by 1.34 ft				Depth increases by 2.0 ft			
85	4.17	7.08	0.78	1.00	5.51	0.74	1.29	1.54	6.17	5.08	1.61	1.80
88	6.17	7.13	0.81	1.03	7.51	0.79	1.32	1.56	8.17	5.13	1.64	1.83
99	7.71	7.20	0.84	1.06	9.05	0.86	1.36	1.60	9.71	5.20	1.68	1.86
103	8.66	7.51	1.22	1.24	10.00	1.17	1.91	1.77	10.66	5.51	2.32	2.04
118	8.69	7.41	0.93	1.18	10.03	1.07	1.47	1.72	10.69	5.41	1.80	1.98
121	8.40	7.41	1.17	1.18	9.74	1.07	1.84	1.72	10.40	5.41	2.25	1.98

Table 23. Stable leeside armor stone required for crest elevation of storm surge plus design wave height if depth increases by 1.34 ft (NRC-I plus subsidence) or 2.0 ft (NRC-II plus subsidence).

Station	Depth, MTL (ft)	Free-board, MTL (ft)	Weight Leeside Armor W(50) (tons)	Trans Wave Ht (ft)	Depth, MTL (ft)	Free-board, MTL (ft)	Weight Leeside Armor W(50) (tons)	Trans Wave Ht (ft)	Depth, MTL (ft)	Free-board, MTL (ft)	Weight Leeside Armor W(50) (tons)	Trans Wave Ht (ft)
	No change in depth				Depth increases by 1.34 ft				Depth increases by 2.0 ft			
85	4.17	4.17	0.28	0.00	5.51	2.83	0.57	0.70	6.17	2.17	0.76	0.97
88	6.17	4.27	0.29	0.00	7.51	2.93	0.57	0.71	8.17	2.27	0.76	0.97
99	7.71	4.40	0.29	0.00	9.05	3.06	0.58	0.72	9.71	2.40	0.77	0.99
103	8.66	5.02	0.40	0.00	10.00	3.68	0.78	0.77	10.66	3.02	1.01	1.03
118	8.69	4.82	0.31	0.00	10.03	3.48	0.61	0.76	10.69	2.82	0.80	1.02
121	8.40	4.82	0.39	0.00	9.74	3.48	0.76	0.76	10.40	2.82	1.00	1.02

3.8 Site visit July 2013

The site for the root of the north jetty discussed in this report up to this point was selected during a site visit by CHL and District personnel in October 2012. The site was re-visited in July 2013, and it was found that the site had eroded significantly. In Figure 70, the "x" marks the location of the north jetty root that was selected in October 2012. At that time, the point was on the shoreline. The picture in Figure 70 was taken shortly before high tide and the depth between the shoreline and the point is about 6 in. There is concern that the site will continue to erode and ultimately flank the jetty.

If the shoreward segment of the north jetty were simply extended to the new shoreline, the jetty would be anchored in an area with an elevation that did not appear to be more than 1 ft above the water level (near high tide). The nearest point that appeared to be more resistive of erosion is marked in Figure 70 with an "o." The elevation there appeared to be close to 3 ft and the ground was held in place with a tangle of roots.

The location of the new point for the root of the north jetty is shown by the blue dot in Figure 71. If the offshore segment of the north jetty is left in place and the shoreward segment redirected straight to the new point, the length of the Alt 4 north jetty will be increased from 546 ft to 757 ft. The new jetty footprint with the modified landward terminus of the north jetty is expected to produce essentially the same wave-reduction benefits as the modeled footprints, so no changes are necessary in the jetty cross-sectional design.

Table 24 is an update of Table 1, and gives the state plane coordinates of key locations for the structures in each of the alternatives with the change in location of the north jetty root. In Table 24 all distance units have been converted from meters to feet.

Figure 70. Looking east towards original site of proposed north jetty root.

Figure 71. Location of key points on the north jetty.
The recommended revised location for the root is the blue dot.

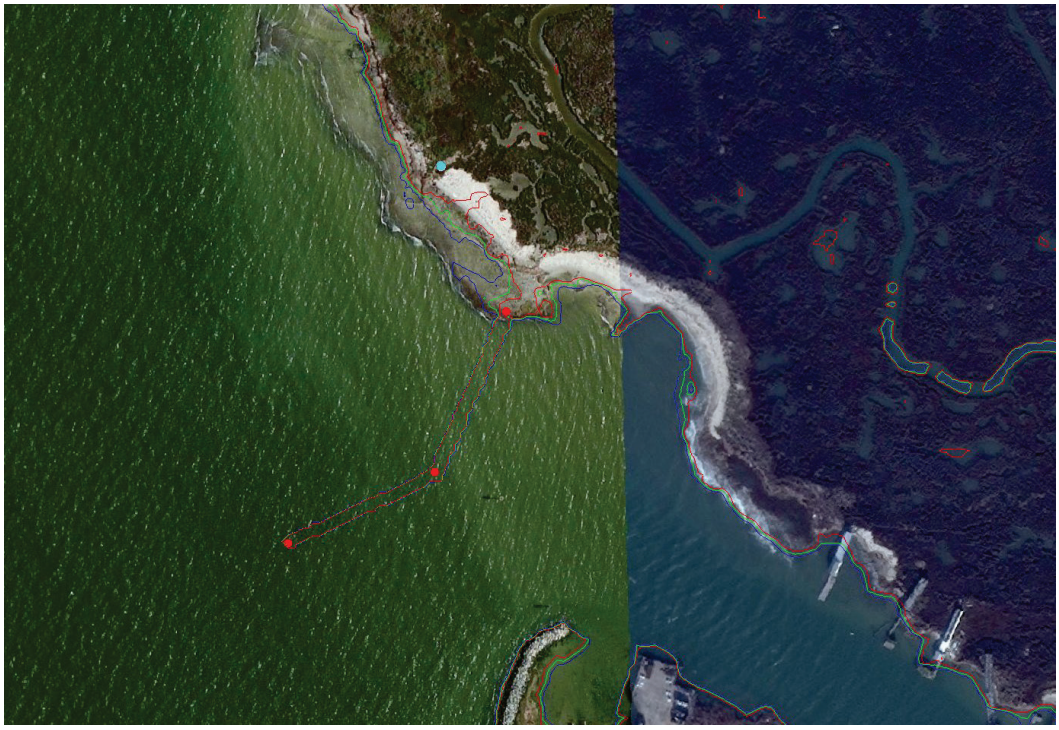

Table 24. Location (footprint) of alternatives in state plane coordinates, ft.

		Alt 1	Alt 2	Alt 3	Alt 4	Alt 5
North Jetty	Type	Straight	Dogleg	Dogleg	Dogleg	Straight
	Landward End Easting (ft)	12205238	12205238	12205238	12205238	12205238
	Landward End Northing (ft)	3836792	3836792	3836792	3836792	3836792
	Turning Point Easting (ft)		12205228	12205228	12205228	
	Turning Point Northing (ft)		3836298	3836298	3836298	
	Seaward End Easting (ft)	12205228	12204992	12204992	12204992	12205228
	Seaward End Northing (ft)	3836298	3836183	3836183	3836183	3836298
	Shore Segment Length (ft)		494	494	494	
	Bay segment Length (ft)		263	263	263	
	Tot Length (ft)	494	757	757	757	494
South Spur Jetty	Type	None	None	Straight	Straight	Straight
	Landward End Easting (ft)			12205366	12205376	12205376
	Landward End Northing (ft)			3835980	3836016	3836016
	Seaward End Easting (ft)			12205366	12205294	12205294
	Seaward End Northing (ft)			3836111	3836118	3836118
	Length (ft)			131	131	131

4 Conclusions

This report documents numerical wave and flow modeling for evaluation of jetties on a shallow draft navigation channel on Tangier Island, VA, located in the south Chesapeake Bay. CENAO is considering the construction of structures to protect the western entrance of the channel and reduce the wave energy in the lee of the structures. Five alternatives and the existing channel geometry were investigated by numerical models. All five alternatives included a breakwater system that connects to the north shoreline. Alternatives 3, 4, and 5 included an optional short structure (spur) joining to the south shoreline. A number of advances to CMS-Wave were necessary to address this project's special needs. The CIRP funded these developments to improve model's capabilities. These included development and testing of the full-plane and parent-child capability for hurricanes and northeasters in an estuary, and developing pre- and post-processing analysis codes for model setup and providing wave parameters for structural design calculations required at and around structures.

Structural designs were estimated based on numerical wave and hydrodynamic modeling conducted for 50 yr design wind speeds, waves, and water-level conditions. The 50 yr wind speed was considered as idealized condition and was based on a previous study by Basco and Shin (1993). Different structure alternatives were evaluated to determine an optimal design as determined by the level of wave-energy reduction in the navigation channel. The hydrodynamic modeling study results (e.g., wave height, period, direction, and water level) along the western side of the proposed structure footprint were used in the preliminary wave-control structural design calculations. These calculations included structural stability, run-up/overtopping, and transmission through and over the structure.

Overall, Alternative 4 performed better than other alternatives for the conditions evaluated, as shown in Figures 29, 31, 33, 36-38, and 42-47; and in Tables 6-8 and 12. Consequently, based upon the level of wave reduction shown in the modeling results, the modified footprint of Alternative 4, as provided in Table 24, is recommended for use as the design structure location. However, some of the other alternatives also provided

considerable wave-reduction benefits. A comparison of the alternatives indicated that the three that included a south spur jetty (Alternatives 3, 4, and 5) outperformed the other two (Alternatives 1 and 2, with no south spur) in reducing wave energy in the channel. This is shown in the figures and tables listed above.

In addition, it should be noted that the geometry of the channel itself, even without any jetty structure, strongly dampens the propagating waves. For example, station 50 is approximately 300 m (1000 ft) down the channel from the western entrance. As shown by the red line (the without project line) in Figures 29, 31, and 33, by the time that waves have propagated this distance down the channel, their energy has dissipated to the extent that their height is only of the order of 10 to 20 percent of their former height in the bay. These three figures (and others) show that the greatest benefits to be accrued by any of the alternatives will occur in this westernmost 1000 ft (300 m) of the Tangier Island boat canal. Most of the docks and processing sheds that line both sides of the channel are to the east (further down the channel) of this position. Thus, while this report shows that Alternative 4 provides the greatest wave-reduction benefits of any of the alternatives, it is recognized that multiple criteria may be used in the selection process of the optimal alternative.

The following results are based upon the choice of Alternative 4 as the construction footprint. Stable armor stone sizes for both the seaside and leeside of a conventional multi-layer rubble-mound jetty are determined at each of six save stations on the proposed jetties. Three different crest elevations for the jetties were considered (Tables 13, 14, and 15): storm surge plus one-half design wave height, storm surge plus one design wave height, and storm surge plus 1.5 times the design wave height. Based on the size of the armor stones, cross-sectional areas were calculated for the seaside armor, leeside armor, and a combined core plus under-layers (Table 16). The lowest crest elevation (storm surge plus one-half design wave height) appears to offer sufficient protection while being the least costly.

Structures with low crest elevation are particularly susceptible to leeside damage by overtopping waves. Armor stone sizes for the seaside and leeside were therefore calculated separately for the different configurations considered (Table 17).

Transmitted wave heights were calculated at each save station for each of the crest elevations considered. Transmitted wave heights were also calculated for the expected freeboard after 50 yrs of the most likely sea-level rise (NRC-I) and also for the larger sea-level rise expected as an upper limit (NRC-II) (Tables 22 and 23). In both cases, a constant rate of subsidence for Chesapeake Bay was included. However, the larger wave heights that would result from the greater depths were not determined. Not included in the calculations was local settling caused by the weight of the structure on the in situ material.

The structures described above allow some overtopping with transmitted wave heights during the design storm event of about 1 ft. However, the proposed jetty crest elevation is considerably higher than the island to which the main jetty is attached. At the design water level, much of the island will be inundated leaving the jetty exposed as an island. A low-crested structure, with crest elevation approximating the highest land elevations in the vicinity of the structure root (crest elevation= 3.3 ft), was also examined. Although the low-crested structure will obviously have greater transmission, it will be less expensive to build and still provide a high level of energy reduction. The wave-height reduction factors in Tables 6 through 11 were based on a crest elevation of 3.3 ft.

A site visit to the island in July 2013 found that the point of land that had been selected as the anchor point of the north jetty had significantly eroded. At high tide, the point was completely surrounded by water and cut off from the main part of the island. Extending the jetty through the selected point and straight back to the island was not recommended as the island at that location was low-lying and additional erosion was expected. A new location for the jetty root was selected at the nearest point that offered at least some elevation and appeared more resistant to erosion.

The design was based on a design storm with a return period of 50 yrs. Not only is the design storm expected to occur during the life of the structure, but a more severe storm is obviously possible. The design equations assume a low level of damage during the design event. Because of the difficulty in obtaining repair and maintenance funds for coastal structures, it may be prudent to use a more extreme design storm or include a level of over-design to minimize any damage that may occur. As was noted in Chapter 2, the focus of this study was on wave modeling to develop means for wave-energy reduction in the navigation canal. If required for the final

design, the modeling estimates for flow and sediment transport should be validated either with field data or compared to the estimates obtained from other two- or three-dimensional hydrodynamic models.

References

Basco, D.R. and Shin C.S. 1993. Design Wave Information for Chesapeake Bay and Major Tributaries in Virginia. Technical Report, No. 93-1. Dept. of Civil Engineering, The Coastal Engineering Institute, Old Dominion University. Norfolk, Virginia.

Boon, J.D., J.M. Brubaker, and D.R. Forrest. 2010. Chesapeake Bay Land Subsidence and Sea Level Change. VIMS Special Report 425 in Applied Science and Ocean Engineering. November 2010.

Church, J.A., and N.J. White. 2011. Sea-Level Rise from the Late 19th to the Early 21st century. Surv. Geophys (2011) 32:585-602.

CIRIA, CUR, CETMEF (2007). The Rock Manual. The use of rock in hydraulic engineering (2nd edition). C683, CIRIA, London.

Demirbilek, Z., L. Lin, and G.P. Bass. 2005. Prediction of Storm-Induced High Water in Chesapeake Bay. Proc. of Solutions to Coastal Disasters 2005, ASCE, Charleston, SC, 187-201.

Demirbilek, Z., L. Lin, and A. Zundel. 2007. WABED model in the SMS: Part 2. Graphical interface. Tech. Note ERDC/CHL CHETN-I-74, U.S. Army Engineer R&D Center, Vicksburg, MS.

Demirbilek, Z. and J. Rosati. 2011. Verification and Validation of the Coastal Modeling System, Report 1: Summary Report, ERDC/CHL Technical Report 11-10, U.S. Army Corps of Engineers Research and Development Center, Vicksburg, MS.

Houston, J.R. 2012. Global Sea Level Projections to 2100 Using Methodology of the Intergovernmental Panel on Climate Change. J. Waterway, Port, Coastal, and Ocean Engr.

Hudson, R.Y. 1959. Laboratory Investigation of Rubble-Mound Breakwaters, J. Wtrwy. and Harb. Div., ASCE, 85(WW3), 93-121.

Lin, L., Z. Demirbilek, R. Thomas, and J. Rosati. 2011. Verification and Validation of the Coastal Modeling System, Report 2: CMS-Wave, ERDC/CHL Technical Report 11-10, U.S. Army Corps of Engineers Research and Development Center, Vicksburg, MS.

Lin, L., Z. Demirbilek, and H. Mase. 2011. Recent Capabilities of CMS-Wave: A Coastal Wave Model for Inlets and Navigation Projects. Proceedings, Symposium to Honor Dr. Nicholas Kraus. Journal of Coastal Research, Special Issue 59,7-14.

Lin, L., Z. Demirbilek, H. Mase, and F. Yamada. 2008. CMS-Wave: A Nearshore Spectral Wave Processes Model for Coastal Inlets and Navigation Projects. Coastal and Hydraulics Laboratory Technical Report ERDC/CHL TR-08-13. Vicksburg, MS: U.S. Army Engineer Research and Development Center.

Lin, L., and Z. Demirbilek. 2005. Evaluation of two numerical wave models with inlet physical model. Journal of Waterway, Port, Coastal, and Ocean Engineering 131(4):149-161, ASCE.

Melby, J.A. and N. Kobayashi. 2011. Stone armor damage initiation and progression based on the maximum wave momentum flux. Journal of Coastal Research, 27(1), 110–119.

Melby, J. A. 2009. "Rubble Mound Stone Armor Stability and Damage Prediction," Technical Report in press, Coastal and Hydraulics Laboratory, US Army Engineer R&D Center, Vicksburg, MS.

Melby, J. A., and S. A. Hughes (2004). "Armor Stability Based on Wave Momentum Flux," Proc. of Coastal Structures 2003, ASCE, Reston, VA, 53 – 65.

Sanchez, A., W. Wu, T. Beck, H. Li, J. Rosati, R. Thomas, J. D. Rosati, Z. Demirbilek, M. Brown, and C. Reed. .2011a. Verification and Validation of the Coastal Modeling System, Report 3: CMS-Flow Hydrodynamics, ERDC/CHL Technical Report 11-10, U.S. Army Corps of Engineers Research and Development Center, Vicksburg, MS.

Sanchez, A., W. Wu, T. Beck, H. Li, J. Rosati, R. Thomas, J. D. Rosati, Z. Demirbilek, M. Brown, and C. Reed. .2011b. Verification and Validation of the Coastal Modeling System, Report 4: CMS-Flow Sediment Transport and Morphology Change, ERDC/CHL Technical Report 11-10, U.S. Army Corps of Engineers Research and Development Center, Vicksburg, MS.

Shore Protection Manual (1984). 4th Ed., 2 Vol, U.S. Army Engineer Waterways Experiment Station, U.S. Government Printing Office, Washington, DC.

USACE. 2011. Sea-Level Change Considerations for Civil Works Programs. Engineering Circular EC 1165-2-212. 1 October 2011.

Van Gent, M.R.A., and B. Pozueta (2004). "Rear-Side Stability of Rubble Mound Structures," Proc. ICCE 2004, ASCE, V4, Reston, VA, 3481-3493.

Vidal, C., M. A. Losada, and E. P. D. Mansard (1995). "Stability of Low-Crested Rubble-Mound Breakwater Heads," J. Waterway, Port, Coastal, and Ocean Eng, vol. 121, no. 2, pp. 114-122.

Zundel, A. K. (2006). Surface-Water Modeling System Reference Manual – Version 9.2. Provo, UT: Brigham Young University Environmental Modeling Research Laboratory.

Appendix A: Description of CMS

The Coastal Modeling System (CMS) was used for the numerical modeling estimates of waves, currents, and sediment transport at Tangier Island. A brief description of the CMS is provided here for completeness.

As shown in Figure A-1, the CMS is an integrated suite of numerical models for waves, flows, and sediment transport and morphology change in coastal areas. This modeling system includes representation of relevant nearshore processes for practical applications of navigation channel performance, and sediment management at coastal inlets and adjacent beaches. The development and enhancement of CMS capabilities continues to evolve as a research and engineering tool for desk-top computers. CMS uses the Surface-water Modeling System (SMS) (Zundel 2006) interface for grid generation and model setup, as well as plotting and post-processing. The Verification and Validation (V&V) Report 1 (Demirbilek and Rosati 2011) and Report 2 (Lin et al. 2011) have detailed information about the CMS-Wave features, and evaluation of model's performance skills in a variety of applications. Report 3 and Report 4 by Sanchez et al. (2011a and 2011b) describe coupling of wave-flow models, and hydrodynamic and sediment transport and morphology change aspects of CMS-Flow. The performance of CMS for a number of applications is summarized in Report 1 and details are described in the three companion V&V Reports 2, 3, and 4.

Figure A- 1. The CMS framework and its components.

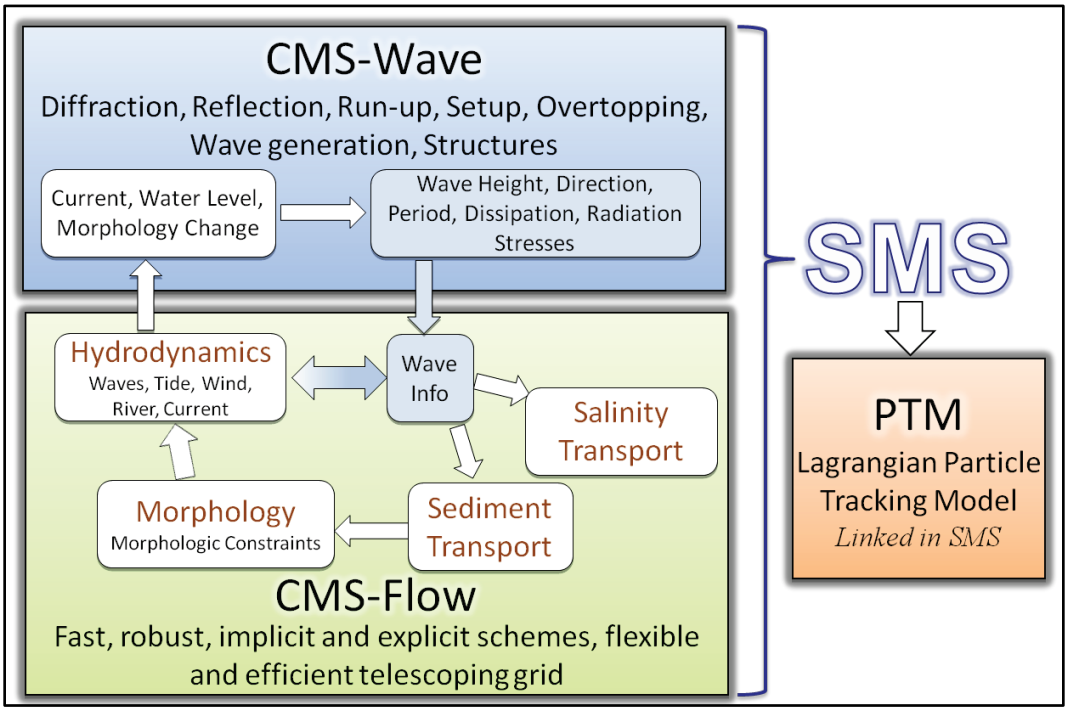

The CMS-Wave, a spectral wave model, is used in this study given the large extent of modeling domain over which wave estimates were required. Wind-wave generation and growth, diffraction, reflection, dissipation due to bottom friction, white-capping and breaking, wave-current interaction, wave run-up, wave setup, and wave transmission through structures are the main wave processes included in the CMS-Wave.

CMS-Wave model solves the steady-state wave-action balance equation on a non-uniform Cartesian grid to simulate steady-state spectral transformation of directional random waves. CMS-Wave is designed to simulate wave processes with ambient currents at coastal inlets and in navigation channels. The model can be used either in half-plane or full-plane mode for spectral wave transformation (Lin et al. 2008; Demirbilek et al. 2007). The half-plane mode is default because in this mode CMS-Wave can run more efficiently as waves are transformed primarily from the seaward boundary toward shore. See Lin et al. (2011 and 2008) for features of the model and step-by-step instructions with examples for application of CMS-Wave to a variety of coastal inlets, ports, structures, and other navigation problems. Publications listed in the V&V reports and this report provide additional information about the CMS-Wave and its engineering applications. Additional information about CMS-Wave is available from the CIRP website: http://cirp.usace.army.mil/wiki/CMS-Wave

The CMS-Flow, a two-dimensional shallow-water wave model, was used for hydrodynamic modeling (calculation of water level and current) in this study. The implicit solver of the flow model was used in this study. This circulation model provides estimates of water level and current given the tides, winds, and river flows as boundary conditions. CMS-Flow calculates hydrodynamic (depth-averaged circulation), sediment transport, and morphology change, and salinity due to tides, winds, and waves.

The hydrodynamic model solves the conservative form of the shallow-water equations that includes terms for the Coriolis force, wind stress, wave stress, bottom stress, vegetation-flow drag, bottom friction, wave roller, and turbulent diffusion. Governing equations are solved using the finite volume method on a non-uniform Cartesian grid. See the V&V Reports 3 & 4 by Sanchez et al. (2011a and 2011b) for the preparation of model at coastal inlet applications. Additional information about CMS-Flow is available from the CIRP website: http://cirp.usace.army.mil/wiki/CMS-Flow

CMS-Flow modeling task included specification of winds and water levels to the model. The effects of waves on the circulation were input to the CMS-Flow and have been included in the simulations performed for this study.

There are three sediment transport models available in CMS-Flow: a sediment mass balance model, an equilibrium advection-diffusion model, and a non-equilibrium advection-diffusion model. Depth-averaged salinity transport is simulated with the standard advection-diffusion model and includes evaporation and precipitation. The V&V Report 1, Report 3, and Report 4 describe the integrated wave-flow-sediment transport and morphology change aspects of CMS-Flow. The performance of CMS-Flow is described for a number of applications in the V&V reports.

Appendix B: Datums

Horizontal datums

The horizontal datum used for coordinate data input into the models was NAD83, State Plane Virginia, South (Federal Information Processing Standard state code: 4502) in meters.

Vertical datums

The vertical datum used in this study was MTL (mean tide level) in meters, based on NOAA benchmark at Bishops Head, Hoopers Strait, Maryland (Station 8571421). The station information is given as follows:

Station ID: 8571421 PUBLICATION DATE: 11/19/2012
Name: BISHOPS HEAD, HOOPERS STRAIT, MARYLAND

NOAA Chart: 12261 Latitude: 38° 13.2' N
USGS Quad: WINGATE Longitude: 76° 2.3' W

Tidal datums at BISHOPS HEAD, HOOPERS STRAIT based on:
LENGTH OF SERIES: 6 YEARS
TIME PERIOD: Sep 05 - Aug 09 & April 10 - March 12
TIDAL EPOCH: 1983-2001

CONTROL TIDE STATION: 8571892 CAMBRIDGE, CHOPTANK RIVER
Elevations of tidal datums referred to Mean Lower Low Water (MLLW), in meters:

HIGHEST OBSERVED WATER LEVEL (10/30/2012)		= 1.309
MEAN HIGHER HIGH WATER	MHHW	= 0.624
MEAN HIGH WATER	MHW	= 0.575
North American Vertical Datum	NAVD88	=0.380
MEAN SEA LEVEL	MSL	= 0.307
MEAN TIDE LEVEL	MTL	= 0.307
MEAN LOW WATER	MLW	= 0.039
MEAN LOWER LOW WATER	MLLW	= 0.000
LOWEST OBSERVED WATER LEVEL (01/03/2008)		= -0.559

The data above were obtained from the website:
http://tidesandcurrents.noaa.gov/data_menu.shtml?stn=8571421%20Bishops%20Head,%20MD&type=Bench%20Mark%20Data%20Sheets

REPORT DOCUMENTATION PAGE

Form Approved
OMB No. 0704-0188

1. REPORT DATE (DD-MM-YYYY)	2. REPORT TYPE	3. DATES COVERED (From - To)
March 2015	Final	

4. TITLE AND SUBTITLE
Modeling Study for Tangier Island Jetties, Tangier Island, VA

5a. CONTRACT NUMBER

5b. GRANT NUMBER

5c. PROGRAM ELEMENT NUMBER

6. AUTHOR(S)
Zeki Demirbilek, Lihwa Lin, Donald L. Ward, and David B. King

5d. PROJECT NUMBER

5e. TASK NUMBER

5f. WORK UNIT NUMBER

7. PERFORMING ORGANIZATION NAME(S) AND ADDRESS(ES)
Coastal and Hydraulics Laboratory
U.S. Army Engineer Research and Development Center
3909 Halls Ferry Road
Vicksburg, MS 39180

8. PERFORMING ORGANIZATION REPORT NUMBER
ERDC/CHL TR-14-8

9. SPONSORING / MONITORING AGENCY NAME(S) AND ADDRESS(ES)
U.S. Army Engineer District, Norfolk
803 Front Street
Norfolk, VA 23510

Headquarters, U.S. Army Corps of Engineers
Washington, DC 20314-1000

10. SPONSOR/MONITOR'S ACRONYM(S)
HQUSACE

11. SPONSOR/MONITOR'S REPORT NUMBER(S)

12. DISTRIBUTION / AVAILABILITY STATEMENT
Approved for public release; distribution is unlimited.

13. SUPPLEMENTARY NOTES

14. ABSTRACT

This report documents numerical wave and flow modeling for evaluation of the jetties on a shallow draft navigation channel on Tangier Island, VA, located in Chesapeake Bay. Because it is heavily used by the local fishing fleet, the U.S. Army Engineer District, Norfolk (CENAO) maintains the Tangier Island boat canal. CENAO is considering the construction of structures to protect the western entrance of the channel and reduce the wave energy in the lee of the structures, and asked the U.S. Army Engineer Research and Development Center (ERDC), Coastal and Hydraulics Laboratory (CHL) to perform a numerical modeling study to investigate how waves and hydrodynamics would be affected by structures, to identify the optimal location for the structures, and to develop a preliminary structure design. The primary goal of the study was to develop a quantitative estimate of waves and wave reduction in the canal for a relative comparison of alternatives investigated and for the preliminary structural design calculations.

CMS-Wave, a spectral wave model, was used to estimate waves in Chesapeake Bay and propagate waves into the entrance channel and boat canal. The numerical modeling results indicated that maximum wave energy reduction inside the canal was obtained using a dog-leg jetty connecting to the north shoreline and a spur on the south shoreline.

15. SUBJECT TERMS
Numerical modeling, evaluation, hydrodynamics, wave reduction, Tangier Island, VA

16. SECURITY CLASSIFICATION OF:			17. LIMITATION OF ABSTRACT	18. NUMBER OF PAGES	19a. NAME OF RESPONSIBLE PERSON
a. REPORT	b. ABSTRACT	c. THIS PAGE			19b. TELEPHONE NUMBER (include area code)
Unclassified	Unclassified	Unclassified		110	